Doctoral theses at NTNU, 2020:335

Benoit Loranger

Laboratory investigation of frost susceptibility of crushed rock aggregates and field assessment of frost heave and frost depth

Doctoral thesis

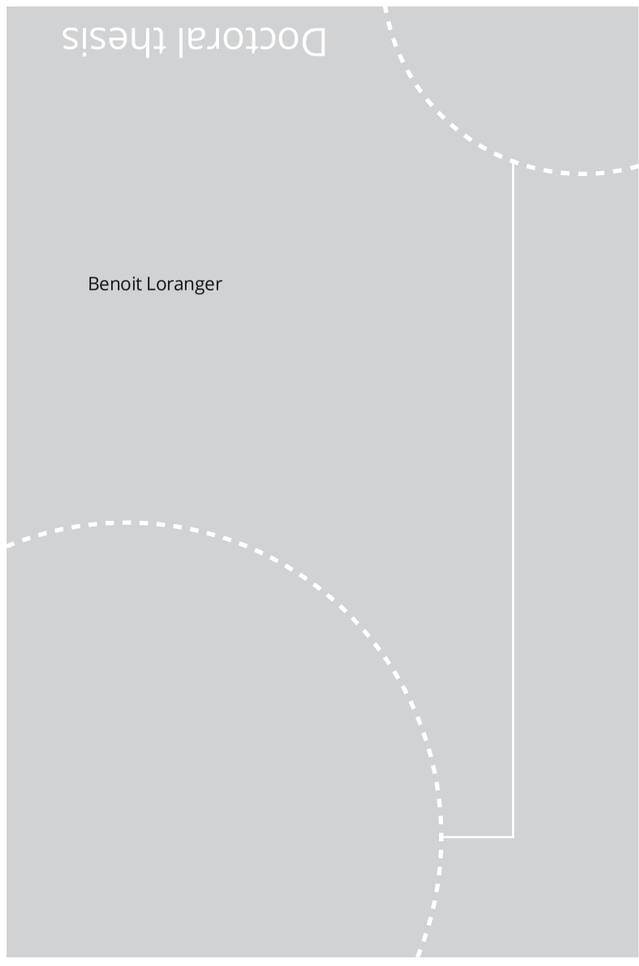

ISBN 978-82-326-5016-3 (printed ver.)
ISBN 978-82-326-5017-0 (electronic ver.)
ISSN 1503-8181

NTNU
Norwegian University of
Science and Technology

NTNU
Norwegian University of Science and Technology
Thesis for the Degree of
Philosophiae Doctor
Faculty of Engineering
Department of Civil and Environmental
Engineering

Doctoral theses at NTNU, 2020:335

NTNU
Norwegian University of
Science and Technology

NTNU

Benoit Loranger

Laboratory investigation of frost susceptibility of crushed rock aggregates and field assessment of frost heave and frost depth

Thesis for the Degree of Philosophiae Doctor

Trondheim, November 2020

Norwegian University of Science and Technology
Faculty of Engineering
Department of Civil and Environmental Engineering

NTNU
Norwegian University of
Science and Technology

NTNU
Norwegian University of Science and Technology

Thesis for the Degree of Philosophiae Doctor

Faculty of Engineering
Department of Civil and Environmental Engineering

ISBN 978-82-326-5016-3 (printed ver.)
ISBN 978-82-326-5017-0 (electronic ver.)
ISSN 1503-8181

Doctoral theses at NTNU, 2020:335

Printed by NTNU Grafisk senter

To my family

PREFACE

This PhD thesis is a part of the Frost Protection of Roads and Railways (FROST) project, supported mainly by the Research Council of Norway under grant 246826/O70. The following public administrations and private partners are associated with this project: the Norwegian Public Roads Administration (*Statens Vegvesen*), the National Rail Administration (Bane Nor), Laval University, SINTEF, Glasopor and Leca. The project involved two PhD researchers who performed a dual analysis of frost susceptibility and heat transfer in crushed rock aggregates used in pavement infrastructure. This thesis focuses mainly on the frost susceptibility of such aggregates.

The main supervisor of this thesis and associated papers was Professor Inge Hoff at the department of civil and environmental engineering at the Norwegian University of Science and Technology (NTNU), in Trondheim. Elena Scibilia, researcher in the same NTNU department, and Professor Guy Doré from the department of civil and water engineering at Laval University in Quebec City (Canada) were co-supervisors.

The committee for the appraisal of this thesis comprises the following members:

Professor Pauli Kolisoja (first opponent).
Tempere University of Technology, Finland

Chief Engineer Geir Berntsen (second opponent)
Norwegian Public Road Administration, Norway

Associate professor Helge Mork
Norwegian University of Science and Technology, Norway

The supervisors of this study were:

Professor Inge Hoff
Norwegian University of Science and Technology, Norway

Researcher Elena Scibilia
Norwegian University of Science and Technology, Norway

Professor Guy Doré
Laval University, Canada

ACKNOWLEDGEMENTS

First I would like to thank Professor Inge Hoff for giving me the opportunity to take part in this project, in which I am deeply interested. Thanks too to my co-supervisor Elena Scibilia, who managed to bring about so much collaboration between diverse entities. Many thanks to my co-supervisor Professor Guy Doré, who has guided and commented on most of the scientific work.

Special thanks to all of the partners involved in this project: the Norwegian Public Roads Administration (NPRA), the Norwegian National Railway Administration (NNRA), SINTEF, Leca and Glasopor, and for their significant contributions at many advisory board meetings. More specifically, I thank Kjell Arne Skoglund (NPRA) for the many discussions about road and railway design and future challenges Thanks to Jostein Aksnes (NPRA) for explaining Norwegian standards and procedures to me, and to Karlis Rieksts, who was doing his PhD on thermal behaviour on the same project, for our most interesting discussions.

I would like to thank Denis St-Laurent at the Quebec Ministry of Transport (MTQ) and Henry Gustavsson from Aalto University, who were involved in the SSR model analysis, for their very interesting discussions, which made a significant contribution to this research. A special thanks to Seppo Saarelainen for in-depth discussions about the SSR model and so many other design-related subjects. His experience and passion are contagious and have inspired me throughout this study.

I thank Bent Lervik and Jan Erik Molde for their considerable help with the laboratory setup, field test site construction and technical support. Thanks to Per Asbjørn Østensen for the data acquisition setup for laboratory and field test site. And my thanks for precious help processing the numerous laboratory tests necessary for the study go to Zahra Rahimi, Kaja Eriksen, Sandeep Shrestha, Parasmani Tripathi, Siri Stolpestad, Vadim Simonsen and Olga Levochckina.

As this project involved so many collaborators I would like to thank everybody else involved in one of the many aspects of this Ph.D., with apologies for not mentioning them all by name.

For my parents Lise and Michel Loranger and their belief in this adventure, and my children Camille, Maëlle, Stella and Éliana for their accompaniment over the years, I am deeply grateful. Their existence is the reason I continued to work on this important project.

Finally, thanks to Julie, my dear partner, with whom I have lived this adventure. Thanks for all the scientific discussion and precious advice, and for encouraging me at the most difficult moments. Thank you for all the support you have given me over all these years, for believing in this project.

ABSTRACT

In Nordic countries that experience seasonal frost, understanding how it affects the service life of linear transport infrastructures such as roads and railways is essential. Frost action both regroup frost heave and thaw weakening processes. This research focuses on frost heave, which occurs when three conditions are met: freezing temperature, water availability and frost-susceptible materials. Frost susceptibility is therefore defined as the ability of an unbound granular material (natural soil or crushed rock aggregate) to form ice lenses due to cryosuction, which is the suction of water to the frost front. Frost heave in a frost-susceptible material lifts the layers above the freezing front. Many kinds of damage are attributable to frost heave, such as cracks in and unevenness of the road surface, making it uncomfortable and even dangerous for road users. Frost heave and subsequent thawing can significantly reduce the service life of roads and are accompanied by high associated maintenance and reparation costs. Knowledge of the frost susceptibility of the materials comprising the different layers of transport infrastructure is therefore crucial to optimal frost design.

This research mainly aimed to characterize the frost susceptibility of crushed rock aggregates. Laboratory experiments using a multi-ring frost cell were carried out to estimate the segregation potential of the 0-4 mm fraction of crushed rock aggregates. Twenty-four tests performed on nine different rock types found that crushed rock aggregates with a fines content of <63 µm between 11.6% to 25.5% are highly frost susceptible. The study found poor correlation between <63 µm fines content and segregation potential. The latter was used to characterize the frost susceptibility of the different crushed rock aggregates primarily for its capacity to estimate frost heave magnitude easily. The use of a grain size criterion, as presently used in Norway, seems to be efficient for dividing non-frost-susceptible from frost-susceptible aggregates, but does not allow estimation of crushed rock aggregates' segregation potential with a good degree of confidence.

As frost heave tests require a costly laboratory setup and specialist personnel, the segregation potentials of crushed rock materials were estimated using material index properties such as initial water content, liquid limit, mean particle size of the fine fraction and specific surface area of the fine fraction. This method is used by the Quebec Ministry of Transportation for soils, and the goal here was to assess the suitability of the methodology for use with crushed rock aggregates. It was found that estimation from material indexes gave segregation potential results within a range of ±15% compared to those obtained from frost heave tests. There was a direct correlation between the specific surface area of the fine fraction of a crushed rock aggregate and its segregation potential, from which an equation was developed. The study showed that the crushing phase had an effect on the frost susceptibility of the tested crushed rocks. Aggregates are more frost susceptible after the first crushing stage than after the third or fourth crushing stages. The hypothesis that the fine fraction is enriched by weak minerals at the first crushing could explain this behaviour, but further research is necessary before this theory can be presented with confidence.

The design was optimized by modelling three road sections with different frost protection layers using the SSR model and the I3C ME software. The fully-instrumented test site is situated in the Røros municipality where harsh winters are the norm, with the freezing index of an average winter equal to that of regions

such as Oslo, Trondheim, Narvik, Tromsø etc. It was found that the SSR model is suitable for both frost penetration and frost heave estimation for thick (2.05 meters) layered road structures. The SSR also permitted the back-calculation of key parameters such as dry density, moisture content and segregation potential, making it useful for assessing existing infrastructure parameters. Using a segregation potential function, i.e. segregation potential according to time, was found to produce optimal frost heave estimations in a transient thermal regime.

LIST OF PUBLICATIONS

I. Loranger, B., Hoff, I., Scibilia, E. and Doré, G. (2019a). Frost heave laboratory investigation on crushed rock aggregates. Québec 2019: 18th International Conference on Cold Regions Engineering and the 8th Canadian Permafrost Conference. Quebec City, Canada. (August 18th to 22nd 2019).

II. Loranger, B., Rieksts, K., Hoff, I. and Scibilia, E. (2019b). Frost depth and frost protection capacity of crushed rock aggregates based on particle size distribution. Québec 2019: 18th International Conference on Cold Regions Engineering and the 8th Canadian Permafrost Conference. Quebec City, Canada. (August 18th to 22nd 2019).

III. Loranger, B., Doré, G., Hoff, I. and Scibilia, E. (2020a). Assessing soil index parameters to determine the frost susceptibility of crushed rock aggregates. Submitted to Cold Regions of Science and Technology Journal (May 12th 2020).

IV. Loranger, B., Doré, G., Hoff, I. and Scibilia, E. (2020b). Evaluation of the SSR model on thick-layered road structures using the I3C-ME frost module and analyses of key parameters. Submitted to the Journal of Cold Regions of Science and Technology (July 7th 2020).

Other significant contribution (not analyzed in the thesis)

A. Loranger, B., Kuznetsova, E., Hoff, I., Aksnes, L. and Skoglund, K.A. (2017). Evaluation of Norwegian gradation based regulation for frost susceptibility of crushed rock aggregates in roads and railways. 10th International Conference of the bearing capacity of roads, railways and airfield. Athens, Greece. (June 28th to 30th 2017).

B. Rieksts, K., Loranger, B., Hoff, I. and Scibilia, E. (2019). In situ thermal performance of lightweight aggregates expanded clay and foam glass in road structures. Québec 2019: 18th International Conference on Cold Regions Engineering and the 8th Canadian Permafrost Conference. Quebec City, Canada. (August 18th to 22nd 2019).

C. Kjelstrup, S., Ghoreishian Amiri, S.A., Loranger, B. and Grimstad, G. (2020). Transport coefficients and pressure conditions for growth of ice lens in frozen soil. Submitted to Acta Geotechnica journal (July 2nd 2020).

TABLE OF CONTENTS

1. INTRODUCTION

This introduction chapter is divided into four sections: 1.1 research background; 1.2 research objectives and scope; 1.3 research approach; and 1.4 thesis structure.

1.1 Background

Frost heave-related damage to roads and railway infrastructure is a problem in countries that experience seasonal frost. Roads and railways are relatively thick infrastructures covering long distances and frequently pass through varied soil deposits, climatic and hydrologic conditions. The economic and design challenges of ensuring a stable, secure and durable infrastructure are numerous.

The road system in Norway, with its relatively low population density, is extensive, resulting in significant budget restriction. The best frost design scenario would prevent the frost front reaching frost-susceptible sub-grade soil and control all construction materials for frost-susceptibility. This approach is already in place for main roads in Norway, but is not always realizable with the budget allocated to secondary and low-volume roads, which represent around 70% of the country's road system.

Road damage related to frost heave appears in different forms, mainly as unevenness (differential heaving) and as longitudinal and transversal cracks. When not repaired, frost-related damage, especially where salts are present, has a cumulative effect as cracks allow water to enter the upper layer of the system as happens on most roads. Lack of maintenance reduces the service life of a road, significantly raising the net cost of the infrastructure. Furthermore, unmaintained roads will eventually require costly rehabilitation.

The cold winters of 2009-2010 and 2010-2011 in south-eastern Norway led to frost action-related complications on the transport infrastructure network. The consequences of the frost action were numerous; e.g. the speed limit of the fast train to and from Oslo airport was significantly reduced for several months, and premature aging and/or differential heaving issues were observed on several newly-built road sections. The maintenance costs for these road sections were significantly higher than those first estimated. Some sections were planned to be completely reconstructed due to severe frost heave and frost action. Two hypotheses were suggested to explain frost design failure and consequent frost heave-related damage: i) frost penetrated deeper than estimated (sub-grade heave) and ii) blasted and crushed aggregates produced substantial heave (pavement-layer heave).

Norway's newest roads are built entirely of crushed rock aggregates and include a frost protection layer between the sub-base and the sub-grade soil. The design system to qualify the frost susceptibility of crushed aggregates is based on a grain-sized criterion, mostly on the basis of what is known about natural gravel and natural soil. Crushed rock aggregates have gradually replaced natural gravel over the last decades for many reasons including the ease of local production, the depletion of natural gravel resources,

ecological reasons (i.e. water stream protection and transport distances), their superior mechanical properties and better quality control (i.e. shape, mineralogy, fine content and grading curves). The Norwegian Public Roads Administration revised its requirements in the 2014 Road Construction Handbook N200 and again in 2018. A wide variety of aggregates was allowed in the frost protection layer before the 2014 revision as untreated blast rock from levelling and cuts. The 2014 revision prohibited the use of untreated blasted rock aggregates to prevent heterogeneity-related problems, as well as accommodating better particle size distribution. Specifically, i) the maximum particle size was set to 500 mm or half the thickness of the frost protection layer, ii) at least 30% must be <90 mm fraction, and iii) the percentage of allowed fines (<63 microns) was set at 2-15%, calculated from material <22.4 mm fraction. The 2018 revision reduced the percentage of allowed fines to 2-7%, calculated from material <90 mm fraction. These changes were mostly based on empirical experience.

The Frost Protection of Roads and Railways (FROST) project was established to investigate frost heave, frost penetration, thermal properties and heat transfer in crushed rock aggregates. This thesis focuses on the frost susceptibility of crushed rock aggregates and field validation of frost depth and frost heave in such materials. Questions were raised about crushed rock's frost susceptibility. There have been several studies of this subject over the last decades, but few have presented criteria for frost heave calculation. Calculations of frost heave is invariably related to frost penetration as the frost front position in function of time have to be known to estimate the heave contribution of the material found at designated depth. This study uses and extends previous studies on this subject, of which the principles are summarized in the next paragraphs.

Grain size was judged a reliable criterion for dividing non-frost susceptible and frost susceptible materials (Chamberlain, 1981), but does not allow estimation of heave magnitude, and its precision when predicting the frost susceptibility of base and subbase materials is disputable, as reported by Janoo et al. (1997, cited in Konrad and Lemieux, 2005). Segregation potential, developed by Konrad and Morgenstern (1981) was chosen as the frost heave criterion as it has been proven reliable for estimating heave magnitude in linear transportation infrastructure (Konrad, 1980; Konrad and Morgenstern, 1982a; Konrad 1994; Konrad 1999; St-Laurent, 2006). The segregation potential of fine fractions in crushed rock aggregates has been investigated by Konrad (2005), who presents six different crushed rock aggregates: four sedimentary, one volcanic and one plutonic. His study suggests that crushed rock aggregates may be quite frost susceptible. The same study also presents a methodology for estimating the segregation potential of geomaterials and soils using index parameters such as the liquid limit, specific surface area and the 50% passing of the fine <75 um. Bilodeau (2009) investigated the segregation potential of three crushed or partially crushed 0-20 mm rock aggregates, as widely used in Canada and the US; and Konrad and Lemieux (2005) present an investigation of the segregation potential of three 0-20 mm crushed rock aggregates.

Saarelainen's (1992) frost penetration investigation inspired this study. Saarelainen calls his model the SSR model. It also integrates segregation potential to compute both frost heave according to frost depth. Saarelainen's investigation was performed on six Finnish sites and was found to estimate both frost heave and frost depth accurately. The Quebec Ministry of Transport included the SSR model in its practice in

2006, with extended validation presented by St-Laurent (2012). Further validation was provided by Saarelainen et al. (2015). The model uses almost the same input parameters as a more classical method (dry density, thermal conductivity, water content, grain density, freezing index etc.), making it easy to implement. Its ability to calculate both frost heave and frost depth makes it a powerful design and optimisation tool.

To recapitulate, a grain-size criterion as the one existing in the Norwegian regulation permit to divide frost and non-frost susceptible material with a reasonable accuracy but i) the heaving magnitude is not calculated, that could lead to unexpected or faster infrastructure degradation and service life loss and ii) it is an empirical criterion, limiting design optimization and development. The leading work on which this thesis is based are the studies from Konrad (2005) on frost susceptibility of crushed rock aggregates, from Konrad and Lemieux (2005) on the determination of SP using index parameters and from Saarelainen (1992) on the SSR model.

1.2 Research objectives and scope

The main objective of this research is the investigation of the frost susceptibility of crushed rock aggregates for linear transportation infrastructures. The crushed rock aggregates are defined as processed rock material from quarry production, blasted beforehand, which goes through several crushing and screening steps to arrive at a final graded product. The frost susceptibility being wide in its meaning, it was therefore divided in smaller research entities that connected all together. The first part of the work focuses on determining the frost susceptibility of different types of crushed rock aggregates commonly found in Norway using their segregation potential. As frost heave tests are costly and time-consuming, the next part investigates the possibility of determining the segregation potential for crushed rock aggregates satisfactorily using soil index parameters. The determination of frost depth in function of time is necessary for estimating frost heave magnitude using the segregation potential. The third part evaluates calculation of frost depth in layered roads and railway structures with frost protection layers of different grading and mineralogy, and compares the results with in situ measurement of a test site. The last section assesses a heat balance model at the frost front that permit to calculate both frost depth and heave according to time and freezing index magnitude. The results from the model were also compared to in situ measurement at a test site.

This research is considered relevant to improving knowledge of the frost susceptibility of crushed rock and transport infrastructure design optimization. Ultimately, it proposes the use of relatively simple calculation tools to numerically predict the behavior of transport infrastructure under freezing stress. The general objective is to improve knowledge of frost design by moving from a rigid empirical system to knowledge-based design optimization.

The work completed for the realisation of these objectives included:

a) Investigate actual Norwegian design guidelines regarding regulations on crushed rock aggregates.

b) Produce a literature review on crushed rock aggregate's segregation potentials.
c) Gather different crushed rock aggregates of various mineralogy and different locations in Norway.
d) Perform and a full geotechnical characterization of crushed rock aggregates, including full particle size distribution, grain density, X-ray diffraction, specific surface area, liquid limit and hydraulic conductivity.
e) Build the laboratory frost heave test setup and calibrate it.
f) Perform frost heave tests on 0-4 mm fraction of crushed rock aggregates
g) Support and participate in the construction and follow up of data at the Røros experimental site.
h) Analyse and modelling of frost depth and frost heave at the Røros experimental test site.

1.3 Research approach

This research focused on design, the common goal of each investigation being to improve knowledge about the studied concept and its applicability for design purposes. The main direction that was pointed out was to i) assess and improve knowledge about the frost susceptibility of crushed rock aggregates, ii) analyse observed and estimated frost depth into different frost protection layers, iii) validate the results of the analysis of the frost susceptibility of crushed rock material via a simple laboratory test and iv) determine a valid model for thick-layered infrastructure.

The research was conducted on one specific objective at a time. Paper A presents Norway's frost design challenges and fully describes the Røros experimental test site. The main part of the study was to install and calibrate the newly acquired frost heave cell constructed at Laval University, Quebec, Canada. A set of seven different crushed rock aggregates of varying mineralogy reflecting, to our best knowledge, Norway's commonest rock types were chosen for testing following determination of their segregation potential. This work is presented in Paper I. Frost penetration of the road sections' different frost protection layers is analyzed in Paper II and Paper B. In parallel, an in-depth crushed rock index parameters measurements were performed on all crushed rock aggregates tested in the frost heave cell. This allowed assessment of the use of Konrad's (2005) normalized segregation potential concept and is presented in Paper III. Finally, road sections' different frost protection layers were fully modelled using the SSR model integrated with the I3C-ME software to assess the use of the model with thick-layered pavement structures. The results are presented in Paper IV.

This is a paper thesis, with a summary of the theory, methodology and main research outputs presented in the following pages. All relevant literature reviews, specific methodologies and detailed analyses are presented in the published papers.

2. FROST ACTION ON TRANSPORTATION INFRASTRUCTURE

Roads in cold climates may be subject to frost heave problems during the cold season and to weakening as a result of the spring thaw (Andersland and Ladanyi, 2004). These effects are commonly divided into frost heave and spring thaw events, but are inseparable elements of frost action. They generate damage including various types of differential deformation, different asphalt cracking patterns and loss of bearing capacity.

Frost heave normally occurs when the frost front reaches a frost-susceptible subgrade soil beneath a road's foundation (Doré, 1997) (Figure 1). Deformation can be due to the ice segregation phenomenon (the creation of ice lenses). Ice segregation can also occur in the pavement material when the fine content is not adequately controlled. In a typical road structure with ca 10 cm of asphalt, 30 cm of crushed rock aggregate (0-20 mm grading) and ca 50 cm of gravelly sand subbase, around 10 mm of frost heave is expected before the frost front reaches the subgrade soil, where there is only a small percentage of fines (Bilodeau, 2009). Doré et al. (1998, cited by Bilodeau, 2009) found 8-10 mm heave from a 0-20 mm base layer in a Canadian field test in Quebec. Konrad and Lemieux (2005), also in Quebec, found that a frost heave magnitude of ca 10 mm was caused solely by the base layer freezing.

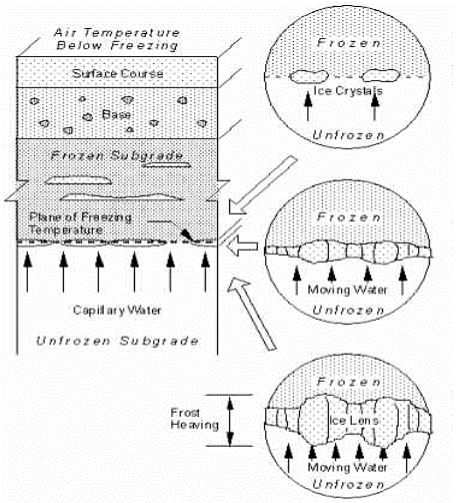

Figure 1: Frost segregation in a road infrastructure (Mahoney et al. 1986)

Frost heave can be uniform, or can create differential deformation when the underlying frost susceptible material is distributed heterogeneously. A constant uniform road infrastructure heave will cause little or no problems during the winter period apart from the possible occurrence of longitudinal cracks in the center of the road. These cracks are formed because roadside embankments insulated by snow generate deeper frost penetration (and subsequent heave) in the centerline compared to at the road's edges (Zubeck & Doré, 2009) (Figure 2).

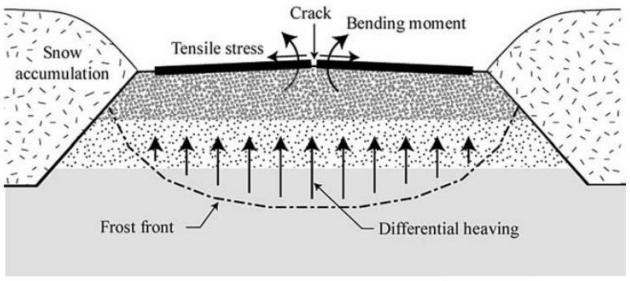

Figure 2: Longitudinal cracking formation in the centerline (Zubeck and Doré, 2009)

Spring thaw of the road has various consequences. As for frost penetration in winter, thaw penetration happens faster in the centerline than on the roadsides. The surface water remains in the upper part of the road because it cannot drain vertically nor horizontally due to the underlying and side frozen layer. This 'pool' phenomenon drastically increases the interstitial pore pressure and therefore decreases significantly (sometimes almost totally) the effective bearing capacity of the top layers (Figure 3). This effect is enhanced by frost heaving as it been demonstrated by Uthus (2007) and Konrad (2008) that water content is expected to raise in crushed rock aggregates layers by cryosuction when the frost front progress downward.

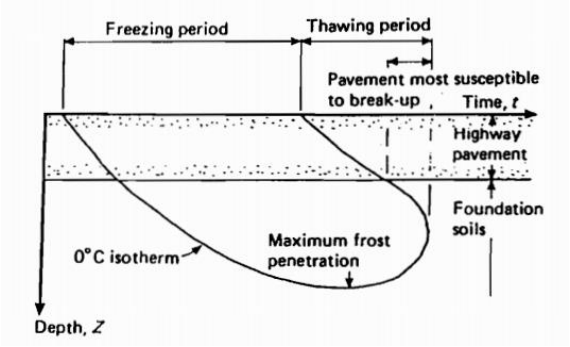

Figure 3: Seasonal ground freezing beneath a pavement structure (Andersland and Ladanyi, 2004)

This phenomenon leads to the creation of settlements, cracks, holes and rutting. The same problems also affects deeper structure layers as the thaw front progress in depth. A large amount of water from ice lenses melting will create a water super-saturation of the material with the same effect as previously described.

In Norway, considerable costs are directly linked to frost action year after year (Hoff et al., 2002). According to the press article in *Teknisk Ukeblad - Bygg* (2014), the average costs of road construction for the Norwegian Public Road Administration (NPRA) ranges from a) 50 to 90 million kroners per kilometer for a 2-lanes, 6.5 meters wide road to b) 140 to 230 million kroners per kilometer for a 4-lanes, 19-22 meters wide road. There is few financial analysis on how much cost frost related damage. An example was found

in two articles from *Teknisk Ukeblad - Bygg* (2010a and 2010b) where portion of a 10 km stretch on highway 2 between Kløfta and Nybakk experience severe frost heave in 2010. This stretch was somehow new, built in 2007. The repair cost were estimated between 40 to 45 millions Norwegian kroner. According to the project manager at that time, the error came from the design phase, which point out the importance of having a solid comprehension of material properties and climate. It is therefore important that those large investments for road building are to be protected by avoiding any deterioration and then assure and their service life expectancy.

3. FROST DESIGN IN NORWAY

The frost susceptibility of soil is based on fine particle passing percentage by mass. This criterion was mainly developed by Nordal in the 1960s, based on Casagrande's conclusions (1932). The Frost I Jord committee (1976) created today's frost design. The frost susceptibility of a granular outbound material is divided into four categories ranging from non-frost susceptible (T1) to highly frost susceptible (T4) depending on its fractions < 2, 20 and 200 microns calculated from the <22.4 mm fraction. Table 1 presents the T1 to T4 frost susceptibility classes.

Table 1: Frost susceptibility classes (modified from Frost I Jord, 1976; Handbook N200, 2014 & 2018)

Frost susceptibility	Class	Material < 22,4 mm		
		Mass %		
		< 2 µm	< 20 µm	< 200 µm
Non/ Negligible	T1	--	< 3	--
Low	T2	--	3-12	--
Moderate	T3	>40[1)]	> 12	< 50
High	T4	< 40	> 12	> 50

1) Soils with more than 40% of < 2 µm are considered as moderatly frost susceptible (T3).

The first step in evaluating the need for a frost protection layer is to assess the material class of the sub-grade (natural) soil. If a construction is to be placed on a T3- or T4-class soil, frost protection must be included in the design. Main roads are designed to prevent frost penetrating a potentially frost susceptible sub-grade (Figure 4). The thickness of each of the road's layers is therefore adjusted to ensure this.

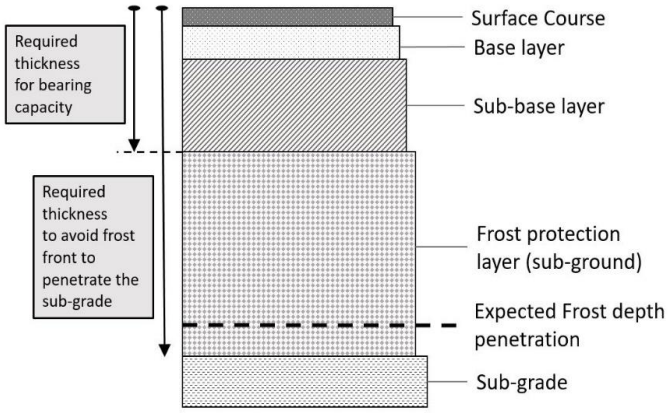

Figure 4: Typical Norwegian road structure designed for main roads built on a frost-susceptible subgrade

When considering the secondary roads, accounting for 70% of the country's road network, the design is based on limiting differential frost heave, but without calculating frost heaving magnitude. The design is therefore based on engineering judgment, and would be prone to vary at different degree according to

the designer experience. It is known that frost heave affect to variable degree those infrastructures, but no allowed frost heave limits nor any frost heave magnitude estimation methods are presently integrated to frost protection design in those cases.

Table 2 resumes the different road class according to the mean average daily traffic (ADT), number of lanes, sub-grade soil's group, statistical period of return of the design freezing index, FI (noted F_{10} and F_{100} for 10 and 100 years period of return) and the allowed maximum infrastructure total thickness.

Table 2: Norway frost protection design chart (modified from Handbook N200, 2018)

ADT	Lanes	Sub-grade Soil's group	FI period of return	Structure maximum thickness (m) [1)]
> 8000	≥ 4	T3, T4	F_{100}	2.4
> 8000	< 4	T3, T4	F_{10}	2.4
1501-8000		T3, T4	F_{10}	1.8
≤ 1500		T3, T4	Measures to prevent differential frost heave to be assessed [2)]	1.8

[1)] The term 'maximum' in this context means that the specified thickness is normally sufficient to avoid unacceptable frost heave, although the frost depth is greater than maximum structure thickness.

[2)] Measures to prevent differential frost heave should be based be based on the F_{10} frost index return period.

Maximum layer thickness were decided empirically, mainly to avoid creep and deformation of the natural sub-grade but also for economical considerations. The freezing indexes for the whole of Norway can be found online at http://www.vegvesen.no/kart/visning/frostsonekart. This is believed to be a serious improvement to climatic data accessibility and precision compared to the table format in Handbook N200 (2014).

A frequent way of estimating frost depth from road authorities is to use a modification of Stefan's equation, to include heat capacity. Equation 1 shows the modified Stefan's solution that adds sensible heat to the latent heat factor (ISO-13793). The total amount of sensible heat in the frozen layer is obtained by multiplying the volumetric heat capacity by the mean annual air temperature (T_m). The depth to which sensible heat is considered varies from designer to designer; one to two meters being regularly used. The cooling effect decreases linearly downwards from the freezing front to the selected depth.

Equation 1

$$FD = \sqrt{\frac{7200 \cdot FI_s \cdot \lambda_f}{L + C \cdot T_m}}$$

where FI_s is the surface freezing index (°C·h), λ_f is the thermal conductivity of the frozen ground (W/(m·°C)), L is the latent heat of water in the soil ($L_w \cdot w_{vol}$ = J/m^3), C is the specific heat capacity of unfrozen ground (J/(m^3·°C)) and T_m is mean air annual temperature (°C).

It is possible to calculate the necessary FI for the frost front to penetrate a depth h in layer *i* (FI_i) in a multi-layered system from the integration of the modified Stefan's solution for a multi-layered system (Nordal, 1989).

Equation 2

$$FI_i = f \cdot L_i \cdot h_i \cdot \left(\frac{h_1}{\lambda_1} + \frac{h_2}{\lambda_2} + \cdots + \frac{h_{i-1}}{\lambda_{i-1}} + \frac{h_i}{2\lambda_i}\right)$$

where FI_i is the freezing index necessary for the frost front to reach h_i in layer i, i is the number of layers considered, f is a conversion factor from MJ to W·h (1 MJ = 277.78 W·h), L_i is the soil's latent heat in layer i (MJ/m^3), h_i is the frozen thickness of layer i (m), and h_i/λ_i is the thermal resistance of layer i (°C/W). Total estimated frost penetration is calculated from the sum of the contributive FI_s for each layer.

4. THEORY AND APPLICATION

The relevant literature and concept found on segregation potential and on the SSR model used for this study are presented in this section. Frost heave according to the segregation potential of crushed rock aggregates is presented in section 4.1 and the SSR model is presented in section 4.2.

4.1 Frost heave and segregation potential

Frost heave is the uplifting of the ground surface due to ice formation. Three conditions are necessary for frost heave to occur: a sub-freezing temperature, access to water, and a frost susceptible soil (Chamberlain, 1981; Konrad, 1999). The frost susceptibility of a soil refers to its ability to form ice lenses. Chamberlain (1981) states that more than a hundred methods for evaluating soil frost susceptibility were proposed between 1929 and 1981. Most are based on grain-size, but only a few allow the estimation of expected heave. This thesis does not describe all theories and methods for determining frost heave but to focus on the frost susceptibility of crushed rock using the segregation potential.

The theory of segregation potential was first developed to find a way of including frost heave magnitude in pipeline design in discontinuous permafrost areas, as a solution to both the imprecision of empirical methods and the complexity of fundamental thermodynamic analysis (Konrad, 1980).

Empirical methods require long-term observation and are mostly site-specific, making their application to other sites difficult (Konrad, 1980). As an example of empirical methodology, Kivikoski (1983, cited by Saarelainen, 1992) relates frost heave to frost penetration at test sites in Finland over a 30-year period. Figure 5 presents the relationship developed using only the square root of the freezing index with fit parameters. The test site was a partially paved road maintenance yard with ca 25 cm of gravel on top of a sandy silt. The site was followed from 1959 to 1982 to develop the empirical relations. The average values (ave) and ±5 % interval confidence (5% and 95%) of the magnitude of heave (h) and frost penetration (z_f) are presented. Different road administration used this empirical relationship (i.e. $z_f = a\sqrt{FI} \pm b$) to estimate frost depth in typical road structures (Stenberg, 1994).

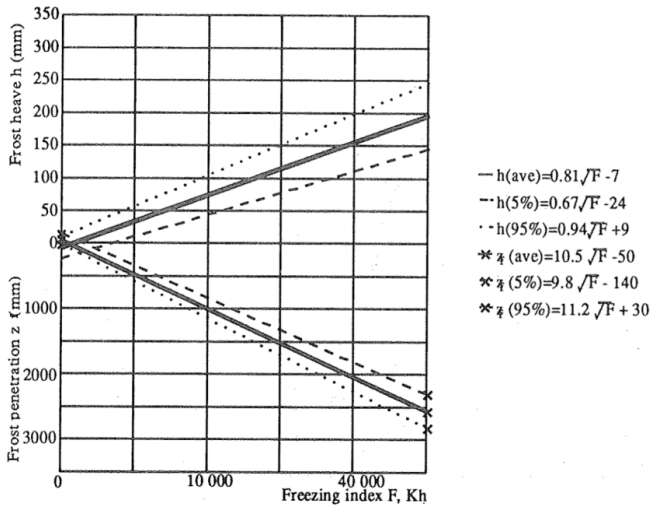

Figure 5: Empirical relation between frost heave and frost penetration in function of the freezing index developed at the Piipola test site in Finland from 1959 to 1982 (Kikovski, 1983)

Sætersdal in the frost I jord (frost actions in soils) research project (1976) proposed an empirical methodology to estimate frost heave magnitude.

Equation 3

$$h = \beta \cdot \frac{\Delta FI}{93000 \cdot \sum \frac{z_i}{\lambda_i}}$$

where h is the heave (m), β is the frost heave factor developed by Sætersdal (ibid), ΔFI is the freezing index contribution from when it reaches a frost susceptible underlying subgrade (°C·h), $\sum \frac{z_i}{\lambda_i}$ is the sum of the thermal resistivity of the non-frost susceptible layers above the subgrade (m^2·°C), z_i is the thickness of layer i (m) and λ_i is the frozen thermal conductivity of layer i (W·m/°C). β has values from 0.1 to 0.7 for less to more frost susceptible soil. At my knowledge, this methodology does not appear to be frequently use nowadays due to the complexity of determining the ΔFI and particularly the β with precision. The frost heave factor was investigated on a great number of test roads by the Swedish National Road and Transport Research Institute and integrated in their early design (Stenberg, 1994).

All criteria based on grain size for determining frost heave magnitude have proven imprecise for the purpose, and are therefore mainly used for qualitative classification (Chamberlain, 1981).

Fundamental thermodynamic analysis requires accurate measurement of unfrozen water content and the hydraulic conductivity of the partially frozen zone (frozen fringe) and unfrozen water content, all of which are difficult to measure precisely in practice and are costly and time-consuming to perform (Konrad, 1980). Some models include the chemical potential of water and the system's entropy , osmotic pressure and enthalpy, as in the model developed by Loch (1978) using the Gibbs-Duhem equation. These parameters

are not practically measurable for engineering application. The large amount of data required by certain models makes them hard to use for engineering purposes, often leading to the application of default values for unknown parameters, raising the uncertainty of the output.

Konrad (1980) observed that for the same soil, the velocity of water intake rose linearly compared to the thermal gradient applied during a frost heave test, as shown in Figure 6 for the Devon silt.

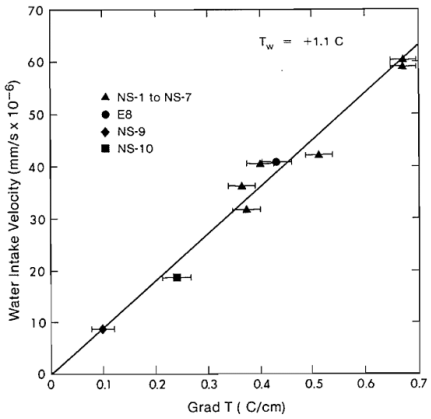

Figure 6: Relation between water intake velocity and temperature gradient at the beginning of the steady state regime (Konrad, 1980)

Figure 7 presents the temperature, hydraulic conductivity and suction profile in the frozen fringe.

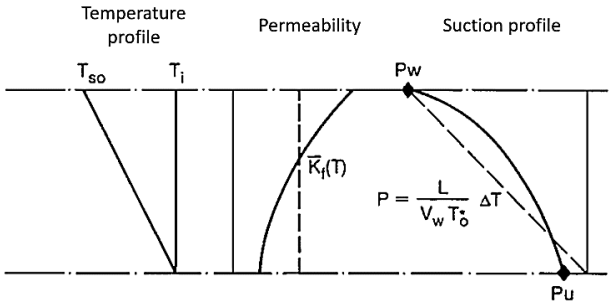

Figure 7: Temperature profile, permeability (inverse of hydraulic conductivity) and suction profile at the beginning of the steady state in the frozen fringe (modified from Konrad and Morgenstern, 1981). The doted lines present the simplified relation for hydraulic conductivity and suction used in the segregation potential theory

The segregation potential (SP) is defined as a relationship between water intake velocity and thermal gradient at the beginning of the steady state (Konrad and Morgenstern, 1981). When no overburden pressure is applied, the segregation potential is express as SP_0:

Equation 4

$$SP_0 = {}^{V}/_{\nabla T}$$

where ∇T is the temperature gradient (°C/mm) in the frozen fringe, v is the water intake velocity (mm/d) at thermal steady state. The SP_0 is therefore expressed in mm²/°C·day. Some works also express SP in mm²/°C·h, or mm²/°C·s. In this text I use SP or SP_0, which are to be considered equal when the overburden pressure = 0, as explained further below.

The SP merges the suction profile and the mean hydraulic conductivity of the frozen fringe, therefore simplifying the parameters needed for more complex models. The complete development of the equation can be consulted in Konrad (1980) and Konrad and Morgenstern (1980, 1981) and is summarized in Equation 5 from Konrad 1994.

Equation 5

$$v = \frac{P_w - P_u}{d} K_f = \left(\frac{P_w - P_u}{T_s} K_f\right) \nabla T = SP \cdot \nabla T$$

where P_w is the suction pressure at the base of the ice lens, P_u is the suction pressure at the frost front, d is the fringe thickness at the beginning of the steady state's start time, T_s is the segregation freezing temperature and K_f is the mean permeability of the frozen fringe.

Segregation potential theory allowed estimation of heave magnitude in the field (Konrad and Morgenstern, 1982a). The proposed relation is expressed in Equation 6.

Equation 6

$$h = 1.09 \cdot \sum SP \cdot \nabla T_{-} \cdot dt$$

where h is the segregational heave, ∇T_{-} is the thermal gradient in the frozen soil and dt is the duration of the freezing period. In field estimation the SP for field have to be corrected for overburden pressure. The SP according to overburden pressure is obtained from Konrad and Morgenstern (1982b):

Equation 7

$$SP = SP_0 e^{-\sigma a}$$

where SP is the segregation potential (mm²/°C·h) accommodated for overburden pressure, SP_0 is the segregation potential without any overburden pressure, σ is the overburden pressure (MPa), and 'a' is a parameter of soil sensitivity to overburden pressure (MPa^{-1}). The 'a' parameter can be estimated with the percentage of clay particles <2 μm using Figure 8 (Knutsson et al. 1985).

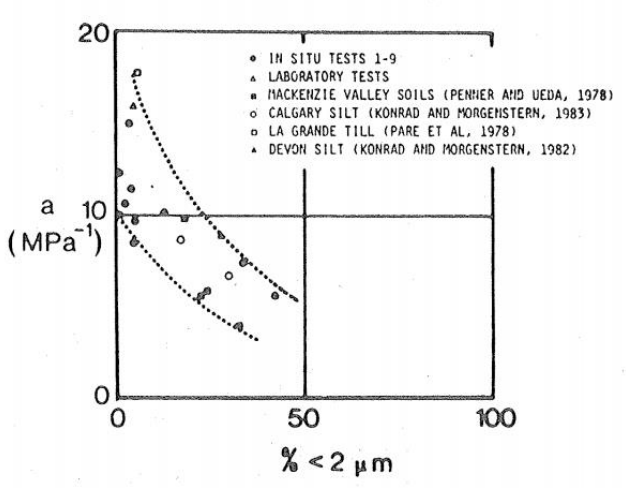

Figure 8: Sensitivity to overburden pressure parameter 'a' in function clay particle % (Knutsson et al., 1985)

Other methods of calculating a soil's sensitivity to overburden pressure 'a' can be found in Konrad (2005) where it is related to the mean particle diameter in the fine fraction < 80 µm (d_{50ff}).

Equation 8

$$a = 5(d_{50ff})^{0.45}$$

4.1.1 Factors influencing the segregation potential

According to Konrad (1999), the key parameters that govern a material's frost susceptibility are its particle size distribution, mineralogy, texture and overburden pressure. The particle size distribution is important because it dictate the critical fine content at which the coarse pore fraction are filled with fine fraction. A coarse matrix soil with the coarse pore fraction filled with fines is more frost susceptible than one not, or partially filled with fines (Bilodeau, 2009). The mineralogy of the fines content is known to affect the susceptibility to frost. Brandl (2008) enumerates the mineralogy criteria used in Austria, which does not correlate directly with the segregation potential. In general mineralogy and texture affect unfrozen water content, dry density and porosity, which are very important in the hydraulic conductivity of the frozen fringe during freezing (Konrad, 1999). The overburden pressure has the effect of lowering the freezing segregation temperature of a soil, decreasing its frost susceptibility. In general clay has low and sand high sensibility to overburden pressure.

Figure 9 presents the structure profile of a typical Canadian road, typically built with ca 20-30 cm of a 0-20 mm graded base layer and ca 50-60 cm of sand as a filter layer noted subbase. This type of structure is common around the world. The figure presents the water content and pore pressure profiles according to depth and water level.

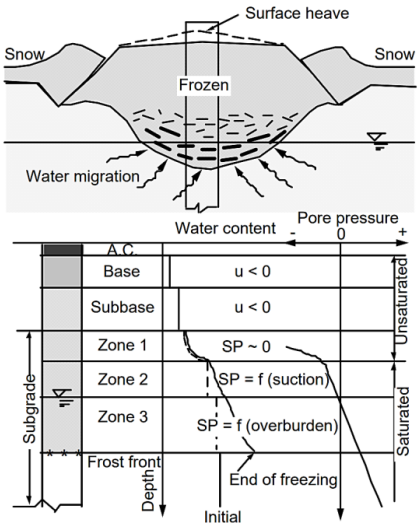

Figure 9: Suction and water content profile according to water table and frost depth in a typical Canadian road structure (Konrad, 2014)

As the figure shows, SP will be ≈ 0 at the limit of the capillary rise of the soil, will be in function of the suction above the water table level and in function of the overburden pressure below the water table level. The suction was investigated by Konrad and Morgenstern (1982a) in Devon silt (Figure 10).

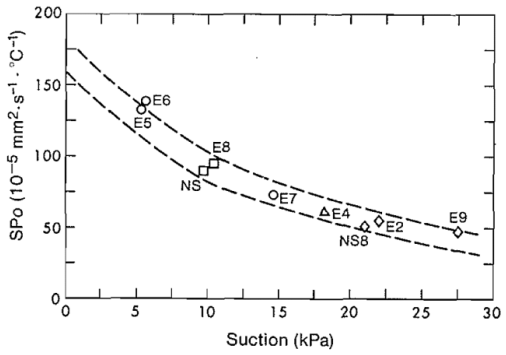

Figure 10: Segregation potential in function of suction at the frost front in Devon silt (Konrad and Morgenstern, 1981)

According to Konrad and Morgenstern (1981), the suction at the frost front,ΔP, can be estimated by applying Darcy's law to unfrozen soil only, using Equation 9.

Equation 9

$$\Delta P = |P_u - P_b| = \frac{v \cdot l_u}{K_u}$$

where P_u is suction pressure at the frost front, P_b is suction pressure at the bottom of the unfrozen soil sample, v is water flux, l_u is the length of unfrozen soil sample and K_u is the permeability of the unfrozen soil.

The rate of cooling also has a direct effect on the segregation potential, as described in Konrad (1980) and Konrad and Morgenstern (1982a), who plot segregation potential, suction pressure and rate of cooling to create the frost heave envelope for Devon silt in Figure 11.

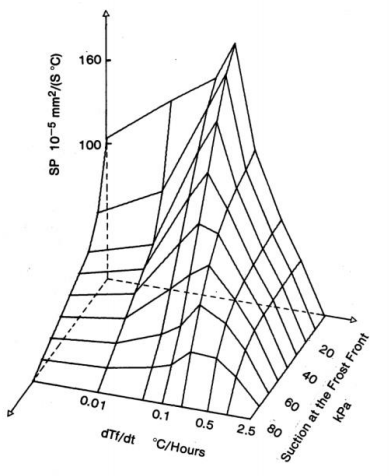

Figure 11: Segregation potential in function of suction at the frost front and rate of cooling in Devon silt (Konrad, 1980)

It is therefore important that the segregation potential is a 3D envelope, and not a single 2D relation. For engineering purposes, the laboratory test therefore limits the suction at the frost front by putting the 0°C isotherm near the base of the sample at a relatively low rate of cooling. The 2D interpretation have then its limitation, as discussed by Nixon (1991). The rate of cooling should represent that expected in the field to determine representative segregation potential from a frost heave test (Konrad 1994).

Konrad (1999) has empirically estimated segregation potential using soil index properties, based mainly on the work of Rieke (1983). An empirical relationship was developed using the specific surface and d_{50ff} and validated for highly frost susceptible till. The $d50_{ff}$ is the 50% passing fraction in mass, measured on the <80 µm fraction. Konrad found that the shape and mineralogy of the fines content influenced the unfrozen water content in the frozen fringe. Konrad (1999) explained that unfrozen water content can be categorised as capillary (or pore) water and adsorbed water. Capillary water can move easily in the soil pores and adsorbed water cannot. The adsorbed water was found to be proportional to the specific surface area. An empirical relationship between d_{50ff} and capillary water (inversely related to the specific surface area (Ss)) for clay-fines related soils was developed at a water content ratio over liquid limit (w/w_L) ≈ 0.7. This relationship was developed for all types of soil and geomaterials and is presented in the segregation potential and crushed rock aggregates section of Konrad's 2005 study.

4.1.2 Segregation potential of crushed rock aggregates

The frost susceptibility of clean and free draining crushed rock aggregates ranges from negligible to low (FHA, 2017). A relatively high fines content, however, can make crushed rock aggregate frost-susceptible. The definition of fine material varies from < 80 µm in Canada to < 75 µm in the US and < 63 µm in Europe. The maximum fines content possible to limit frost susceptibility to a 'low' or 'low to medium' Cold Region Research Laboratory (CRREL) category ranges from ca 8-12% for a 0-20 mm crushed rock aggregate (Chamberlain, 1981). A fines content of <20 µm is often included in grain-based criterion as developed by Casagrande (1931, cited by Chamberlain, 1981). The fine content that is allowed in materials by different transportation administrations varies significantly (Chamberlain, 1981). Some agencies that use grain-size based criteria combine this with other restrictions such as plasticity index (e.g. CRREL, 1981), capillarity (e.g. Finnish Transport Infrastructure Agency), and mineralogy (e.g. Austrian Federal Road Administration) criteria. Figure 12 presents segregation potential as a function of % passing 0.02 mm (20 µm), adapted by the Quebec Ministry of Transport (MTQ) from the frost susceptibility classification chart of the US Army Corps of Engineers, Cold Region Research Laboratory (CRREL, 1981). The soil/aggregate taxonomy is based on the United Soil Classification System (USCS). Figure 12 illustrates the variability of the average segregation potential of coarser aggregates. A well-graded gravel (GW) with 2% passing 0.02 mm can therefore be characterized as having a frost susceptibility varying between negligible and medium, which does not provide sufficient accuracy for high-class road projects.

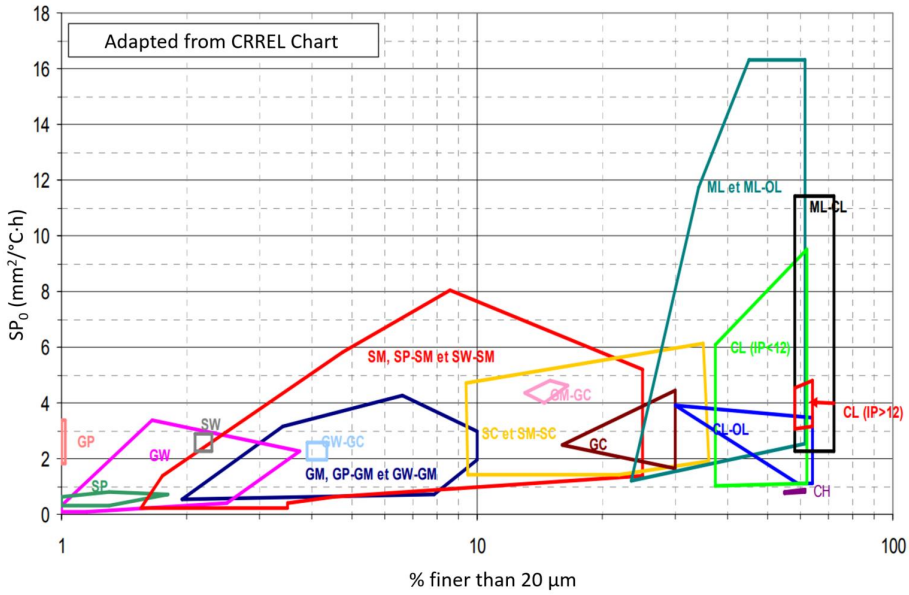

Figure 12: SP_0 in function of % passing 20 µm, and according to USCS soils taxonomy, adapted from the 1981 CRREL Chart (modified from St-Laurent, 2006)

Basing frost susceptibility calculation on grain-size therefore has flaws as with a given fines content it can vary significantly and the heave rate is difficult to transpose to specific field conditions. It can be concluded that trying to estimate the magnitude of heave using soil classification and fines content of < 75 or 20 µm, could lead to significant errors.

Most of segregation potential development was done for subgrade soils, as silt and clay are the most frost susceptible soils. The main studies on the segregation potential of crushed rock aggregates are Konrad (2005), Konrad and Lemieux (2005), Nurmikolu (2005), Konrad (2008) and Bilodeau (2009). The main direction and findings of their work are presented in the next paragraphs.

Konrad (2005) tested the < 80 µm fraction of basalt, dolostone, granite, limestone, quartzite and greywacke and determined that the SP of crushed rock aggregate fines ranges from medium to very high, with associated SP of 84-310 $mm^2/°C \cdot d$. Tests by Rieke (1983) were used to develop a normalized SP, allowing the estimation of SP_0 for clay fines and non-clay fines granular materials. Normalized SP involved the estimation of empirical $SP_{0\ ref}$ and Ss_{ref}. Normalized SP (i.e. $SP_0/SP_{0\ ref}$) has a linear relationship with Ss/Ss_{ref} when non-clay fines drive the frost heave response ($Ss/Ss_{ref} < 1$), and an exponential relationship when driven by clay fines ($Ss/Ss_{ref} > 1$). The relationship takes different forms depending on the w/w_L ratio (equations 10 to 13).

- If $Ss/Ss_{ref} < 1$ (non-clay mineralogy dominance in frost heave behaviour)

for $w/w_L = 0.7 \pm 0.1$ → $$SP_{0.n} = SP_{0\,ref} \cdot {Ss}/{Ss_{ref}}$$ *Equation 10*

for $w/w_L > 0.8$ → $$SP_{0.n} = SP_{0\,ref} \cdot \left(0.08 + 1.42\left({Ss}/{Ss_{ref}}\right)\right)$$ *Equation 11*

- If $Ss/Ss_{ref} > 1$ (clay mineralogy dominance in frost heave behaviour)

for $w/w_L = 0.7 \pm 0.1$ → $$SP_{0.n} = SP_{0\,ref} \cdot \left({Ss}/{Ss_{ref}}\right)^{-0.85}$$ *Equation 12*

for $w/w_L > 0.8$ → $$SP_{0.n} = SP_{0\,ref} \cdot 1.5\left({Ss}/{Ss_{ref}}\right)^{-0.55}$$ *Equation 13*

It was shown that crushed rock aggregates follow the relationship of $Ss/Ss_{ref} < 1$ and $w/wL > 0.8$, as shown by the results for "fines Qc" (representing the crushed rock aggregates studied by Konrad in 2005), in Figure 13.

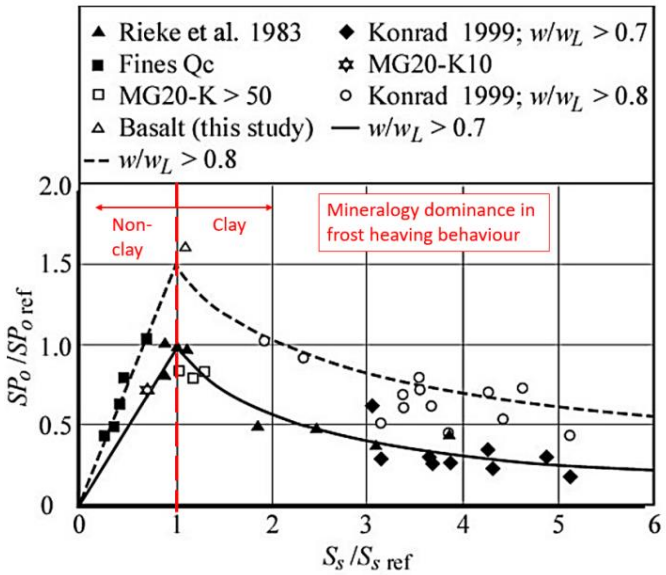

Figure 13: Normalized segregation potential as a function of normalized specific surface area. Fines Qc and basalt are crushed rock aggregates (modified from Konrad, 2005).

The equation 10 to 13 established a relationship between Ss and SP. Ss had an effect on the unfrozen water content, dimension and tortuosity of water channels (Konrad, 2005; Bilodeau, 2009). Frost susceptibility increases with increasing Ss in aggregates with a relatively small fine content. When Ss reaches a higher value the increased volume of adsorbed water in the material matrix has the effect of reducing the water channel dimensions (and increasing tortuosity, described in Konrad, 1999), resulting in a reduction of the hydraulic conductivity of the frozen fringe and therefore also of frost susceptibility.

Konrad and Lemieux (2005) studied the effect of different fines % in 0-20 mm graded crushed rock aggregates (base material).They tested different percentages (5, 10 and 15% of < 80 µm) of granitic fines in a 0-20 mm fraction, varying the percentage of the clay content (10, 50, 75 and 100% of kaolinite) in the fines. They demonstrated that segregation potential can be medium to high even at a low percentage of fines. A set of graphs showing the relationship between frost heave rate and thermal gradient for 5, 10 and 15% fines containing 10, 50 and 75% of kaolinite clay were produced from their work. The segregation potential according to the same 5 variation of fines and kaolinite clay were also presented. Frost heave rates and segregation potential were proven to increase with an increasing percentage of fines. Frost heave rates and segregation potential also increased with the increasing proportion of kaolinite clay in the granitic fines fraction. Figure 14 present an example showing the heaving rate according to thermal gradient for a crushed rock with fine content of 5 percent in which the percentage of kaolinite clay varied from 10 to 75 percent.

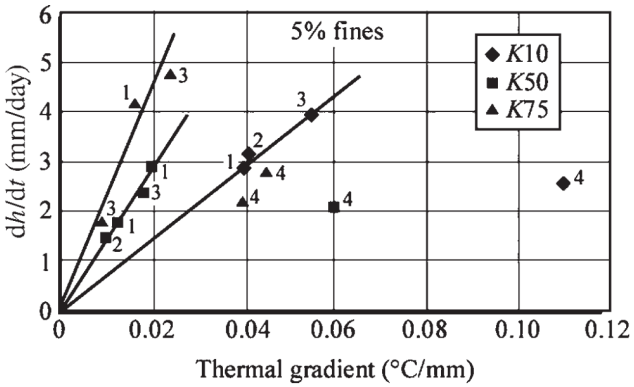

Figure 14: Frost heave rate according to temperature gradient for a 0-20 mm graded crushed rock base that contain 5% of granitic fines and a proportion of kaolinite clay in the 5% fines of 10, 50 and 100%, defined by K10, K50 and K100. Numbers 1 to 4 are the freeze run numbers (Konrad and Lemieux, 2005)

Nurmikolu (2005) studied 132 frost heave tests on 0-31.5 mm graded ballast of different crushed rock aggregates used in railway infrastructures. Most of the aggregates were gathered in situ in order to estimate the effect of long-term ballast degradation. Some of the tests were performed on new crushed rock aggregates. Different rock types including mainly granite but also granodiorite, mica-schist, mica-gneiss, talc pyroxenite and cordierite-mica gneiss were tested. Nurmikolu used the frost heave coefficient, which is the same as segregation potential, for his analysis. The fine contents <63 µm of the tested aggregates were mainly between 5 and 6%. His results showed different SP values, mainly from ca 24-40 $mm^2/°C·d$ for fines content of 5-6%. One typical frost heave test as analysed in Finland is presented in Figure 15. The SP is determined when the frost heave coefficient stabilizes during the frost heave test, here being about 1.3 $mm^2/K·h$ (≈31 $mm^2/°C·h$).

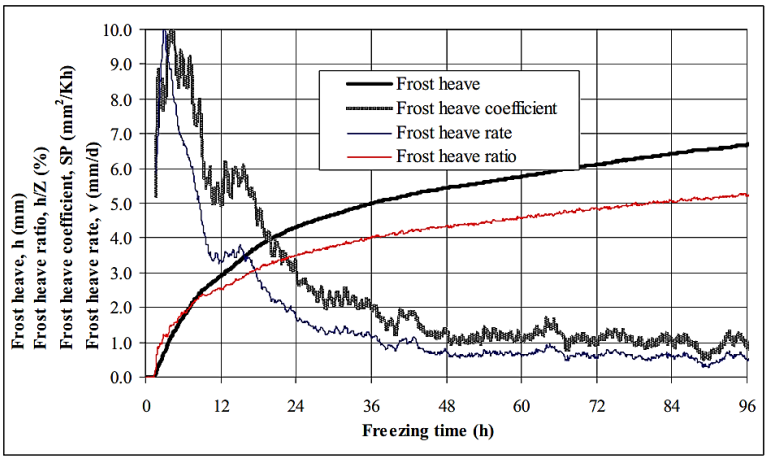

Figure 15: Frost heave test interpretation of a 0-31.5 mm ballast material with ~ 5% of fines <63 µm (Nurmikolu, 2005)

Konrad (2008) performed ramped-freezing tests on three base granular materials (0-20 mm) with a < 80 µm fines content of up to 7%, and degrees of saturation near 60%. A gneiss with biotite, a limestone and a monzonite were tested. The measured SPs were ca 20 $mm^2/°C·d$, which are classified as low. Konrad observes that water drawn to the freezing front during the frost heave test must be considered when analysing the behaviour of the material to frost action. In other words, not all of the water entering the system turned to ice, leading to a significant rise in the water content of the unfrozen part and a decrease in the dry density of the material. The water drawn and the rate of cooling effect can be expressed using a modified segregation potential, SP_w. Konrad suggests that the normalized segregation potential method can be applied to determine the SP_0 of a granular base material.

Bilodeau (2009) performed frost heave tests on three 0-5 mm graded rock types: a limestone, a basalt and a gneiss, each with six different pre-established particle size distributions, making a total of 18 tests. He tested fine content percentages of (<80 µm) of 2, 4.5 and 7%, measuring their segregation potential under a 7 kPa overburden pressure in all tests (SP_{7kPa}). The gneiss in general showed a very low segregation potential, the limestone a low segregation potential and the basalt a low to medium segregation potential. He developed a relationship linking the segregation potential to a statistical complex variable named ϒ, which is function of the curvature index of the fines (C_uF), the specific surface area of the fines (S_sF) and the porosity of the fine fraction (n_f). Figure 16 shows the relation between SP and ϒ. This relationship was developed to estimate the segregation potential of crushed rock aggregates with low fines content.

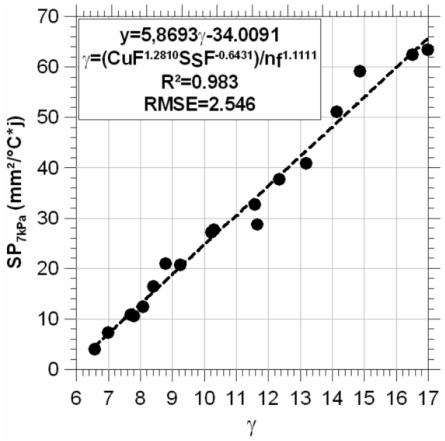

Figure 16: Relationship between SP and ϒ (Bilodeau, 2009)

A relationship exist between fine fraction porosity (n_f) and coarse fraction porosity (n_c). The segregation potential of a granular material will be maximal when the n_c is entirely filled by the fine fraction, and will be lower when the n_c is partially filled with the fine fraction. Konrad (1999) estimated that the coarse fraction porosity is filled when having a fine content (<75 µm) of ca 15% and more. The n_f reflects the water flow tortuosity in pore channels and was thoroughly described by Côté and Konrad (2003). Fine fraction porosity was defined by Côté and Konrad (2003) using Equation 14.

Equation 14

$$n_f = {}^{n}/_{(n+(1-n)\cdot fines\ \%)} = {}^{(n_c - fines\ \%)}/_{(n_c(1-fines\ \%))}$$

where n_f is the fine fraction porosity (< 80 µm), n is the porosity, n_c is the coarse fraction porosity (> 80 µm) and $fines\ \%$ is the fine particles content (< 80 µm). A lower fine fraction porosity will lead to higher tortuosity of the flow channels to the segregation front, for materials with a relatively low amount of fines %. as demonstrated by Konrad (2005) and shown in Figure 13.

4.2 SSR Model theory

The Seppo Saarelainen Routanousu (SSR) model was developed in 1992 in Finland with the intention of calculating frost depth and resulting frost heave to an acceptable degree of accuracy (Saarelainen, 1992). The model is based on the heat flux balance at the frost front in frost-susceptible soils, and can be expressed, with all heat flow parameters in the equation in W/m^2, as:

Equation 15

$$q_- = q_+ + q_f + q_s$$

where $q_- = \lambda_f \nabla T_-$ is the heat flow through the frozen layers, $q_+ = \lambda_f \nabla T_+$ is the heat flow to the freezing front coming from the unfrozen layers underneath, q_f is the heat flow released by pore water freezing, q_s is the heat flow released by ice segregation (water flow drawn by cryosuction effect). Figure 17 presents the schematic of the parameters included in the SSR model.

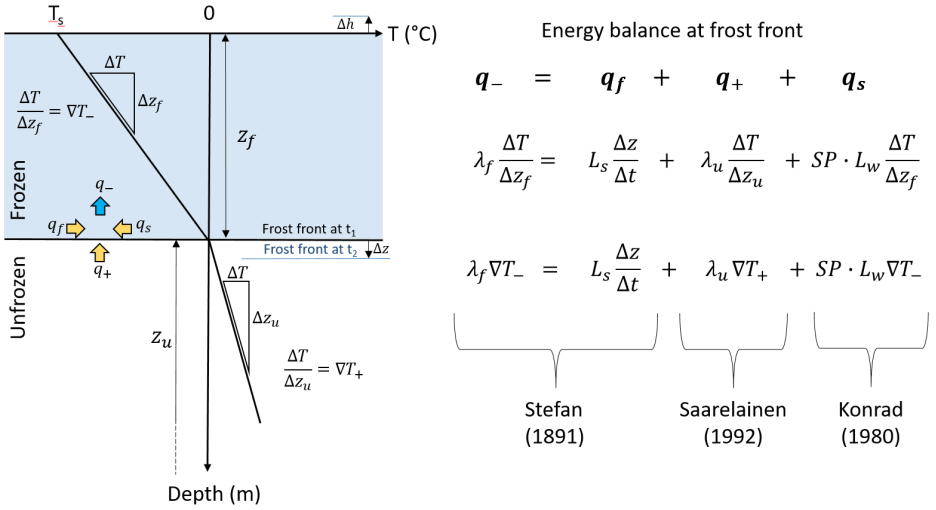

Figure 17: Heat balance equation at the frost front with associated parameters (modified from Côté and Konrad, 2009)

The left part of Figure 17 represents an idealized temperature distribution used to determine the heat flux balance at the frost front, while the right part of the figure represents the development of the heat flux balance equation using soil and material parameters. The equation's first term (q_f) comes from the solution developed by Stefan in 1891 and considers the release of latent heat into the conductive heat flux in the frozen layer. The second term (q_+) is the conductive heat flux from the underlying unfrozen ground introduced by Saarelainen for the SSR model based on an empirical relationship between mean annual air temperature and thermal gradient developed by Skaven-Haug (1971). Finally, the heat flux from the release of latent heat produced by segregational ice formation (q_s) was modelled using Konrad and Morgenstern's (1981) segregation potential theory. Therefore the equation can be developed as:

Equation 16

$$\lambda_f \nabla T_- = \lambda_u \nabla T_+ + L_s \frac{\Delta z}{\Delta t} + L_w v$$

where the rate of water flow to the freezing front is modeled using the segregation potential theory

Equation 17

$$v = dv/dt = SP\ \nabla T_-$$

where λ_f is the thermal conductivity of the frozen layers (W/°C·m), ∇T_- is the thermal gradient in the frozen layers (°C/m), λ_u is the thermal conductivity of the unfrozen layers (W/°C·m), ∇T_+ is the thermal gradient in the unfrozen layers (°C/m), L_s is the volumetric latent heat of soil fusion at the freezing front (W·h/ m^3), L_w is the volumetric latent heat of water fusion (W·h/ m^3), Δz is the increase in frost penetration during the time increment (m), Δt is the time increment (h), v is the water flow rate (dv/dt) induced by ice segregation (m/h) and SP is the soil's segregation potential at the freezing front (m^2/°C·h), also called the frost heave coefficient in the Finnish literature (Saarelainen et al., 2015).

When adapted to a multi-layered system, as much transportation infrastructure is, Equation 16 can be re-written as:

Equation 18

$$\lambda_f \frac{(T_f - T_s)}{z^*} = \lambda_u \nabla T_+ + L_s \frac{\Delta z}{\Delta t} + L_w\ SP\ \frac{(T_f - T_s)}{z^*}$$

where T_f is the freezing temperature of soil (°C), T_s is the average surface temperature during period of time dt (°C), $z^* = \lambda_{fz} \sum(z_i/\lambda_{fi}) + 0.5\ \Delta z$, where λ_{fz} is the average thermal conductivity of the frozen layers, when reaching half of the calculated penetration during the increment time, dt. Figure 4 shows details of the development of z^*, expressed as:

Equation 19

$$\lambda_{fz} = \frac{z + \frac{\Delta z}{2}}{\frac{z}{\lambda_z} + \frac{\Delta z}{2\lambda_{\Delta z}}} \rightarrow \lambda_{fz} = \frac{z + \frac{\Delta z}{2}}{\sum(z_i/\lambda_{fi})} \rightarrow \lambda_{fz} \sum(z_i/\lambda_{fi}) - \frac{\Delta z}{2} = z$$

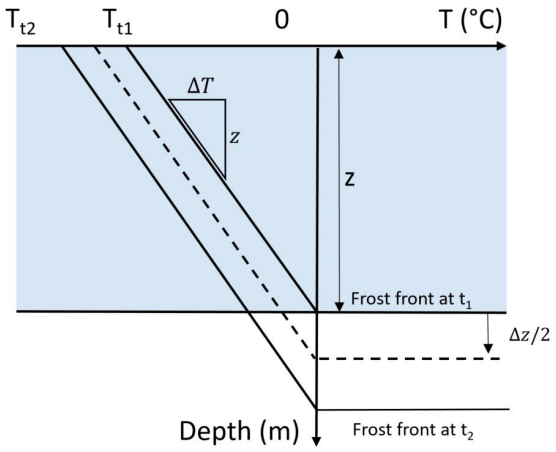

Figure 18: Computation of average thermal conductivity details

where $z^* = z + \Delta z$, $L_s = L_w \cdot w\left(\rho_d/\rho_s\right)$, w is the gravimetric water content ($w = M_w/M_s$), L_w is the volumetric latent heat of water fusion ($333 \cdot 10^3\ {}^{kJ}/_{m^3} = 92.5 \cdot 10^3\ {}^{W \cdot h}/_{m^3}$), $\Delta z/\Delta t$ is the rate of frost penetration (m/h). $SP = SP_0\ e^{-a\sigma}$ where SP_0 is the segregation potential without overburden pressure, σ is the overburden pressure at the freezing front (MPa) and a is the overburden sensitivity of the soil (MPa^{-1}). SP is expressed in $mm^2/°C \cdot h$.

To compute the frost penetration increment Δz at each time step in Equation 5, the Saarelainen iterative solution (1992) is presented as Equation 20:

Equation 20

$$\Delta z = (T_f - T_s)dt\frac{(1 - SP \cdot L_w/\lambda_{fz})}{(L_{fz} \cdot \sum(z_i/\lambda_{fi}))} - \frac{S \cdot \nabla T_+ \cdot \lambda_{uz}\ dt}{L_{fz}}$$

where Δz is the increase in frost penetration during the time increment (m), $(T_f - T_s)dt$ is the freezing index, FI (°C·h), which equals $T_s dt$ when T_f is approximated as 0°C, SP is the segregation potential of the soil at the freezing front under actual overburden stress ($m^2/°C \cdot h$), λ_{fz} is thermal conductivity near the freezing front (W/°C·m), L_{fz} is the volumetric latent heat of the fusion of soil at the freezing front ($W \cdot h/\ m^3$) and $\sum(z_i/\lambda_{fi})$ is the sum of all frozen layers thermal resistance, in $m^2.°C/W$, z_i and λ_{fi} being the thickness of frozen layer i (m) and the thermal conductivity of frozen layer i (W/°C·m) respectively. Note that Δz is also present in the following expression (in **bold**), making this solution iterative.

Equation 21

$$\sum(z_i/\lambda_{fi}) = R_{fz} = \frac{z_1 + z_2 + \cdots + \mathbf{\Delta z}}{\lambda_1 + \lambda_2 + \cdots + 2\lambda_{fz}}$$

where S is a coefficient describing the intensity of heat flow from the ground, with $S = 1$ in November to $S = 0.7$ in April, ∇T_+ is the temperature gradient of unfrozen ground at the freezing front (°C/m) and λ_{uz} is the thermal conductivity of the unfrozen soil at the freezing front (W/°C·m).

The magnitude of heave is computed using a two-time step, one step considering segregated ice using the SP and the other considering pore water freezing. The heave of the segregated ice is compiled at each time step, using the SP of the actual layer in the freezing process (Equation 22):

Equation 22

$$\Delta h_s = 1.09 \cdot [SP \cdot \nabla T_-]\, dt = 1.09 \cdot SP \cdot \frac{(T_f - T_s)dt}{(\lambda_{fz} \sum(z_i/\lambda_{fi}))}$$

where Δh is the increment in heave due to ice segregation (m). The expansion of pore water when freezing, $\Delta h_{p,}$ must be taken into account for soils whose degree of saturation exceeds 85-90% (Orlov et al., 1977, cited in Saarelainen, 1992). The heave from pore water expansion is computed using Equation 23:

Equation 23

$$\Delta h_p = 0.09 \cdot \Delta z \cdot w \cdot {}^{\rho_d}/_{\rho_w} = 0.09 \cdot \Delta z \cdot Sr \cdot n$$

where Sr and n are the degree of saturation and porosity respectively. The total amount of frost heave is computed as:

Equation 24

$$\Delta h = \Delta h_s + \Delta h_p$$

5. RESEARCH METHODOLOGY

Research methodology includes three sections that describe the laboratory work, the fieldwork and the modelling work executed during this research.

5.1 Laboratory

Frost heave tests were performed to measure the frost susceptibility of crushed rock aggregates. In parallel, the crushed rock aggregates were characterized to determine the relevant index parameters.

5.1.1 Frost heave test

A multi-ring frost heave cell was constructed at Laval University, Canada, and shipped to NTNU. The whole experimental setup had to use this kind of cell to determine the frost heave susceptibility of the different crushed rock aggregates tested, as described in section 5.1.3. The frost cell setup is presented in Figure 19. The frost heave tests were used for Paper I and Paper III results and analysis.

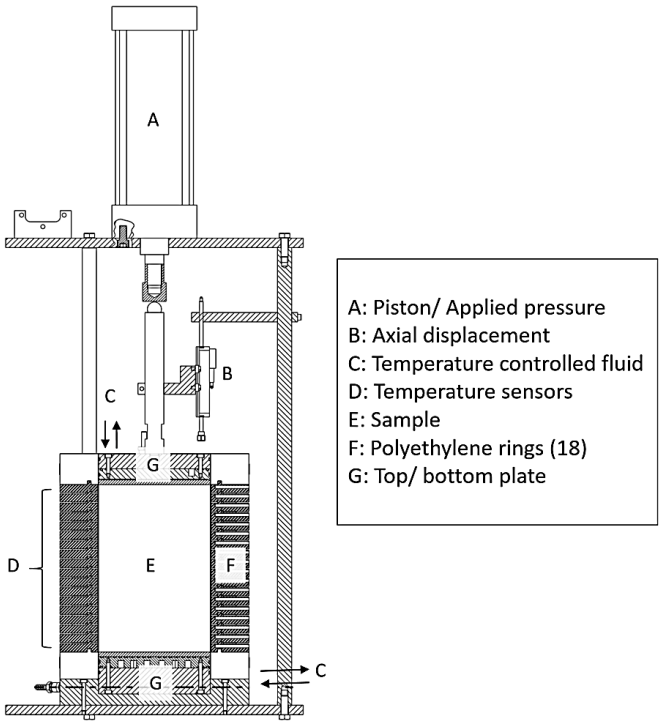

Figure 19: Multi-rings frost heave cell

The frost cell consists of 18 rings made of high-density polyethylene and with a 150 mm diameter, and accommodates sample heights of up to 200 mm (225 mm with rubber spacers between rings). Eighteen thermistors with a 0.1°C accuracy were inserted into each ring with the tip of each one secured with epoxy glue flush with the outside diameter side of the sample, to measure the temperature every 11.1 mm. The cell was insulated during the test to minimize radial heat transfer. The cell's 50 mm thick wall was rigid enough to resist radial pressure during ice formation. The sample was placed between two cooling plates from which the temperature was imposed using two cryostat units.

A rubber membrane was placed on the sample after being placed on the base plate. A split ring at the base was tightened with a steel collar to seal the membrane. Rings were inserted on the sample one by one and another split ring sealed the sample at the top. The multi-ring cell included an air piston, allowing pressure control during the test. No vertical pressure was imposed in this study. A potentiometer was used to measure heave with 0.01 mm precision. The water was free to flow inside the sample for the 24-hour conditioning phase, with water level placed 3-4 cm higher than the sample top. The water level was lowered at ca 0.5-1 cm upper than the base of the sample prior to the freezing phase. A glass recipient with a cork in which a glass tube had been inserted (a Marriotte's bottle) was used to create a constant pressure head at a chosen height, therefore allowing water to flow only via cryosuction.

The cell was placed in a fridge to further limit temperature variation during test, conditioning the sample at 2°C before starting the freezing. The freezing was applied from the top with a target temperature of -4°C. Samples were submitted to freezing for a 96-hour period. All the data were recorded at 5-minute intervals using a data acquisition system (18 temperature, heaving and water mass). The positions of the rings during the tests were measured using graduations on the frame, allowing thermistor height correction versus time for the segregation potential calculation.

The methodology for determining segregation potential is a graphical interpretation, as described in the Quebec Transport Administration (MTQ) LC-22.331 standard, based on the procedure described by Konrad (1987). It was adapted from the original version, which was developed for fine grained-soils (silt and clay), without a compaction phase (samples are placed in cells with relatively high water content followed by a consolidation phase) and uses a split-mold freezing cell type (with no height variation among the thermistors).

The principle of the method is to use both frost depth vs. time, and temperature profile graphs in order to discover the moment at which the temperature regime changes from a transient to a steady state. This moment defines the time at which the rate of heave and the temperature gradient in the frozen fringe can be considered for calculation, and indicates when the last ice lens in the sample begins to grow.

5.1.2 Soil index parameter

Different soil index parameters were measured for all crushed rock aggregates. The first reason was to estimate the fine particle size distribution in order to, first compare the Norwegian grain-size criterion and

second, assess the soil index parameters necessary to estimate the normalized segregation potential proposed by Konrad (2005). European/Norwegian (Handbook R210, 2015) and American (ASTM) standard were used for testing. The following characterization tests were performed on the different crushed rock aggregates:

i) particles size distribution by washing and coarse fraction sieving, i.e. >63 or 75 µm (Handbook R210 (131); ASTM C136)
ii) particles size distribution of the fine fraction using hydrometer analysis (Handbook R210 (214); ASTM D7928).
iii) particle density ρ_s (Handbook R210 (213); ASTM D854)
iv) liquid limit w_L (Handbook R210 (216))
v) Specific surface area of different fraction (<250, <125 and <75 µm) using Santamarina et al. (2002) which is a modified version of the ASTM C837
vi) Mineralogical composition using X-ray diffraction (Geology department, NTNU)

5.1.3 Materials

The crushed rock aggregate samples came from the Aplitt, Hadeland, Hellvik, Legruvbakken, Vassfjell, Lørenskog and Velde quarries in Norway and the PEB and Drapeau quarries in Canada. All crushed rock aggregates were tested using a multi-ring frost heave cell. The 0-4 mm fraction was primarily tested. The required fraction was obtained directly from the quarry or sieved down from a larger fraction, generally 0-16, 0-20 or 0-31.5 mm. Two series of Lørenskog and one of Vassfjell crushed rock aggregates were tested at different steps of the crushing process. For the Lørenskog sample this included two series of tests on the 0-4 mm fraction obtained from the first step of crushing, the cone crushing (3rd step) and the VSI crushing phase (4th step). The Vassfjell tests included a 0-4 mm fraction from blasted materials, subbus (a mixture from the 1st,2nd and 3rd crushing phases) and the 3rd crushing phase (from a cone crusher). Three fillers from the Velde quarry, coarse, intermediate and fine, from an air classifier, including the VSI Lørenskog aggregates for the coarser fraction (0.125-4 mm) and Velde for the finer fraction (0-0.125 mm), were used in a series of tests. A sample that used VSI Lørenskog with the same proportion of coarser and finer fractions as the Velde fillers was also produced.

5.2 Field test

5.2.1 Description of site

A full-scale test site was built in fall 2016 at 62°33’29.13’’N/ 11°19’31.26’’E, south-west of Røros, in the southernmost part of the Trøndelag region in central Norway (Figure 20). The field test was built contractors (crushed rock handling) and NTNU personnel (instrumentation installation and positioning).

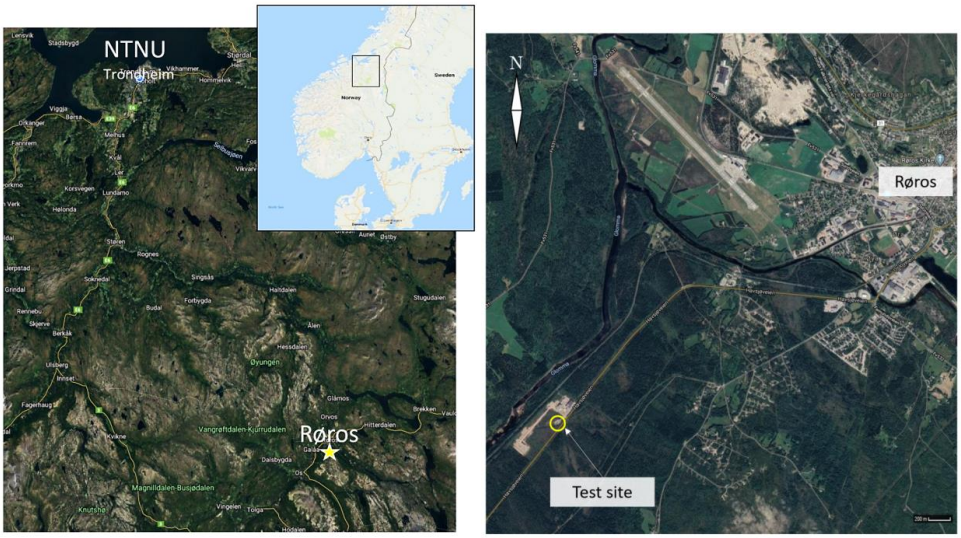

Figure 20: Røros location, Central Norway

The test site, built to measure the thermal response of different construction materials, is composed of six road sections and four railway sections, each 8 meters long by 6 meters wide (Figure 21). The site is beside the Rv30 road and experiences no vehicle traffic apart from snow removal maintenance in winter. This site was an important part of this investigation for comparing with our laboratory results and theoretical calculations on the different materials.

Our primary objective for all sections was to investigate frost penetration and consequent frost heave, if any. Road sections 1-3 were used to investigate different grading of the same rock type in the frost protection layer. The gradation were based on limits proposed in Handbook N200 (2014), therefore the grading were ranged from the finest grading allowed to an open-coarse grading, and subsequent frost penetration behaviour were analysed according to winter temperature using the freezing index. Road sections 4-6 were used to investigate different grading and types of lightweight aggregate used as an insulation layer. Railway sections 1-4 were used to investigate both grading and different rock types in the-sub ballast or reinforcement layer and to analyse their effect on frost penetration. All sections are fully described bellow.

Røros was chosen as the location of the test site for its rigorous winters. The freezing index period of return over 2, 10 and 100 years (F_2, F_{10} and F_{100}) are 21000, 39000 and 61000 °C·h respectively. Many populated regions in Norway have a F_{100} of around 20000°C·h (Table 3). The Røros test site allowed to test what is considered as a F_{100} period of return winter in populated areas as Trondheim and Oslo, therefore being of great interest in design performance analysis. The site was designed using Handbook N200 (2014) with a 10-year freezing index return period.

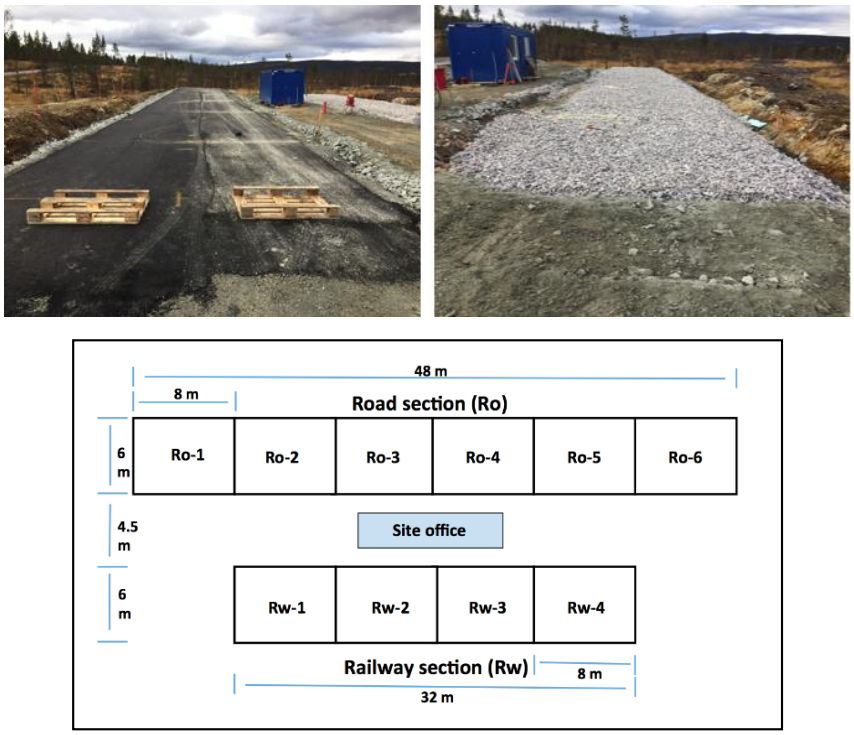

Figure 21: Røros test site road section (top left) and railway section (top right) after construction (2016). Bottom picture shows section's dimension and positions on site

Table 3: Mean annual temperature (MAT) and freezing index for 2-, 5- and 10-year periods of return (F_2, F_{10} and F_{100}) in different areas in Norway

Locality	MAT	FI_2	FI_{10}	FI_{100}
Røros	0.2	21000	39000	61000
Oslo	6.4	5000	12000	21000
Bergen	7.6	1000	2000	4000
Trondhein	5.3	4000	11000	19000
Tromsø	2.8	8000	15000	24000

FI_x: Return period in x years of a freezing index magnitude event

FI in °C·h

The test section was instrumented to measure the following parameters:

a) temperature (°C): 95 T24 duplex insulated thermocouples were embedded on the site: 57 in the road sections, 36 in the railway sections and 2 at different heights beside the construction site office for air temperature;

b) irradiance (W/m^2): a long-wave Kipp & Zonen CGR-3 pyranometer was placed at a height of about 1.5 m. above the top of the construction site office;

c) humidity (%): twelve Eijkelkamp Theta Probe ML3 soil moisture sensors were placed on site: ten in the road test sections and two in the railway sections;

d) frost heave (mm): linear variable differential transformers (LVDT) were placed in all sections, but some failed shortly after installation. Three survey nails were then inserted into the top of every road section for manual vertical deformation measurement using a level meter;

e) heat flux (W/m^2): two Hukseflux HFP01 heat flux plates were placed under two asphalt layer sections.

The positions of all of these instruments are presented in Figure 22, 24 and 26 below, in cross section.

5.2.2 Road test sections

All crushed rock aggregate materials for the road test sections were sourced from the Legruvbakken quarry near Røros municipality. The Geological Survey of Norway (NGU) defines the rock type as fine grain metamorphic hornblende-schist dominated by phyllite. Rock analysis by the Geological Survey of Norway (NGU) found an average mineralogical composition of about 45-50% quartz, 15-20% hornblende, 15% plagioclase or chlorite, and 15-25% of other minerals, mostly silicates, micas and garnet.

The road test section was divided into two distinct parts; the first to analyse the effect of varying particle size distribution in three different frost protection layers (all other layers being the same), and the second to analyse the thermal performance of three lightweight aggregates (two particle size distribution of expanded clay and one of foamglass) used as insulation layers between the sub-base and frost protection layers.

5.2.2.1 Road sections Ro-1, Ro-2 and Ro-3

A cross sections of road sections 1, 2 and 3 (Ro-1, Ro-2, Ro-3) are presented in Figure *22*, showing layer thickness, design and type, and the location of the instruments used. Figure 23 presents the different grading curves of the crushed rock aggregates of which the pavement is composed.

An open, coarse-graded material (20-120 mm) was used as the frost protection layer in Ro-1. This material is characterized by a low percentage of fines and an open pore structure. A fine, well-graded material (0-32 mm) was used in Ro-2 with a fines content (< 63µm) of ≈11-12%. Ro-3 was built using a coarse, well-graded aggregate layer (0-120 mm) qualified as 'typical'; this was used as the reference section. The fraction of fines in this material is believed to be approximately 5-8 %. The exact amount of fines wasn't tested due to loss of material. The road structure lay on 50 cm of silt.

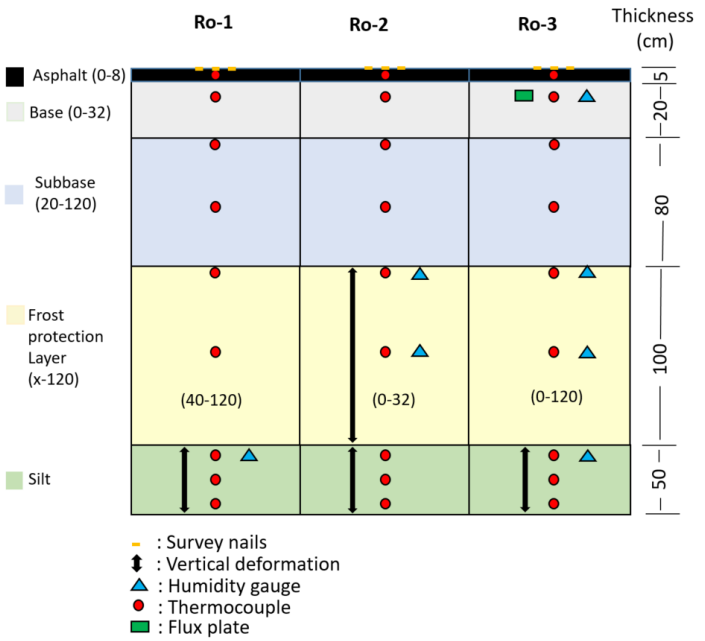

Figure 22: Cross sections of Ro-1, Ro-2 and Ro-3 showing the different particle size distribution of crushed rock aggregates in the different layers (in mm). Here the frost protection layers are investigated

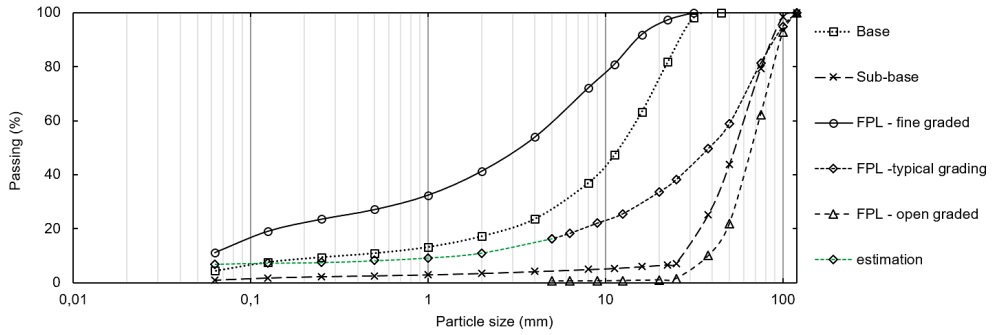

Figure 23: Grading curves of base, sub-base and the three different frost protection layers in Ro-1 (open graded), Ro-2 (fine graded) and Ro-3 (typical grading)

5.2.2.2 Road sections Ro-4, Ro-5 and Ro-6

Cross sections of Ro-4, Ro-5 and Ro-6 are presented in Figure 24, showing layer thickness, design and type, and instrument location. The different grading curves of the lightweight aggregates in the insulation layers are presented in Figure 25.

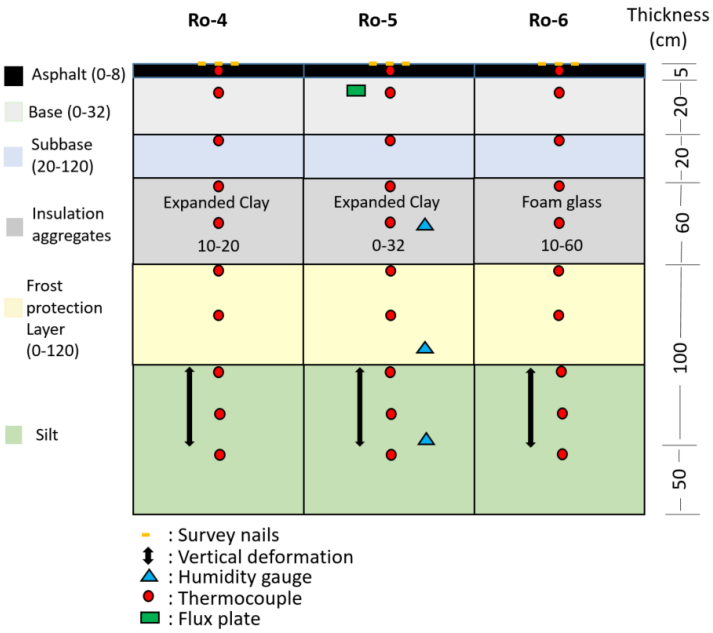

Figure 24: Cross sections of Ro-4, Ro-5 and Ro-6 investigating different grading and type of lightweight aggregates used as insulation layer

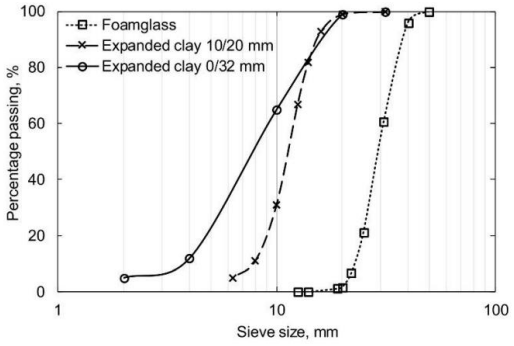

Figure 25: Grading curves of the three different lightweight aggregates used as insulation layer in Ro-4 (expanded clay 10-20 mm), Ro-5 (expanded clay 0-32 mm) and Ro-6 (foamglass 10-60 mm)

The expanded clay aggregates are round whereas the foamglass aggregate particles are cubical, and their installation therefore differed. Insulation is frequently used in Norway's transport infrastructure to limit frost penetration. Two different gradations of expanded clay (10-20 and 0-32 mm) were installed in Ro-4 and Ro-5 respectively and 1 gradation of foam glass (10-60 mm) in the Ro-6 section. All insulation layers were placed at a depth of 45 about cm and were 60 cm thick. Expanded clay is produced by sintering clay

in a special rotary furnace and for use as lightweight fill or frost protection (Øiseth et al. 2005c). Foamglass is produced from recycled glass crushed to powder and heated in a furnace. The insulation capacity of such materials is investigated in Frost I Jord (1976) and further research since (e.g. Bakløkk et al. 2001, Hoff et al. 2000a, 2000b, Øiseth et al. 2005a, 2005b, 2005c, 2006, all cited in Øiseth et al., 2006). Investigation of the thermal properties of lightweight aggregates was mainly carried out by Rieksts (2018) as the other part of the FROST project.

5.2.3 Railway sections

The railway sections were built using different rock types. Slate from the Legruvbakken quarry was used for all frost protection layers and was of the same grading as that used in Ro-3 (typical grading). The behaviour of sub-ballast crushed rock aggregates were investigated in the railway sections. Four different gradations were used: 0-120 and 20-120 in Rw-1 and Rw-2, and 0-250 mm and 20-250 mm in Rw-3 and Rw-4. Two different rock types were also used: a quartzite from the Hanestad quarry (Rw-1 and Rw-2) and a gabbro from the Vassfjell quarry (Rw-3 and Rw-4). Figure 26 presents the details of the railway section design and the instruments used.

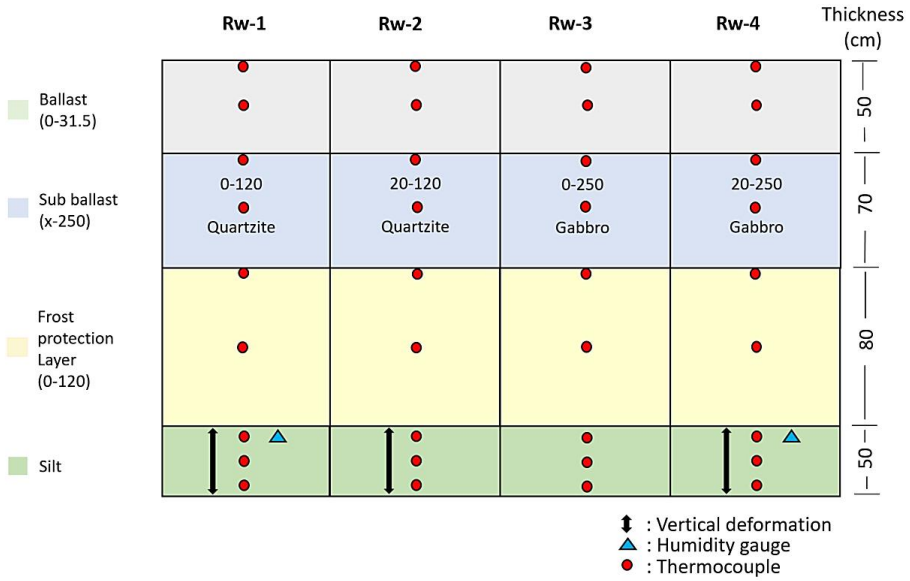

Figure 26: Cross section of sections Rw-1 to Rw-4 where different grading and rock type were investigated.

The different grading curves of the lightweight aggregates in the insulation layer are presented in Figure 27.

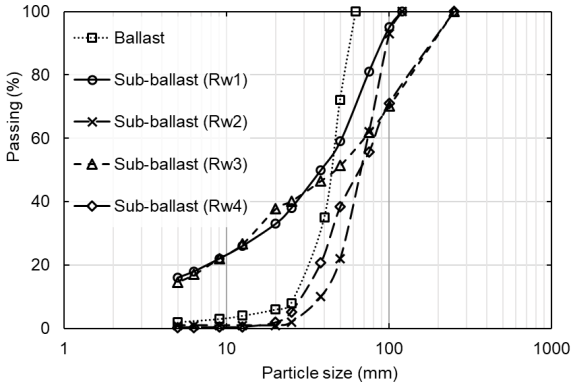

Figure 27: Grading curves of the different sub-ballast and ballast in railway sections.

5.3 Modelling SSR USING I3C-ME

5.3.1 I3C-ME Software

The I3C-ME software was developed for mechanistic-empirical road design by a research chair at Laval University in Quebec City, Canada. 'I3C' stands for the interaction between pavement, load and climate, and 'ME' for mechanical-empirical. The I3C-ME user manual (Doré et al., 2019) thoroughly describes the design process and the software's estimation and analysis methods. This freeware supports complete mechanical and frost design and is relatively easy to adapt and implement for local use. The software includes eight modules, one of which considers frost design (Figure 28).

The I3C-ME frost module was based from the MTQ software CHAUSSEE2. The CHAUSSEE2 software is only available in French and was therefore not presented here. However, CHAUSSEE2 allows to unlock any parameters from any materials, therefore being a bit more practical as there is no need to update the Microsoft Access tables for modifying the different parameters limits. All the calculation for the SSR model evaluation for the I3C-ME comes from the CHAUSSEE2. The analysis from the I3C-ME software for this study were verified using the CHAUSSEE2 software.

The software follows a step-by-step procedure: each module must be completed before moving on to the next. Module 1 requires a general name and information about the project to be inputted. Module 2 concerns the type of road involved, the design objectives and the equivalent single-axle load (ESAL) values. Module 3 characterizes the load, and here default values can be selected. Module 4 offers a choice between using a Quebec climate databank and importing a different one. In Module 5 the materials and layer thicknesses of roads and their resilient modulus are defined. Input from module 4 and 5 are needed for module 7 analysis. Module 6 offers a choice of damage models for the ME analysis. We used Module 7, described below, in this study. Module 8 calculates the ME design results.

Figure 28: I3C-ME software modules, including frost module in red (no. 7)

5.3.1.1 I3C-ME Module 7: Frost analysis

Module 7 has two sub-sections: the input and calculated parameters, and the climatic data analysis coupled with the model results (Figure 29). Each sub-section is explained below.

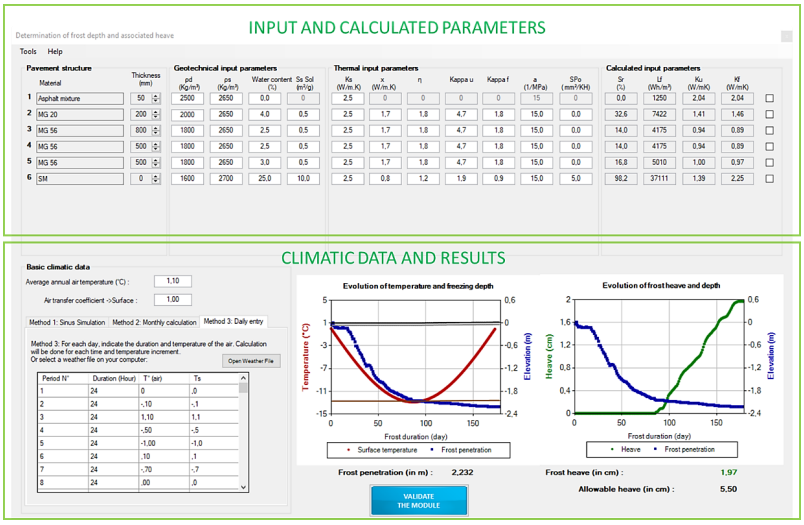

Figure 29: I3C-ME frost module interface

5.3.1.2 Input and calculated parameters

The I3C-ME software input parameters for the frost module are in four blocs: pavement structure, geotechnical input parameters, thermal input parameters, and calculated input parameters (Figure 30 and Figure 31).

Pavement structure / **Geotechnical input parameters**

	Material	Thickness (mm)	ρd (Kg/m³)	ρs (Kg/m³)	Water content (%)	Ss Sol (m²/g)
1	Asphalt mixture	100	2500	2650	0,0	0
2	MG 20	200	2000	2650	4,0	0,5
3	MG 56	800	1800	2650	2,5	0,5
4	MG 56	500	1800	2650	2,5	0,5
5	MG 56	500	1800	2650	3,0	0,5
6	SM	0	1600	2700	25,0	10,0

Figure 30: Left part of the input and calculated parameters section

The names of the pre-determined materials follow MTQ appellation, but as all the other parameters can be changed it is possible to bypass the assigned material names. The only limit is the range of values accepted for each material. New material appellation, default values and parameter ranges can be added using a Microsoft Access table. The layer materials and thicknesses are inputted from module 5. The

geotechnical input parameters include dry density (ρd), grain density (ρs), water content (w) and specific surface area (Ss).

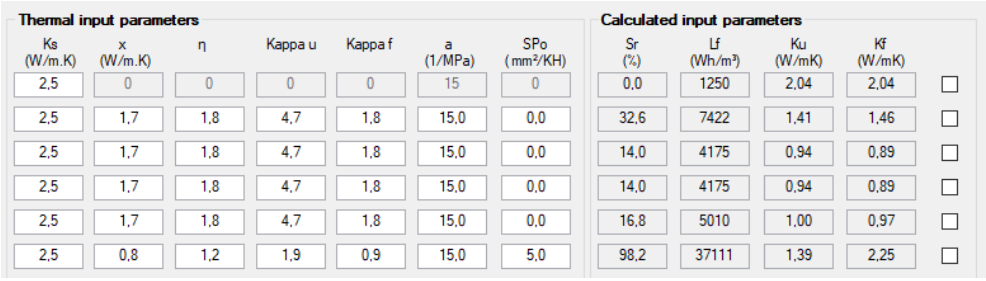

Thermal input parameters

Ks (W/m.K)	x (W/m.K)	η	Kappa u	Kappa f	a (1/MPa)	SPo (mm²/KH)
2,5	0	0	0	0	15	0
2,5	1,7	1,8	4,7	1,8	15,0	0,0
2,5	1,7	1,8	4,7	1,8	15,0	0,0
2,5	1,7	1,8	4,7	1,8	15,0	0,0
2,5	1,7	1,8	4,7	1,8	15,0	0,0
2,5	0,8	1,2	1,9	0,9	15,0	5,0

Calculated input parameters

Sr (%)	Lf (Wh/m³)	Ku (W/mK)	Kf (W/mK)	
0,0	1250	2,04	2,04	☐
32,6	7422	1,41	1,46	☐
14,0	4175	0,94	0,89	☐
14,0	4175	0,94	0,89	☐
16,8	5010	1,00	0,97	☐
98,2	37111	1,39	2,25	☐

Figure 31: Right side of the input and calculated parameters section

The thermal input parameters include the thermal conductivity of the solid (λ_s, called Ks in the software), the 'a' parameter (sensitivity to overburden pressure parameter) and SP_0 (SP without overburden pressure). The four other parameters, χ, η, Ku and Kf, are used to compute the thermal conductivity of the different layers using the Côté-Konrad model (2005). χ and η are two parameters that take into account the effect of particle shape on thermal conductivity. Ku and Kf are granular factors of unfrozen and frozen thermal conductivity respectively. It is possible to choose to compute the thermal conductivities using the Kernsten model (1949), with which Saarelainen obtained good results in his SSR model analysis of natural subgrade soils (pers. comm., 2020). The calculated input parameters are the degree of saturation (Sr), latent heat of fusion (Lf), and unfrozen and frozen computed thermal conductivities. It is possible to bypass the automatic thermal conductivity calculation and enter thermal conductivity values computed using another model or from laboratory experiments.

5.3.1.3 Climatic data and results

The climatic data set is imported from Module 4 by default, but can be changed completely in Module 7. The average annual air temperature and air transfer coefficient (n-factor) must be entered if not using the data from Module 4. There are three calculation methods for compiling the freezing index (in °C·d) to be put into the SSR model: sinus simulation, monthly calculation, and daily entry. Sinus simulation uses a sinus function compiled from average temperature data, the normal air freezing index and the duration of the freezing period. A probabilistic approach or an estimation computes the function, using the standard deviation and recurrence period. The results show the sinus temperature imposition (red curve) along with the evolution of frost depth and heave (Figure 32).

The second option for the climatic data input is to directly enter the monthly FI with the corresponding number of days. This method imposes a constant FI for each month. The data must be entered manually. Figure 33 presents an example of such an approach.

The last option considers all the mean daily average temperature. Any temperature data set can be imported in .txt file format. Climate file formats, described in section 8.2.2 of the CHAUSSEE2 user manual (St-Laurent, 2006) are easy to build. Figure 34 presents an example using the Røros temperature set for winter 2017-18.

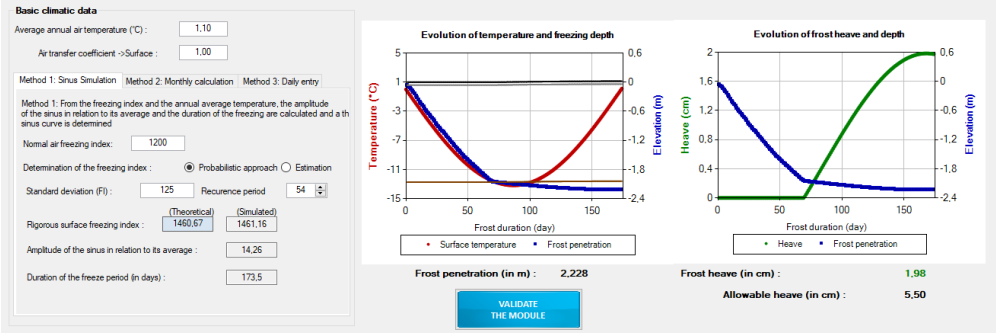

Figure 32: I3C-ME climatic data and SSR results, sinus simulation method

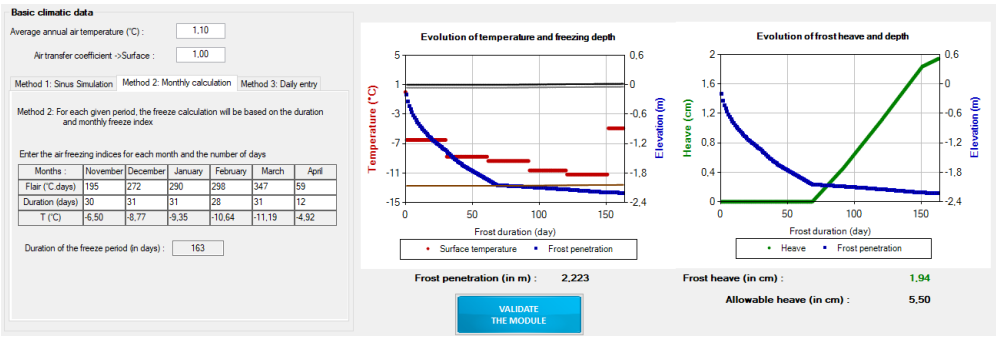

Figure 33: I3C-ME climatic data and SSR results, monthly calculation method

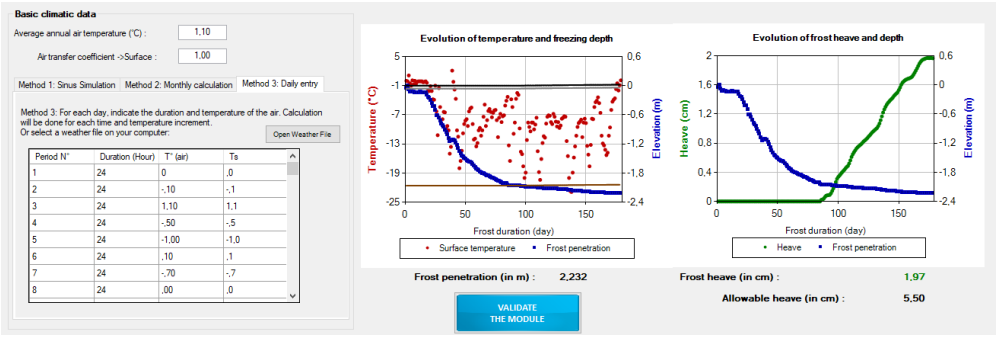

Figure 34: I3C-ME climatic data and SSR results, daily entry method

Modelling the SSR model in the I3C software therefore permits a quick overview of expected frost depth and heave using default parameters, with deeper analysis possible following an extensive study of the material properties, as in the Røros test site analysis. Seeing the results permits the adjustment of uncertain parameters such as water content and segregation potential to fit the values measured on site.

6. RESULTS AND DISCUSSION

This section summarises the main results of this study presented in the papers completed for this thesis. The first part (6.1) describes and discusses the laboratory work studying the segregation potential of crushed rock material (Paper I) and normalized segregation potential, including index parameters (Paper III). The second part (6.2) describes and discusses the field work including the investigation of frost penetration in Ro-1, Ro-2 and Ro-3 (Paper II). The third part (6.3) analyses frost penetration and frost heave in the same three road sections based on modelling and design optimization (Paper IV).

6.1 Laboratory

The laboratory experiments were the cornerstone of this research. An important series of tests was carried out to characterize the index parameters of the different aggregates and to study their behavior when subjected to freezing. This part has two subsections: the first describes the first phase of freezing tests, as presented in Paper I, and the second describes the tests carried out to characterise the different aggregates, and the second phase of the freezing tests for validation purposes, as presented in Paper III.

The first task was to set up the laboratory. A frost heave cell was constructed at Laval University, based on cells used in its pavement laboratory, and shipped to NTNU. The setup involved construction of the compaction mold and installation of the different instrumentation (thermistors, cooling fluids for top and bottom plates, and LVDT). The Marriotte's bottle was prepared using a 3-liter container. The data acquisition was set using LAbView and a full calibration of thermistors, cryostat temperature and LVDT was completed. Administrative complications delayed the arrival of the frost heave cell. The calibration and setup phase were completed at the beginning of 2018, and the first test on crushed rock was carried out in February 2018. I had learnt the methodology and setup requirements for frost heave tests at Laval University Laboratory in 2016 and 2017.

Figure 35 presents the conditioning, freezing and end stages of a frost heave test using the NTNU cell. The third picture shows that the rings in the freezing cell moved apart from one another as lifting due to freezing penetrated downwards, eliminating friction between the sample and the wall of the cell, as is the case for solid, or split cells.

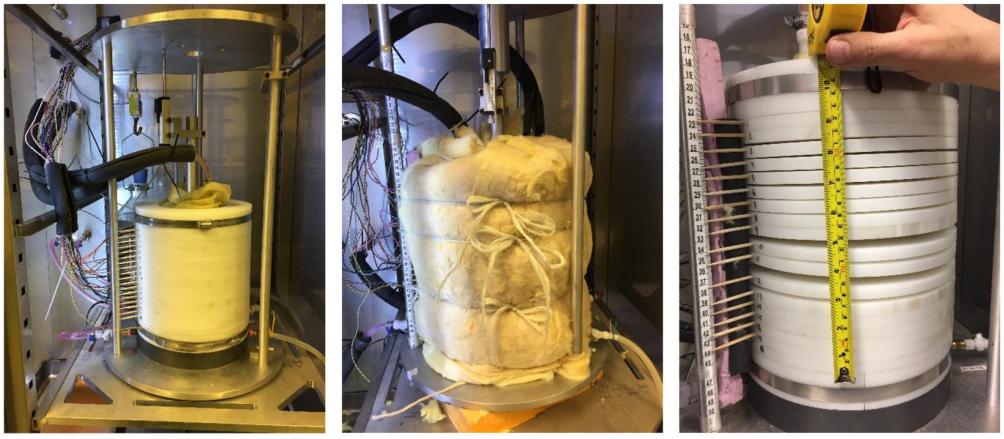

Figure 35: Frost heave test using the multi-ring cell during conditioning phase (left), freezing process (middle) and after the test (right)

6.1.1 Frost heave tests

This part of the study was done in order to extend frost heave susceptibility knowledge of different type of crushed rock aggregates. Crushed rocks from various Norwegian quarries were investigated: Aplitt, Hadeland, Legruvbakken, Vassfjell, Lørenskog and Velde. Those quarry were chosen because they was judged to reflect good quality aggregates of typical rock type in Norway, the exception being Legruvbakken, a slate, which was coming from a small, local quarry, used for the test site construction in Røros.

In total seven different crushed rock aggregates were tested. All samples were tested using the 0-4 mm fraction except for two: one was prepared using a constituted sample (CS) of Lørenskog (>125 µm - 4 mm) and Velde (0 - <125 µm) fractions, and the other was a 0-500 µm grading (Velde). Particular attention was paid to particle size distribution, as the NPRA uses grain size as a criterion for determining frost susceptibility of unbound granular material. The particle size distribution of the different aggregates is presented in Figure 36. Table 4 presents rock type and passing percentage of <63, <20 and <2 µm for each crushed rock aggregates. Mineralogical composition details can be found in Paper I.

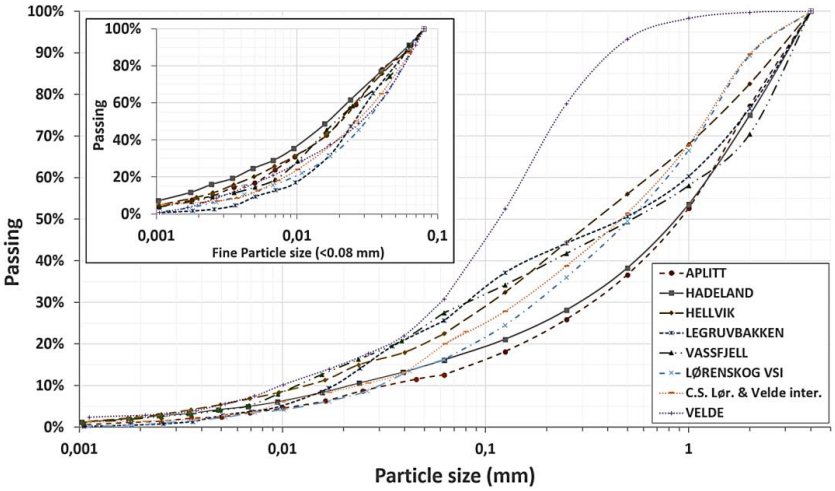

Figure 36: Crushed rock aggregates particle size distribution

Table 4: Different quarries rock type and passing percentage of different fine fractions

Quarry	rock type	< 63 µm %	< 20 µm %	< 2 µm %
Aplitt	Granodiorite	12.5	7.4	1.23
Hadeland	Porphyr	16.1	9.7	2.30
Hellvik	Anortosite	22.4	13.2	2.45
Legruvbakken	Slate	25.6	11.5	0.56
Vassfjell	Gabbro	24.9	14.8	2.05
Lørenskog	Gneiss	16.2	7.1	0.53
C.S. Lør.+ Velde	Gneiss/Granite	20.0	9.1	1.41
Velde	Gneiss/Granite	30.7	15.2	2.83

The frost heave and frost penetration results from tests omitted from Paper I due to space restriction are presented Figure 37. The frost heave results were run for a 96-hour duration. Figure 38 presents the results of the frost heave tests on Aplitt (granodiorite), Hadeland (porphyr) and Vassfjell (gabbro). All of the aggregates except the slate from Legruvbakken showed 20-35 mm of heave after 96 hours. The atypical heave curve of the Legruvbakken aggregate led to the hypothesis that heaving had been compromised in some way and that these results should be used with care. According to Konrad (1994), the coarser pore fraction is filled when fines % < 75 µm are >15%, leading to maximum frost susceptibility potential. The percentage of fines in the Legruvbakken aggregate was ≈25%, leading to the hypothesis that there was issues with water supply during the test.

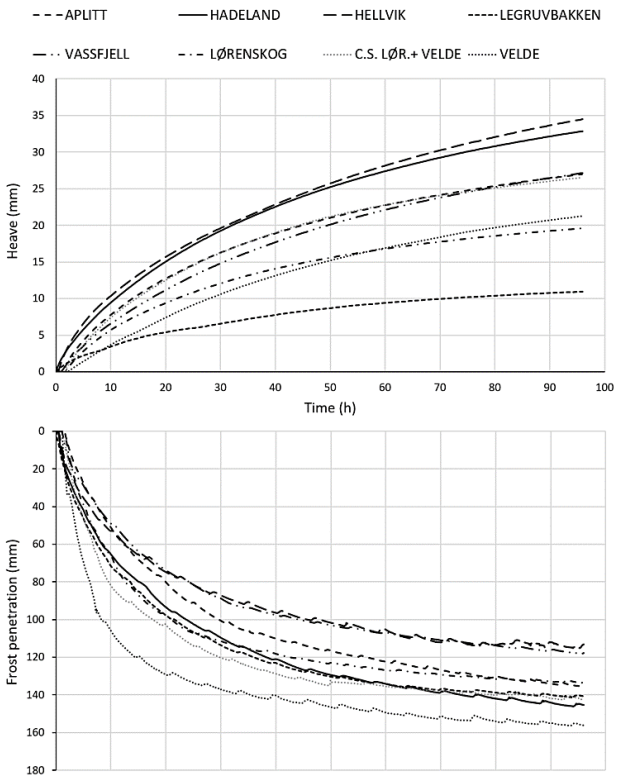

Figure 37: Heave and frost penetration according to time for the 8 tests presented in Paper I

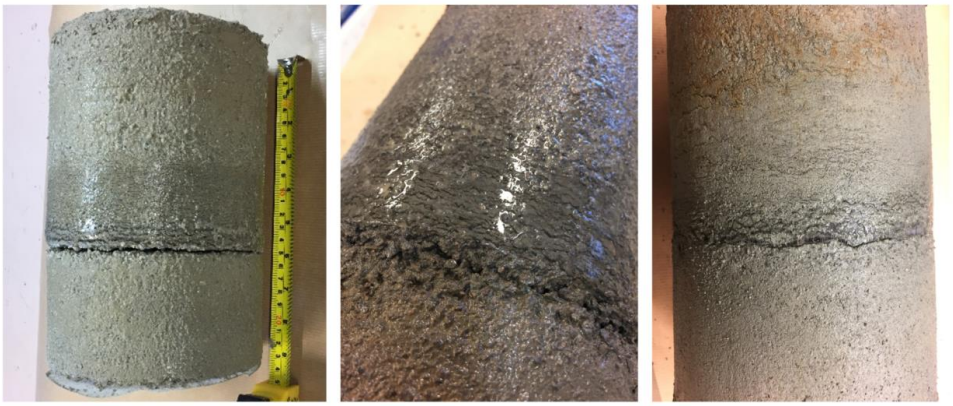

Figure 38: Samples after freezing test for a granodiorite (Aplitt, left), a porphyr (Hadeland, middle) and a Gabbro (Vassfjell, right)

For a better analysis of frost susceptibility, i.e. a material's capacity to generate ice lenses, the segregation potential of all the aggregates was measured. The segregation potential calculation method uses both frost depth vs. time and temperature profile graphs to find the moment at which the temperature regime changes from a transient to a steady state. This moment defines the time at which the rate of heaving and the temperature gradient in the frozen fringe can be considered for calculation, at which the last ice lens in the sample begin to grow. Figure 39 shows an example of a frost heave test on the Hadeland quarry aggregate segregation potential calculation. All the tests were processed in the same way.

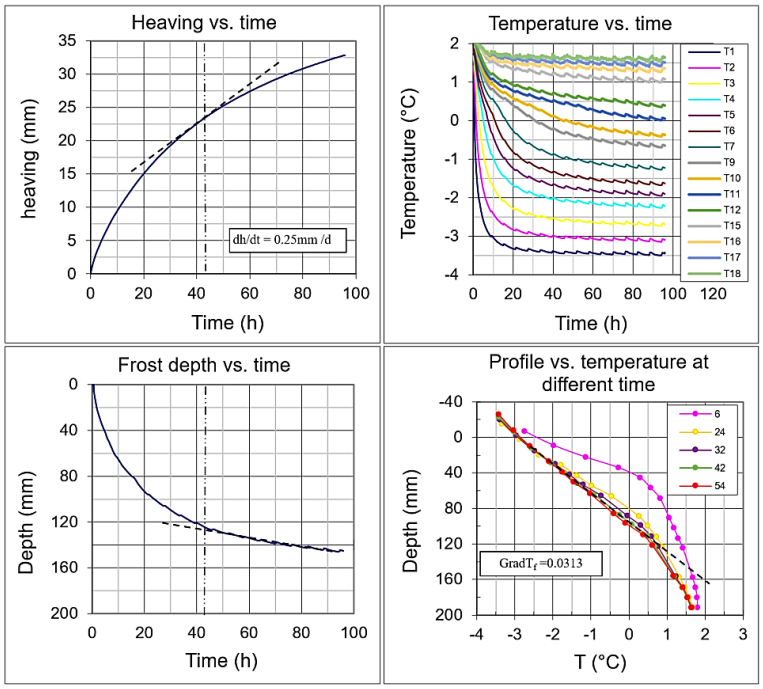

Figure 39: Graphical solution method for SP calculation using the Hadeland frost heave test data

The top right corner of Figure 39 presents the temperature evolution of each thermistor over the 96 hours of the test. Note that three of the thermistors were found to be faulty (T8, T13 and T14) and therefore have not been plotted. The cyclic variation of ± 0.05 °C is caused by the fridge temperature varying during the test due to its evaporator defrost cycle. The left sections of Figure 39 present heaving and frost penetration vs. time respectively. The bottom right section shows temperature profiles at different times in the sample.

The steady state was reached after 42 hours based on a) frost penetration becoming linear and b) the temperature gradient in the fringe becoming constant in the frozen fringe, i.e. between 0.1 and 0°C. At this time the rate of heaving (dh/dt) was 0.25 mm/h and the thermal gradient in the frozen fringe (Grad T_f) was 0.0313 °C/mm. SP is calculated by dividing the rate of heaving by 1.09 time the temperature gradient to accommodate the difference in volume between ice and water. The SP for this 0-4 mm crushed

rock aggregate was 192 $mm^2/°C$-d. Note that the SP here is an SP_0 as the experiment was done without overburden pressure.

Table 5 presents the quarry and rock types again for convenience of reference, with the temperature of the top cold plate (T_c), the bottom warm plate (T_w), the rate of heaving (dh/dt), and the temperature gradient in the frozen fringe (Grad T_f) all at steady state regime, and the SP_0 in both $mm^2/°C·d$ and $mm^2/°C·h$. Note that since SP_0 is calculated from the water velocity intake, the heaving rate has to be divided by 1.09 to accommodate the change in volume between ice and water.

Table 5: Segregation potential of different crushed rock aggregates

Quarry	rock type	T_c (°C)	T_w (°C)	dh/dt (mm/d)	*Grad* T_f (°C/mm)	SP_0 ($mm^2/°C$-d)	SP_0 ($mm^2/°C$-h)
Aplitt	Granodiorite	-3.5	2.0	5.40	0.0333	149	6.2
Hadeland	Porphyr	-3.4	1.6	6.00	0.0313	176	7.3
Hellvik	Anortosite	-3.3	2.2	6.97	0.0324	197	8.2
Legruvbakken	Slate	-3.5	1.9	2.18	0.0333	60	2.5
Vassfjell	Gabbro	-3.2	2.1	7.27	0.0379	111	7.3
Lørenskog	Gneiss	-3.7	1.9	4.00	0.0350	105	4.4
C.S. Lør.+ Velde	Gneiss/Granite	-3.7	1.8	5.33	0.0376	130	5.4
Velde	Gneiss	-4.2	1.1	5.42	0.0253	197	8.2

The Quebec Ministry of Transport (MTQ) uses a qualification chart from SP values presented in Table 6. This same table is interesting because it links SP values to the CRELL (1981) frost heave classification and to the frost heave ratio, in use by diverse authors as Saarelainen (1992, 2015).

Table 6: Frost susceptibility classification according to segregation potential (SP), frost heave rate (CRREL 1981) and frost heave ratio, in use by MTQ, Quebec, Canada (St-Laurent, 2006).

frost-susceptibility	SP $mm^2/°C·h$	SP $mm^2/°C·d$	Frost heave rate mm/d	Frost heave ratio $\Delta h/h_{frozen}$ (%)
Negligible	< 0.5	< 12	< 0.5	< 1
Low	0.5 - 1.5	12 - 35	0.5 - 2	1 - 4
Medium	1.5 - 3	35 -75	2 - 4	4 - 8
High	3 - 8	75 -200	4 - 8	8 - 20
Very high	> 8	> 200	> 8	> 20

Discarding the Legruvbakken sample result, which was considered compromised, the SP_0 of the remaining crushed rock aggregates ranged from 105 to 197 $mm^2/°C·d$. All of them were therefore found to be highly frost susceptible according to MTQ's frost susceptibility classification. These results are within the range of those proposed by Konrad 2005 for six different rock types (basalt, dolostone, granite, limestone, quartzite and greywacke). The investigation then focused on plutonic, and metamorphic from plutonic orogenesis rock types, widening knowledge of their susceptibility to frost heave. According to Neeb of the Norwegian Geological Survey (cited in GEO365, 2015), the commonest crushed rocks produced in Norway are gneiss and gabbro, which contribute 40% of total production, with other crushed plutonic rock such as

syenite and granite also widely produced. This tends to validate the choice of crushed rock aggregates for this study.

Table 1 presented previously in section 3 classifies the frost susceptibility of all granular material, natural soils and crushed rock aggregates from T1 to T4, T1 being non/negligibly frost susceptible as used by NPRA. None of the tested aggregates contained less than 3% of fines < 20 µm, so it was not possible to evaluate the boundary between T1 and T2. T2 material (low frost susceptibility) is characterized by 3-12% of fines < 20 µm content in the mass. The Aplitt, Hadeland, Legruvbakken, Lørenskog and the mixed Lørenskog and Velde samples fell within this range. All of these showed high frost susceptibility except for that from Legruvbakken, which showed moderate susceptibility although the validity of the test on this was in doubt. Four of the quarry samples contained 7.1-9.7% of fines < 20 µm. This leaves no doubt that the criterion of grain size must be used with caution. Nurmikolu (2005) reports a good correlation between the <20 µm fraction and the SP of crushed rock aggregates. This trend was not observed in this study. The <2 µm calculated from the < 80 µm fraction was the one that showed an acceptable trend, with a $R^2 = 0.835$), as shown in Figure 40.

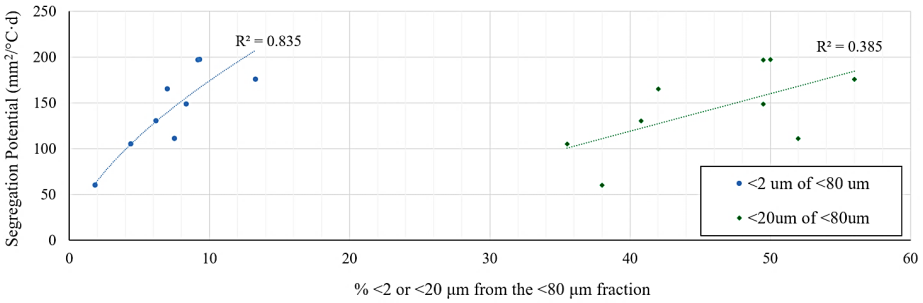

Figure 40: Segregation potential of the <2 and <20 um fraction calculated from the < 80 um fraction

This study was not able to link the magnitude of frost heave susceptibility to particular minerals, as proposed in Brandl's (2008) mineral criterion. Indeed, no relationship was found between different minerals and composition percentage, and their segregation potential. The rock is subject to mineralogy variation when extracted from quarry. One hypothesis is that the XRD analysis were not directly performed on the same exact samples that were tested for frost heave, and therefore may not reflect the 'true' mineralogical composition of the samples. Uthus (2007) discusses how XRD results must be taken as relative values and mineralogical investigation should be approached using XRD, a scanning electron microscope (SEM) and thin layer analysis.

Table 7: Mineralogical content of crushed rock aggregates using XRD

	Aplitt	Hadeland	Hellvik	Legruvbakken	Vassfjell	Lørenskog	Velde*
Quartz	29.0	7.0	0.0	35.8	0.0	28.0	25.0
Plagioclase	37.0	53.7	78.2	32.8	21.3	47.5	30.0
K-Feldspar	13.4	32.0	3.7	4.3	1.7	6.4	35.0
Hornblend	0.6	2.2	0.0	3.9	35.1	0.0	0.0
Epidote	6.0	0.0	6.2	5.7	30.0	0.0	0.0
Pyroxene	0.0	4.3	2.4	0.0	1.0	0.0	0.0
Amphibole	0.0	0.0	0.0	0.0	0.0	14.1	0.0
Chlorite	2.3	0.0	2.3	12.9	9.9	0.0	1.0
Mica	11.8	0.3	6.4	4.6	0.0	4.0	9.0
Others	0.0	0.5	1.0	0.0	1.1	0.0	0.0

* : % estimated from NGU and Velde Industri AS data.

In summary, the frost heave laboratory setup is believed to be well adapted for performing freezing tests on crushed rock aggregates. The SP_0 values for the studied rocks are within the range found in literature for granite, and can be used as reference values for the granodiorite, porphyr, anortosite, slate, gabbro and gneiss. The high frost susceptibility of the 0-4 mm crushed rock aggregates with a relative large percentage of fines was expected, but their evaluation from a grain-size criterion developed firstly for natural soils have to be considered with care.

6.1.2 Determining frost heave susceptibility from the materials' index parameters

The design of linear transport infrastructure is based on predicted performance during its planned service life. A high-class road project requires highly reliable input data, while estimated input values could satisfy the requirements for a secondary road. The budget allowed for a project therefore governs the effort that can be put into evaluating the frost susceptibility of the subgrade and the quality of the aggregates used for the different pavement layers.

The determination of frost heave susceptibility can be classified into four levels, level 1 being the least reliable and level 4, the most reliable.

Level 4, the most reliable form of frost heave determination that can be achieved, measures in situ heaving. However it involves the instrumentation of a site and the mobilization of competent personnel, and therefore while it is the most reliable it is also the most expensive, and is reserved for projects requiring precise input and for study sites.

Level 3 measures frost heave susceptibility using a freezing test in laboratory conditions. It can be divided into sub-levels depending on whether the tests are run on disturbed or undisturbed soils, although this is not relevant in the case of crushed rock materials, which are by nature disturbed. When the tests reproduce site conditions the results have a high level of reliability. It is considered expensive, however, and requires specialized equipment and personnel, and again is suitable for projects requiring highly reliable input data and for material characterization. Most frost susceptibility classifications are based on frost heave tests. Note that levels 3 and 4 are sometimes considered as the same confidence level (Konrad, 2014).

Level 2 relies on the empirical relationship between frost susceptibility and common material index properties measured in the laboratory, such as capillary rise, hydraulic conductivity, Atterberg limits, specific surface area etc. Many such relationships been developed over the years (Chamberlain, 1981) with varying precision. Furthermore, most such relationships are qualitative and are do not allow estimation of the magnitude of frost heave.

Level 1 determination of frost susceptibility involves a qualitative criterion such as grain size. This criterion leads to a pass/fail decision that can have unfortunate consequences. For example while a crushed rock aggregate with 11% of fines <20 µm would be categorized as a T2, the frost heave tests presented in the previous section proved otherwise. This level is however judged sufficient when designing local roads with low average annual daily traffic (AADT).

More than 70% of roads in Norway are secondary roads with AADT of less than 1500 vehicles (pers. comm., Skoglund 2019). The design of these roads must therefore be optimized to fit their limited budgets. A low-cost reliable estimation is needed for the assessment of the frost susceptibility of soils and geo-materials for calculation of the magnitude of frost heave. The estimation should use simple and readily available index properties to keep the costs associated with sample preparation, transport and laboratory testing low.

Paper III investigates the use of Konrad's (2005) normalized SP concept and its validation for crushed rock aggregates. The main results and discussion are presented in the following pages.

The investigation described in Paper III estimated the soil index parameters of 8 different rock types of 23 different crushed rock aggregates. The crushed rock aggregates came from the Aplitt, Hadeland, Hellvik, Legruvbakken, Vassfjell, Lørenskog and Velde quarries in Norway and the PEB and Drapeau quarries in Canada. All crushed rock aggregates tested were processed in the laboratory to calculate the soil indexes needed to estimate their SP from normalized SP ($SP_{0.n}$ in this text). The laboratory results and $SP_{0.n}$ were compared to validate the applicability of the normalized SP method to the various crushed rock aggregates.

All crushed rock aggregates were tested using a multi-ring frost heave cell. The 0-4 mm fraction was primarily tested. The required fraction was obtained directly from the quarry or sieved down from a larger fraction, generally 0-16, 0-20 or 0-31.5 mm. Two series of Lørenskog and one of Vassfjell crushed rock aggregates were tested at different steps in the crushing process. For the Lørenskog aggregate this included two series of tests using the 0-4 mm fraction obtained from the first step of crushing, the cone crushing (3rd step) and the VSI crushing phase (4th step). The Vassfjell tests included a 0-4 mm fraction from blasted materials, subbus (a mixture of rock from the 1st, 2nd and 3rd crushing phase), and the 3rd crushing phase (from a cone crusher). Three fillers from the Velde quarry (coarse, intermediate and fine), from an air classifier, were used in a series of tests including the coarser VSI Lørenskog fraction (0.125-4 mm) aggregate and finer Velde fraction (0-0.125 mm). A sample from VSI Lørenskog with the same proportion of coarser and finer fractions as the Velde fillers was also tested.

The material index parameters or soil index parameters required to estimate the SP of a material are the d_{50ff}, the initial water content (w), the liquid limit (w_L) and the specific surface area (Ss) of the fines. The

d_{50ff} is the average diameter of the <75 µm fraction, which was measured using hydrometer tests. The initial water content was measured from the water content when molding the sample and from the saturation phase before freezing. The water content in the unfrozen sample section rose substantially during the test, as also observed by Konrad (2008). The liquid limit were estimated using the cone penetration method. The specific surface area of the fines fraction (<75 µm) was determined by a modified methylene blue tests using Santamarina's (2002) calculation method. The complete step-by-step procedure for calculating the $SP_{0.n}$ is summarized in section 4.1.2 of this thesis. Figure 41 compares SP estimated from index parameters ($SP_{0.n}$) with those measured in laboratory frost heave tests ($SP_{0\,lab}$).

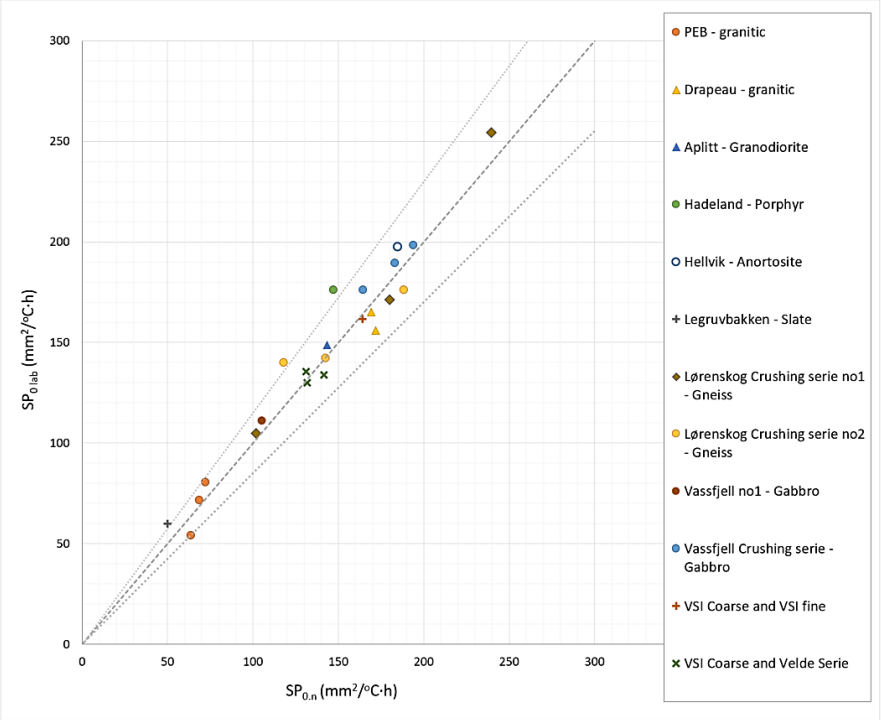

Figure 41: Estimated SP from index parameters ($SP_{0.n}$) compared to measured SP from laboratory experiments ($SP_{0\,lab}$). Dotted lines represents 1:1 relation and ±15% envelope

The methodology for estimating the SP from the index properties as proposed by Konrad (2005) is judged applicable for estimating crushed rock aggregate SP within a ± 15% degree of confidence. The relation can be plotted as a normalized SP relation as presented in Konrad 2005. The $SP_{0\,lab}/SP_{ref}$ is plotted with Ss/Ss_{ref} in Figure 42.

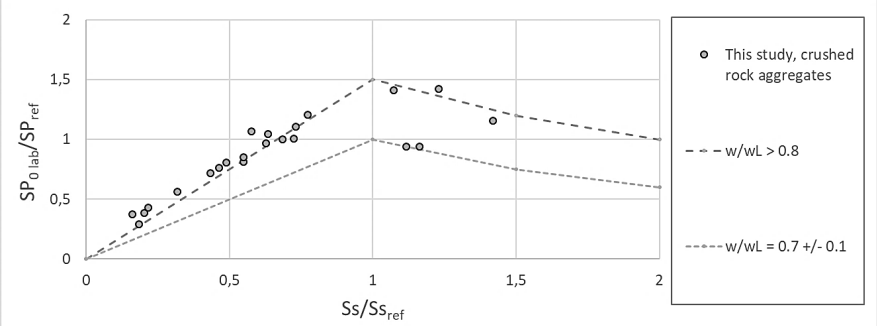

Figure 42: Normalized SP in relation to normalized specific surface area of all studied tests

The normalized SP results are following the same trends that was proposed by Konrad (2005), reinforcing the validity of the method for crushed rock aggregates. It is possible to see that the trend followed the w/wL > 0.8 for almost all data point. It seems to demonstrate, even if the samples were not saturated before the freezing phase in frost heave test, that a significant quantity of water is drawn and held into the unfrozen portion of the sample during the test. The high hydraulic conductivity of such materials is favoring such water movement, as described also by Konrad (2008). This water availability can have a considerable impact on ice segregation. Furthermore, the water content augmentation in the aggregate matrix will result in serious mechanical behaviour issues if undrained, but this was not investigated in this study.

The specific surface area can be an index correlating grain shape and unfrozen water content (Rieke, 1983). Further investigation found that the relationship between the specific surface area and $SP_{0\,lab}$ gave a R^2 = 0.78 for all crushed rock aggregates data in this study, which was judged unsatisfactory. Konrad's (2005) results with crushed rock aggregates showed specific surface areas of mostly < 8 m^2/g, and up to 12 m^2/g for one rock type (basalt). Konrad and Valencia (2008) show that the methylene blue test could overestimate specific surface determination due to asperities on fine particles. The test is based on the principle of a monolayer of molecules on the surface of a grain. This is altered by the methylene blue molecule filling small cracks and asperities, leading to overestimation of the amount of methylene blue solution adsorbed and the specific surface area value (Figure 43).

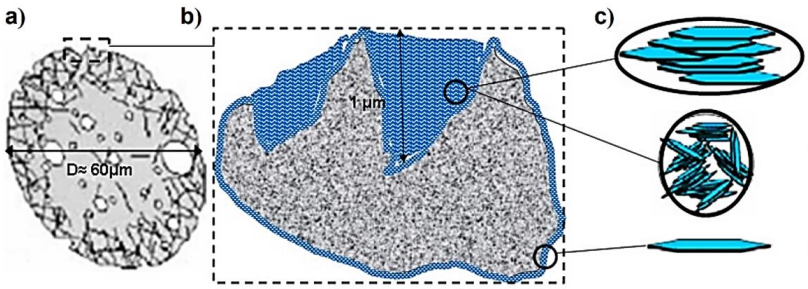

Figure 43: a) Grain surface alteration. b) Methylene blue molecules in asperities. c) Methylene blue molecules possible arrangement (Konrad and Valencia, 2008, modified from Tokunaga et al., 2003).

It was observed that the specific surface area results in this study were showing large variation from the trend when > 8 m^2/g. In fact, early stage of crushing (i.e. Lørenskog 1st stage, Vassfjell subbus and blast crushing) crushed rock aggregates presented specific surface area values of ≈ 12.5 m^2/g. The following hypothesis was that specific surface area variability was due either to the mineralogical content or grain-surface condition, or to a combination of both. It is possible that finer grain sizes are produced at an earlier crushing stage containing softer minerals (e.g. mica and chlorite), lead to soft mineral enrichment in the fine fraction. In subsequent crushing phases harder minerals turn to finer fractions, reducing this effect (Figure 44). The same logic applies to damaged/altered grain surfaces. Blasting rock is known to produce micro-cracking. As rock goes through subsequent crushing phases, the percentage of damaged particles decreases as processing several crushing stages (Figure 45). Two Lørenskog series were tested at 1st stage crushing, 3rd stage cone crushing, and 4th stage VSI crushing. The specific surface area estimates for the 1st stage, cone and VSI crushing were 12.6, 6.7 and 3.7 m^2/g for the first series, and 12.6, 5.4 and 4.5 m^2/g for the second. A Vassfjell blast subbus and 3rd crushing stage were analyzed, the results being 12.4, 12.7 and 7.3 m^2/g. It was, however, impossible to determine which of the hypotheses was applicable at this point. However the results clearly show a reduction of specific surface area as the crushing stages proceed. The blast and subbus aggregates showed similar results, as subbus consists of a mix from the 1st, 2nd and to a lesser extent 3rd crushing stages, resulting in the production of a highly variable material. Further research should be undertaken to validate both hypotheses for different rock types, mineralogical content and crushing methods.

The hypotheses are in agreement with the observations of Uthus (2006), who compared thin sections of three different rocks using X-ray diffraction (XRD) on < 20 µm fractions of a cubical gneiss (fine grain) and a flaky gneiss (foliation, very fine to fine grain) from Norway, and a gneiss from Sweden (fine to medium grain). XRD analysis found the mica content to be much higher in the two Norwegian gneiss and lower in the Swedish gneiss. The study was extended using the same aggregates (Uthus, 2007) to compare the < 63 µm and < 20 µm fractions using XRD analysis. It found that relative mica enrichment was higher in the 20 µm - 63 µm grain-size fraction, with relative quartz impoverishment observed in the same fraction. Table 8 summarizes these results. Micas are, according to Prestvik (1992, cited by Uthus, 2007), softer minerals with weaker chemical bonds. This causes their relative accumulation in the fines when crushed.

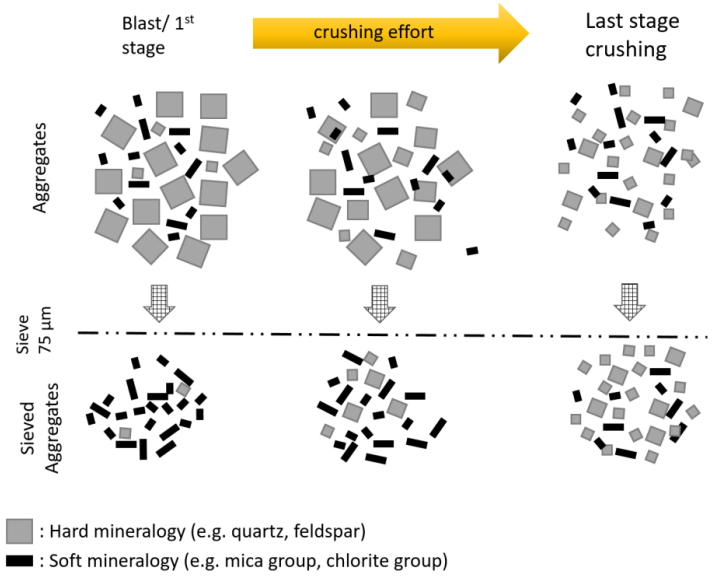

Figure 44: Mineral enrichment concept according to crushing phase

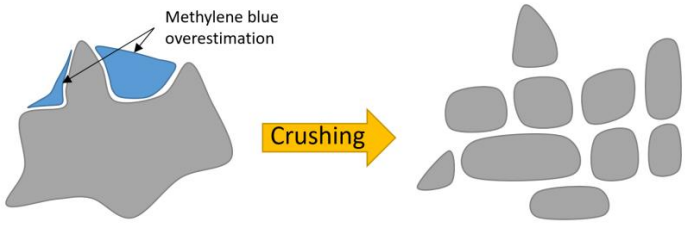

Figure 45: Overestimation of methylene blue on poorly crushed and well crushed fine particles

Table 8: Partial mineralogy variation of 3 gneiss according to different analyses (data from Uthus (2007))

	Cubical gneiss				Flaky gneiss				Swedish gneiss			
Mineralogy	%Q	%P	%F	%M	%Q	%P	%F	%M	%Q	%P	%F	%M
Thin section	47	44*		0	40	50*		8	19	37*		33
XRD < 63 um	12	46	24	14	16	23	18	36	8	34	18	35
XRD < 20 um	27	31	31	6	21	37	16	17	21	53	11	11

Q: quartz; P: plagioclase; F: Alkali fldspar; M: mica
*: thin section measured felspar content (plagioclase and alkali fledspar) together

It was therefore thought that mineral variability in the fine fraction and grain surface irregularities/micro-cracking were responsible for the specific surface area variation. This idea is supported by Konrad and Valencia (2008) with regard to weathered till fines. Crushed rock aggregates with a specific surface area of < 8 m^2/g were therefore used in this study to eliminate the effects of mineral enrichment and methylene blue variation. Note that Konrad 2005 also analyzed basalt with a specific surface area of 12.6 m^2/g

differently from the other crushed rock aggregates used in his study which had a specific surface area of 2.6 to 7.5 m^2/g (Figure 13). The crushed rock aggregates in this study with Ss values < 8 m^2/g showed a good correlation to the segregation potential, with a coefficient of determination of $R^2 = 0.936$, as shown in Figure 46.

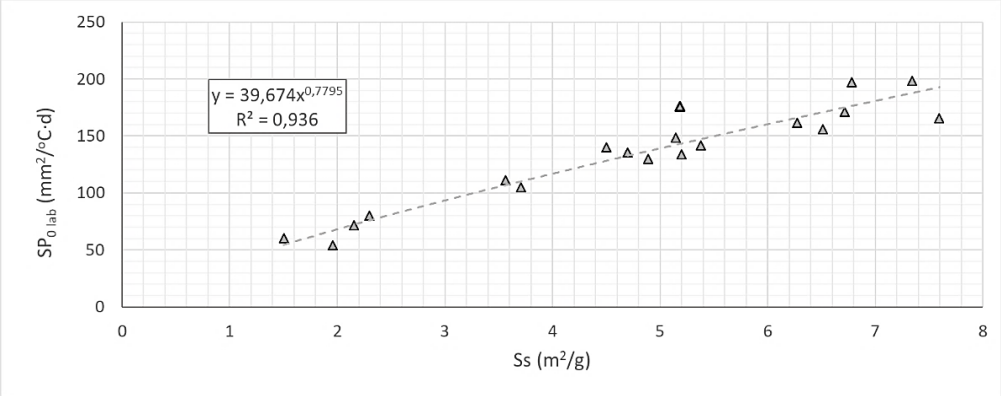

Figure 46: Relation between $SP_{0\,lab}$ and specific surface area, Ss, for Norwegian crushed rock aggregates

The power function linking $SP_{0\,lab}$ to the specific surface area is presented in Equation 25. $SP_{0\,lab}$ and $SP_{0.n}$ were in accordance, and was judged adequate to generalize equation 14 as $SP_{0\,lab} = SP_{0.n} = SP_{0\,CRA}$, or SP_0 for crushed rock aggregates with Ss < 8 m^2/g.

$$SP_{0\,CRA} = 39.674\, S_s^{0.7795} \qquad \textit{Equation 25}$$

Konrad and Valencia (2008) proposed a methodology for correcting overestimation of methylene on weathered till particles which could be a good starting point for evaluating specific surface area values more reliably in early-stage aggregate crushing.

In summary, 23 different crushed rocks from different origins and at different crushing stages were analysed to find the index parameters necessary to estimate the SP using Konrad's (2005) relationship ($SP_{0.n}$). These are the d_{50ff}, the initial water content (w), the liquid limit (w_L) and the specific surface area (Ss) of the fines. All of the crushed rocks were tested in frost heave tests and their SP determined (SP_{lab}). It was found that the normalized SP relationship is applicable to crushed rock aggregates, with a variability of approximately ±15%. It was found that the specific surface area of fines (< 75 µm) is affected by the crushing stage. Early-stage crushing tends to result in overestimation of specific surface area, which can be explained by grain surface irregularities or mineral enrichment. It was found that crushed rock aggregates from last-stage crushing presented a specific surface area of approximately < 8 m^2/g. A relation was developed to estimate SP directly from the specific surface area of fines only, showing a coefficient of determination $R^2 = 0.936$. This suggests that SP is mainly related to the specific surface area, which reflects the grain shape, and indirectly to the mineralogy of the crushed rock aggregates.

6.2 Field test

It is typical to estimate the expected maximum frost depth in road structure in order to choose an adequate design for frost protection purposes. In Norway, the use of a frost protection layer is mandatory on main roads in order to hold the frost front back from a frost susceptible subgrade. The frost protection layer may be used in secondary roads design in order to limit the time length where the frost front is into a frost susceptible subgrade but at the moment, without calculating heaving magnitude.

We investigated frost insulation performance on the three road sections Ro-1, Ro-2 and Ro-3 at the Røros field test site in the winters of 2016-17 and 2017-18. The N200 handbook includes a chart for estimating frost penetration in function of the freezing index, but it presents frost penetration beyond the thicknesses allowed in the regulations and does not take into account the cooling of the underlying subgrade (specific heat effect). However, it is presented as a simple decisional tool that can give a quick idea of the frost protection capacity of different soils and aggregates with different moisture content. Another, more precise calculation method is described in Equation 1 and Equation 2 in section 3 of this thesis.

Figure 47 presents the air and surface temperatures measured from October 2016 to May 2018. The surface freezing indexes were compiled directly from the upper thermocouple in the asphalt layer. The measured *n* factor relating FI_{air} to FI_s was 0.96 and 1.0 in winter 2016-17 and winter 2017-18, with an FI_s of 22630 °C·h and 36683 °C·h respectively. The Road Construction Handbook N200 gives a FI_{air} of 21000 °C·h for a 2-year period of return and a FI_{air} of 32000 °C·h for a 5-year period of return. The mean air temperature was calculated for both years and was equal to 1.3 °C, diverging from the design mean annual temperature of 0.2 °C proposed in the N200 Handbook for the Røros municipality.

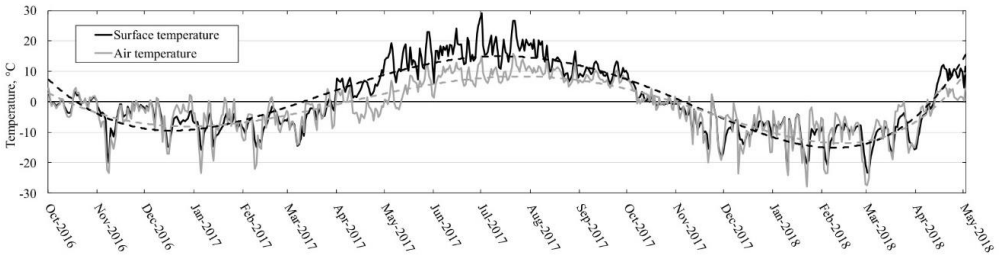

Figure 47: Road surface and air temperature from October 2016 to May 2018 at Røros test site

Table 9 lists the material properties of each soil layer. Material properties were measured under laboratory conditions. Moisture content was obtained from field measurements. Thermal conductivity was calculated based on the model proposed by Côté and Konrad (2005). Asphalt, silt and clay properties values were taken from standard values proposed by Heiersted in frost i jord (1976).

Table 9: Material properties of road section Ro-1, Ro-2 and Ro-3 at Røros test site

	Porosity (n)	ρ_d (kg/m^3)	C (kJ/(m^3·°C))	w (%)	λ_u (W/(m·°C))	λ_f (W/(m·°C))
Asphalt	0.07	2400	1840	0.5	1.45	1.25
Base	0.29	1980	1817	4	1.46	1.46
Subbase	0.42	1623	1218	1	0.51	0.46
FPL – open graded (Ro-1)	0.45	1535	1152	1	0.44	0.41
FPL – fine graded (Ro-2)	0.24	2116	1986	5.5	1.80	1.87
FPL – typical grading (Ro-3)	0.36	1780	1542	2	0.85	0.77
Silt	0.41	1600	2959	26.3	1.50	2.14
Clay	0.50	1400	2725	28.6	1.19	1.70

Frost penetration was compiled from site measurements, using linear interpolation from the thermocouples' temperature and depth. The frost depth evolution in both winters is presented in Figure 48, which shows that the frost front remained inside the frost protection layer during the first winter, and penetrated the subgrade in section Ro-1 and to a lesser extent in Ro-3 during the second winter. As many Norwegian regions have a freezing period of return of 20000 to 25000 °C·h, a road structure such as that of Ro-1, which is the least resistant to frost penetration, was considered sufficient to meet the requirements of the Norwegian standards.

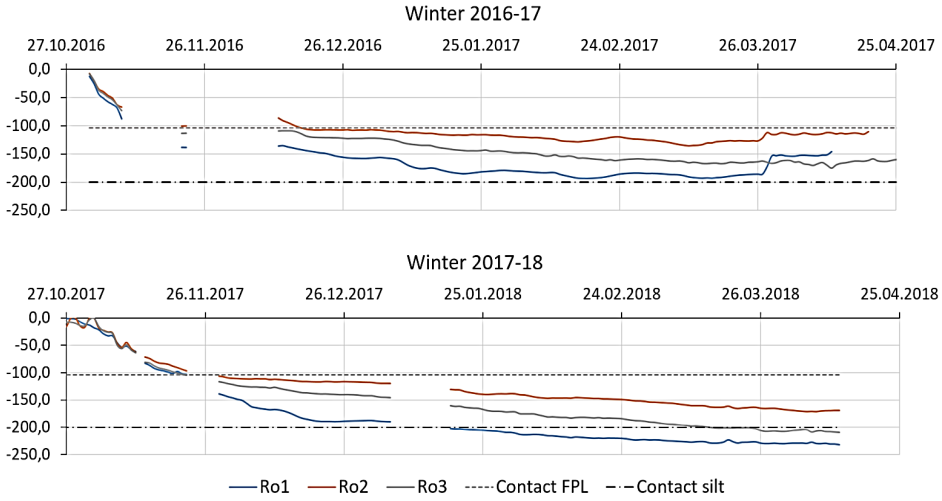

Figure 48: Frost depth evolution of Ro-1 (20-120 mm, open graded), Ro-2 (0-32 mm fine graded) and Ro-3 (0-120, well graded) for winters 2016-17 and 2017-18

Equation 2 (modified Stefan's solution) which calculates contributive freezing index to reach a certain depth in the infrastructure that includes the heat capacity of the underlying unfrozen ground, was used to

estimate frost depth. The spreadsheet developed at the NPRA required the depth of cooling influence and the mean annual temperature to include the heat capacity to the calculations. Required input parameters for the estimation are the layer thicknesses, dry densities, water contents, frozen and unfrozen thermal conductivities, and the material's latent heat and heat capacities. Frost depth was also calculated using Aldrich and Paynter (1953) modified Berggren equation and the same results were achieved. The results are presented in Table 10.

Table 10: Field and calculated frost depth (cm) for winters 2016-17 and 2017-18 at Røros field test site

	2016-2017		2017-2018	
	Field	Calculated	Field	Calculated
Ro-1	194	208	233	216
Ro-2	136	170	171	209
Ro-3	175	208	209	218

The modified Stefan's solution is over-evaluating the frost depth of all sections for 2016-17 winter, with wider variation as the aggregates get finer. For winter 2017-18, the frost depth in section Ro-1 was underestimated, and overestimated in sections Ro-2 and Ro-3. Even if some centimetres of difference can be considered acceptable for design purposes, one should be careful when using this solution. In fact, the necessary FI_s to penetrate the high-water content silt below the frost protection layer implies large FI_s bias. Field observations found that FI_s of roughly 1000 to 1500 $^oC \cdot h$ was necessary to penetrate each cm of silt below the frost protection layers. There is therefore an important difference between calculated and observed depth in terms of the necessary freezing index. Determination of the depth of cooling influence it is not obvious to evaluate. This depth was set at 2 m for our analysis, but was difficult to assess due to the temperature variation on site.

An important observation concerned the use of the mean annual temperature in the equation. The mean annual temperature reference in the N200 Handbook for sites such as Røros is close to 0°C, meaning that frost depth is more or less evaluated without the heat capacity effect, as in the basic Stefan solution. The following short analysis is complementary to Paper II. It was not presented at the conference due to the restricted number of pages allowed, but is judged an interesting contribution.

Mean annual temperature should reflect the temperature of the soil state. Nordal (1989) evaluates a different frost penetration methodology from which equations 1 and 2 in this thesis have been taken. He also presents the Watzinger solution, which proposes to take into account the mean ground temperature before the freezing season begins rather than mean annual temperature, as it reflects the thermal state of the ground better. A small comparison of calculated frost depth was performed using the freezing indexes from winters 2016-17 and 2017-18 with mean annual temperature (T_{ma}) at Røros as stated in the N200 Handbook (=0.2°C) and mean temperature before the freezing season (T_{bf}). The mean annual temperature from the standard was chosen as this would be legitimate to use for the frost design of a new road. The depth of cooling influence was two meters. The temperatures before the freezing season (at the beginning of November) in both winters were set to 4.5, 5.4 and 4.9 °C for Ro-1, Ro-2 and Ro-3 respectively. The results are presented in Table 11.

Table 11: Frost depth (FD) calculated using mean annual temperature (0.2°C) and mean temperature before the freezing season (4.5, 5.4 and 4.9°C), compared to those observed on site in Ro-1, Ro-2 and Ro-3

	2016-2017			2017-2018		
	T_{ma}	T_{bf}	Observed	T_{ma}	T_{bf}	Observed
	FD (cm)	FD (cm)	(cm)	FD (cm)	FD (cm)	(cm)
Ro-1	214	180	194	222	209	233
Ro-2	195	151	136	216	190	171
Ro-3	215	179	175	225	210	209

According to the results, it can be observed that the use of the mean annual temperature before freezing gave better estimations. The use of the mean annual temperature before the freezing season began seemed therefore promising, at least for a test site such as Røros with a low mean annual temperature. Further studies are needed to assess the validity of this method.

The last part of Paper II presents the frost protection capacity of Ro-1, Ro-2 and Ro-3's different frost protection layers. Frost protection capacity is proposed as a performance index defined by the surface freezing index necessary for the frost front to penetrate 1 cm in the frost protection layer. The necessary FI_s from the top of each of the three different frost protection layers to a depth of 50 cm was used to calculate βs as the frost penetration was mainly linear and therefore judged not to be significantly affected by the cooling of the sub-grade silt. Frost protection capacity can provide a quick overview of the three different frost protection layers and roughly estimate the frost depth. The results are presented in Table 12.

Table 12: Frost protection capacity, β (FIs/cm), for winters 2016-17 and 2017-18, and average values for 2016-18

	2016-17 β (FIs/cm)	2017-18 β (FIs/cm)	2016-2018 β (FIs/cm)
Ro-1 (20-120 mm, coarse, open graded)	95	75	85
Ro-2 (0-32 mm, fine, well graded)	395	485	443
Ro-3 (0-120 mm, coarse, well graded)	265	240	253

It takes a surface freezing index contribution as low as 950 °C·h to penetrate 10 cm in a coarse, open graded frost protection layer; 2530 °C·h in a coarse, well graded frost protection layer; and as much as 4430 °C·h in a fine, well graded frost protection layer.

Frost depth estimation with the modified Stefan's solution and with frost protection capacity have the same limitations for analytic purposes as they do not include the wind factor or solar radiation. These climatic factors can be taken into account when correcting the freezing index using the methodology proposed by Dysli (1991).

In summary, the thermal performance of three differently graded frost protection layers at the Røros test site was investigated for winters 2016-17 and 2017-18. All the road structures prevented frost penetrating the subgrade in winter 2016-17, when a surface freezing index of 22630 °C·h was observed. In the winter

of 2017-18, only Ro-2 (fine, well graded 0-32 mm) prevented frost front to penetrate the sub-grade soil when a surface freezing index of 36683 °C·h was observed. Most of Norway's coastal and populated areas have an F_{100} of ≈3000 - 4000 °C·h (i.e. Bergen, Ålesund, Stavanger) to ≈19000 - 24000 °C·h (i.e. Trondheim, Oslo, Narvik, Tromsø). Therefore the frost protection layers with the best cost-benefit ratios would seem to be those composed of coarser, open graded crushed rock material, although the potential for convective effects must be included in the design.

Frost depth estimation using the contributive freezing index tended to over-estimate maximal frost depth, even with a fully characterized site. Fortunately, over-estimation of frost depth is on the safe side from a frost protection point of view, but over-design can have serious budgetary repercussions for a project. It was shown that over-estimation of frost depth can result in a significant bias when considering the contributive freezing index. For example, in Ro-3, overestimating the frost depth by 9 cm in the calculation represents ≈ 9000 °C·h of error in contributive freezing index, so almost 25% more of the 36683 °C·h for the whole 2017-18 winter.

Part of the overestimation in calculation comes from the initial thermal state of the soil under consideration. It was found that most realistic frost depth results were achieved when using mean road temperature before the freezing season, season which began November 1st at Røros.

Finally, the concept of frost protection capacity was proposed for the quick evaluation of frost penetration into a frost protection layer. This concept allows the rough estimation of frost penetration of the frost protection layer and comparison of the relative performances of different crushed rock aggregates **and** other materials.

Paper B: In situ thermal performance of lightweight aggregates expanded clay and foam glass in road structures.

Ro-4, Ro-5 and Ro-6 were also analyzed and the results presented in 2019 at the 18th International Conference on Cold Region Engineering and the 8th Canadian Permafrost Conference. The paper is presented in the annex to this thesis as Paper B. The main conclusion was that the frost front was prevented from reaching the frost protection layer below the insulation layer of all three sections, raising the question of the necessity for a lower frost protection layer when using lightweight aggregates and the N200's decisional chart.

6.3 MODELLING: SSR model assessment for thick-layered road structures

The modelling works is the last study carried out in this research. It wrap up the use of the segregation potential and the analysis of the Røros test site for design optimisation purposes. The SSR model analysis of Saarelainen (1992) and Saarelainen et al. (2015) gave good concordance between modelled and in situ observations. The Quebec Ministry of Transportation incorporated the SSR in its CHAUSSEE 2 software following extensive model validation (St-Laurent, 2006). CHAUSSEE 2's SSR model calculations are the same as those in the I3C-ME software.

6.3.1 Climatic

The winter of 2017-18 was modelled using the I3C-ME software for road sections 1 to 3, testing different grading in frost protection layers. Climatic data for winter 2017-18 was used as it was the coldest winter recorded over the three-year monitoring period. Temperatures were calibrated from thermocouples using moisture content sensors when freezing occurred, as they had not been calibrated prior to installation. The calibrated temperatures produced FI_s values slightly lower than those presented in Paper II, but still of the same magnitude (e.g. 35064 vs 36683 °C·h). The freezing index correction was validated with the data set of temperatures at Røros airport, situated nearby, and with a second temperature sensor (thermistor) situated on site. FI_s were calculated using the mean daily surface temperature (MDST). The mean daily air and surface temperature during the winter season were almost identical, with an n-factor of 0.9955, as Figure 49 shows.

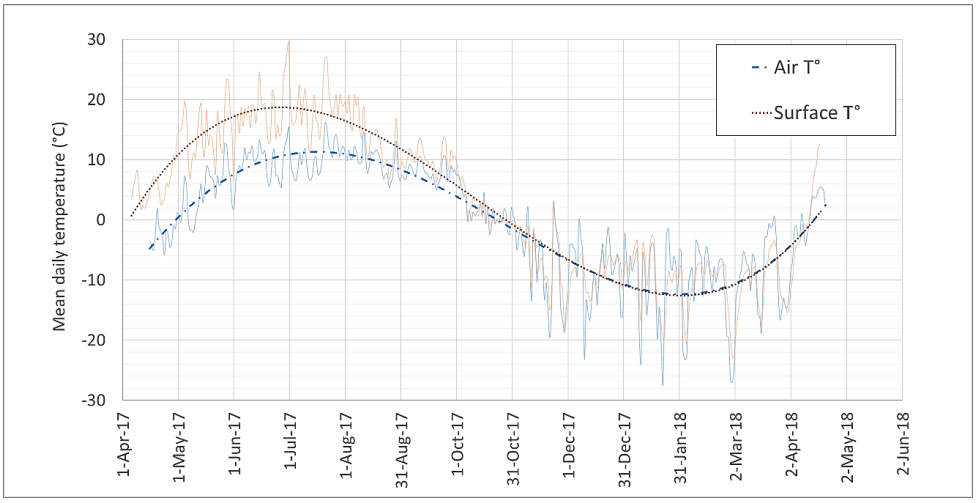

Figure 49: Mean daily air and surface temperatures, April 2017 to May 2018, Røros test site

Samples from the different layers were taken from the test site for further analysis. The rock's mineralogy, dry density (ρ_d), particle density (ρ_s) and thermal conductivity of solid particles (λ_s) were measured under laboratory conditions, mostly by Rieksts (2018). The water content of the different materials was computed from the moisture content sensors on site. In Ro-3's frost protection layer the sensors were installed in a finer matrix and the relative water content was interpolated for a coarser matrix and therefore subject to greater uncertainties. A default water content value was used for sub-base in all sections and for Ro-1's frost protection layer. The frozen and unfrozen thermal conductivities of crushed rock and silt were estimated using laboratory experimentation and the Côté-Konrad (2006) generalized model included in the I3C-ME software. Level measurements taken during the construction of the test site allowed accurate determination of the layer thicknesses in each road section. As the frost did not penetrate the silt layer, no subgrade properties were taken into account in the model. Table 13 lists the porosity, dry density, water content, solid particle thermal conductivity and layer thickness of each

material. The densities of solid particles (ρ_s) were 2788 kg/m^3 and 2750 kg/m^3 for the crushed rock aggregates and silt respectively. The asphalt concrete thickness was revised at 8 cm of thickness, following observation on site.

Table 13: Material properties, road section Ro-1, Ro-2 and Ro-3, Røros test site

	Porosity (n)	ρ_d (kg/m^3)	w (%)	λ_s (W/m·°C)	Ro-1 (cm)	Ro-2 (cm)	Ro-3 (cm)
Asphalt	0.07	2400	0.5	2.5	8	8	8
Base	0.29	1980	4	3.3	23	19	17
Sub-base	0.42	1623	1	3.3	81	84	87
FPL – open graded	0.45	1535	1	3.3	100	---	---
FPL – fine graded	0.24	2116	5.5	3.3	---	90	---
FPL – typical grading	0.36	1780	2	3.3	---	---	93
Silt	0.41	1600	25.0	2.6	50	50	50

6.3.2 Frost depth

The daily temperature entry in the I3C-ME software was used to estimate frost depth, as it showed a better fit with field than methods using sinusoidal simulation and mean monthly temperatures. The first attempt to model frost penetration as a function of time gave good results for total frost depth penetration. However, the rates of frost penetration in crushed rock aggregates were slightly different from those observed in the field and therefore frost penetration rates were compiled for each road section using i) estimated parameters (see **Error! Reference source not found.**) and ii) parameters back calculated to fit the values observed on site. The back calculation of the parameters of the different frost protection layers (FPL) were applied to the water content (Ro-1 and Ro-3) and dry density (Ro-3) to fit the observed frost depths at the test site. The FPLs of Ro-1 and Ro-3 were divided into two distinct layers, allowing for adjustment of the water content in the upper and lower parts, as suggested by Gustavsson and Saarelainen (pers. comm., 2018) when using the SSR. The lower part of the FPL was set to 0.4 m for Ro-1 and 0.3 m for Ro-3. No variation of water content was imposed for Ro-2. The back calculated parameters and initial estimations are presented in Table 14. Where two numbers are separated by a slash, the left-hand number is for the upper part and the right-hand number for the lower part of the frost protection layer.

Table 14: Estimated and adjusted water content and dry density of frost protection layer in each road section

Section (FPL)	Water content (%)		Dry density (kg/m^3)	
	est.	adj.	est.	adj.
Ro-1	1	1.5/2.5	1535	1535
Ro-2	5.5	5.5	2116	2116

Ro-3	2	4/4.5	1780	1850

The back calculated parameters for the different FPLs were considered within realistic limits compared to references in the literature (Frost I Jord, 1976). The back calculated water content in Ro-1 seemed a little high but was acceptable, showing that water content in open, coarse graded crushed rock aggregates may sometimes be underestimated. The back calculated water content for Ro-3 was as expected, as the crushed rock material used in that section was more or less the same as the base layer, which was measured as 4% on site. The slight variation in the dry density of Ro-3 was to accommodate the frost penetration rate to the field observation.

Figures 50, 51 and 52 present the measured and modelled frost depths over time for Ro-1, Ro-2 and Ro-3. Each figure presents different frost depth curves: observed on site, with first estimation values, and with back calculated values (except for Ro-2). Ro-1 also presents frost depth including the convective effect, as discussed below.

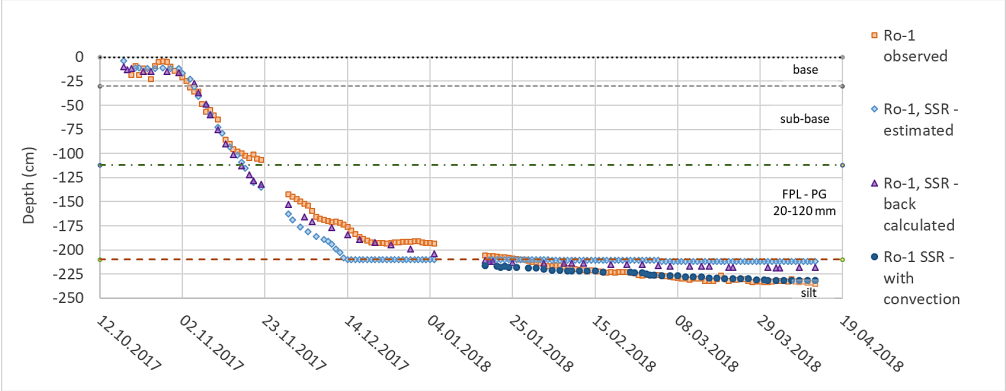

Figure 50: Measured and estimated frost penetration in function of time in road section Ro-1, Røros

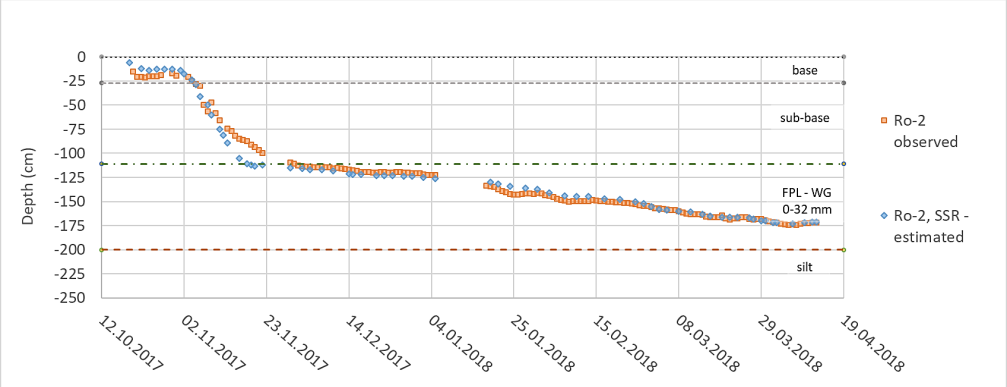

Figure 51: Measured and estimated frost penetration in function of time in road section Ro-2, Røros

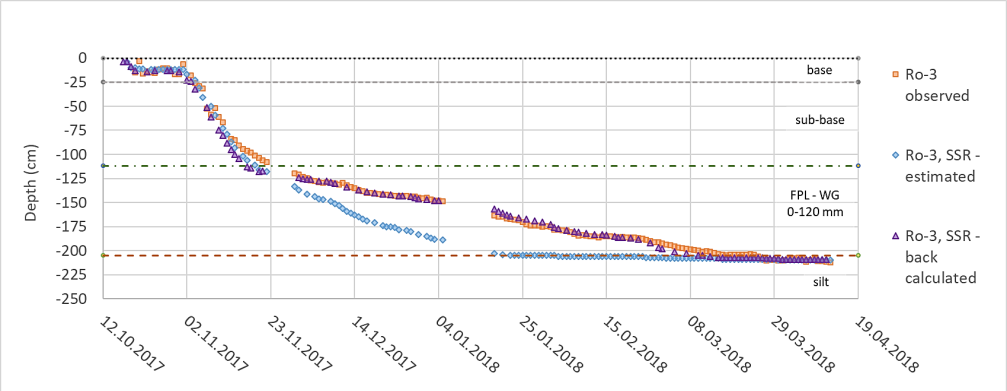

Figure 52: Measured and esyimated frost penetration in function of time in road section Ro-3, Røros

Table 15 presents the maximum frost depth i) observed in situ, ii) calculated with the SSR model using the first parameter estimation presented in Table 13, and iii) calculated using the SSR model with the back calculated parameters to fit in-situ observation.

Table 15: Maximum frost depth from on-site measurement, and from SSR model using estimated and back-calculated water content (Ro-1 and Ro-3) and dry density (Ro-3)

	Maximum frost depth (m)		
	Test site	$SSR_{estim.}$	$SSR_{back\ calculated}$
Ro-1	2.35	2.12	2.19/2.32*
Ro-2	1.74	1.73	n/a
Ro-3	2.12	2.10	2.09

*: with convection

The maximum frost depth penetration in Ro-1, whose frost protection layer consists of an open and coarse gradation, was difficult to model. Rieksts (2018) has shown that convective heat transfer probably occurred in Ro-1, making it difficult to emulate a homogeneous frost penetration. As convection appears only in strong temperature gradient conditions in open-coarse aggregates, the frost penetration rate was probably influenced by both conductive and convective heat transfer to an unknown extent. The winter of 2017-18 was extremely cold from mid-January onwards. The hypothesis is that the frost penetration rate was not affected by convection before mid-January, and then the effect became significant, leading to a high frost rate and maximum frost penetration during the second half of the winter. Convective heat transfer is not considered in the SSR model. It can be approximated by estimating an equivalent thermal conductivity that integrates the contribution of convective heat transfer with conductive thermal conductivity. It was possible to fit the modelled maximum frost depth with the depth observed using an equivalent frozen thermal conductivity of 0.8, 0.85 and 1.3 W/m·°C for the sub-base, the upper and the lower parts of the frost protection layers, respectively. The proposed equivalent thermal conductivity

values are within the range used by Rieksts (2018) for modelling the convective effect in Ro-1. The calculated frost depth using the equivalent frozen thermal conductivity is 2.32 m.

No back calculation was needed to model Ro-2, whose frost protection layer is composed of a crushed rock similar to the material used in the base layer, i.e. a well graded granular material. The first estimation of parameters gave good results since the frost penetration rate and maximum frost depth modelled by the SSR match the observations.

The results of the Ro-3 SSR model were good for calculating maximum frost depth when using the initial estimated values of the input parameters. However, the frost penetration rate was not considered realistic, as it was much more rapid than observed on site. Back calculation of water content suggested 4 and 4.5% for the upper and lower frost protection layers, and a slight increase of 70 kg/m^3 in the dry density of the frost protection layer allowed for a better fit between the modeled and the observed frost penetration rates. These back calculated values appear to be realistic and in agreement with the frost penetration rate observed on site.

It was observed that the most sensitive parameters were water content and porosity, and indirectly, dry density. A slight change in the amount of water content has a significant impact on the overall frost penetration rate and final maximum penetration. One significant finding when varying the water content in the model was that higher water content in material with low water content such as crushed rock did not always have the direct effect of reducing the maximal frost depth. The latent heat effect was observed to slow the frost penetration rate to a certain degree, but the consequent rise in the thermal conductivity of the frozen layers directly enhanced heat extraction, leading to deeper frost penetration. This proved even more critical in layers with very low water content such as the sub-base. The frost front quickly penetrates an unbound crushed rock layer with low water content, which somehow acts as an insulation layer afterwards. For example, an increase from 1% to 2% in water content in the Ro-2 sub-base layer led to a maximum change in the depth of the frost from 1.76 to 2.03 m for winter 2017-18, which is significant. This can be explained by the fact that the frozen thermal conductivity of the sub-base layer increased from ≈0.5 to 0.7 W/°C·m, helping to extract heat faster. This highlights the importance of assessing water content and porosity precisely to increase the reliability of modelling results. More work is needed to assess the soil water characteristic curves (SWCC) of crushed rock aggregates, and more specifically open-coarse aggregates, which to my knowledge are relatively poorly documented. Ongoing work at the E6 test site near Trondheim, where seven different pavement structures are being monitored, is a step towards better assessment and validation of pavement parameters relevant to thermal modelling.

6.3.3 Frost heave

Frost heave tests to determine the segregation potential of the 0-4 mm fraction of the silt and of the Legruvbakken quarry slate were performed using the NTNU frost heave cell. The segregation potential of the silt and the slate were determined as 8.1 and 2.7 mm^2/°C·h respectively. The result for the silt was within expected values for a soil with a high frost susceptibility. The segregation potential for the slate was lower than that of other 0-4 mm crushed rock aggregates studied in Paper I. The segregation potential

value obtained is around half of the average value obtained for rocks with similar mineralogy in the investigation of the segregation potential of crushed rock. The results of frost heave as a function of time during the test showed atypical behaviour, as if it were being restrained. Therefore the segregation potential of the different crushed rock aggregates layers was back calculated from the test site observations.

The magnitude of frost heave on the site was intended to be measured continuously by LVDTs installed at different locations in the soil and frost protection layers, with one in each silt layer and one in the frost protection layer of Ro-2. The sensors stopped emitting signals only a few months after their installation. Heave was therefore computed using a surveyor's level during test-site visits in January, March and April 2018. Figure 53 presents the SSR model with back calculated SP values and in situ frost heave evolution on site.

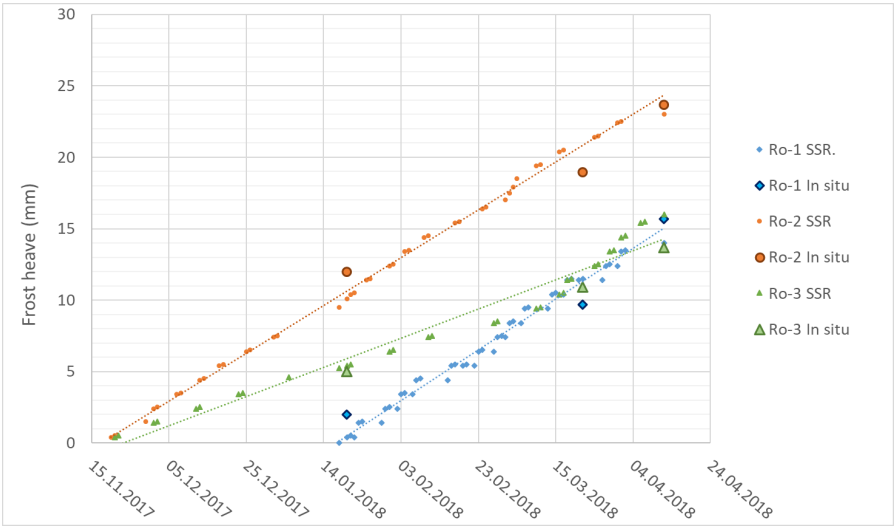

Figure 53: Frost heave measured at the Røros site and estimated using the SSR model at different times during winter 2017-18

Table 16 presents the maximum frost heave observed in situ, calculated with the SSR model using the first parameter estimation presented in Table 13, and calculated using the SSR model with back calculated segregation potentials to fit in-situ frost heave observation.

Table 16: Frost heave measured in situ and with the SSR model, using estimated and back calculated water content (Ro-1 and Ro-3), dry density (Ro-3) and SPs

		Total heave (mm)	
	In situ	$SSR_{estim.}$	$SSR_{back\ calculated}$
Ro-1	16	14	14
Ro-2	24	0	23
Ro-3	14	11	16

The silt SP_0 modelled is similar to that measured in laboratory conditions, i.e. 8.1 $mm^2/°C·h$. The different FPL SP_0s were back calculated from field observations using the SSR model. Table 17 presents the estimated and adjusted SP_0 values for each FPL.

Table 17: Estimated and adjusted segregation potential of the different frost protection layers without overburden pressure (SP_0)

	SP_0 ($mm^2/°C·h$)	
FPL	est.	adj.
Ro-1	0	0
Ro-2	0	4.1/4.1
Ro-3	0	1.3/1.3

As expected, the SP_0 of the crushed rock aggregates measured in the laboratory did not allow to fit in situ frost heave observations to the predicted values. On the other hand, the back calculated SP for Ro-2 was on the high side for a 0-32 mm grading material. However, as the portion of the material smaller than 4 mm was lost during sieving there was no possibility of assessing the estimated SP_0 from the model using the fine content. The validation of the modelled SP_0 was done using SP_0 results from one frost heave test on 0-20 mm crushed granite aggregates with similar fine content. The SP_0 magnitude showed value of 3.4 $mm^2/°C·h$ for fine content (<63 µm) of 6.4%. The SP as a function of time for this crushed rock aggregate is presented in Figure 54.

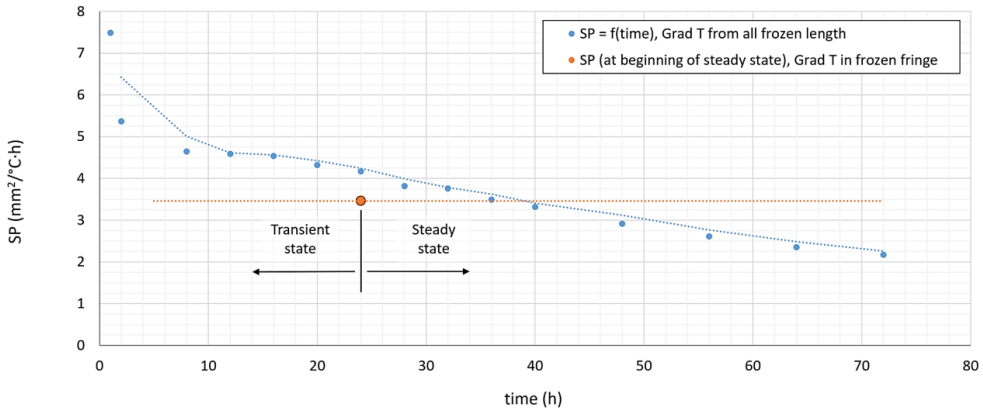

Figure 54: Evolution of segregation potential in 0-20 mm grading of crushed granite aggregate

The SP parameter is applicable when the frost front is in a steady state. As it can be observed in Figure 54, the SP as defined by Konrad (1980) is constant (orange line). However, Konrad (1980) demonstrates that the SP will not be constant in the transient state due to the cryosuction profile and the thickness of the frozen fringe (indirectly, the permeability of the fringe). The SP in function of time was plotted in to observe the SP's evolution as the frost front penetrated the sample (blue line), using the Finnish method. The Finnish method for determining SP uses the SP vs time plot and considers the SP when it become constant, which happens when reaching the steady state. It determines the SP using the thermal gradient of the

total frozen length of the sample rather than the gradient in the frozen fringe. This leads to higher overall SP values (Figure 54), which typically start from 0 with a rapid progression to maximum values and then decline at different rates, depending on the nature of the material, to finally stabilize when reaching a steady state. This means that when the frost front progresses, i.e. in a transient state, the SP can be higher than that obtained in the steady state. This means that the SP in function, measured either in a frost heave test or in situ, could be used to evaluate SP in the transient state.

It was observed that the SP changed significantly as a function of time and temperature regime and a mean value of 4.1 $mm^2/°C·h$ for the Ro-2's frost protection layer seemed realistic. The fact that the SP of crushed rock aggregates varies considerably, as also observed by Zhang et al. (2019), makes it a challenge for the designer to adopt a representative SP when there is no possibility of back calculating from field measurements. Future investigations should include the application of typical transient SP values to thick pavement structures as used in Norway, and in natural soils in thinner structures.

6.3.4 Ground thermal heat flow

The ground thermal gradient (∇T_+) at the frost front was computed for all the freezing seasons. The values were used to assess the Scandinavian ∇T_+ as a function of the mean annual temperature and to back-calculate heat flow q_+. The early February 2018 results were added to Côté and Konrad (2009) graph for comparison. The gradients were calculated using an average value for ±3 days from February 1, giving 1.91, 1.72 and 1.68 °C/m for Ro-1, Ro-2 and Ro-3 respectively (Figure 55). The calculated gradients were observed to be within the range of the Scandinavian ∇T_+ proposed by Skaven-Haug (1971).

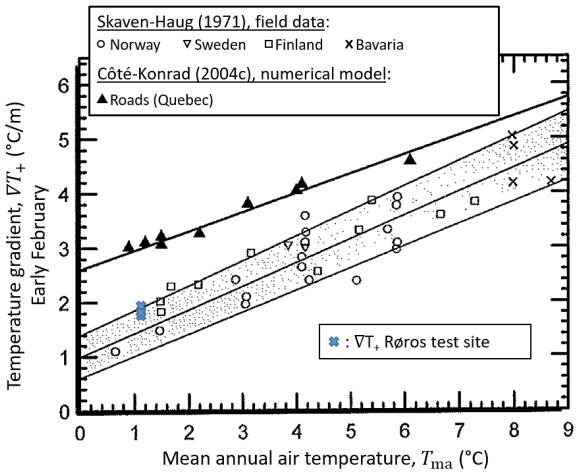

Figure 55: Calculated temperature gradient at the Røros test site, early February, 2018 (modified from Côté and Konrad, 2009)

As the I3C-ME software does not allow modification of the modelled thermal gradient, CHAUSSEE2 was used to find the modelled ∇T_+. An initial gradient of 1.71 °C/m was automatically calculated and corrected using the ground heating coefficient S. The ground heating coefficient in the I3C-ME SSR model is linearly derived from intensities proposed by Saarelainen (1992), and was equal to 1 for November to 0.7 for March. Calculated S for December, January, February and March was 0.66, 0.54, 0.48 and 0.41 respectively. It was observed that the modelled ∇T_+ was lower than the field values at the frost front. The ∇T_+ from the silt layer is added in Figure *56*, which shows that the default ∇T_+ in CHAUSSEE2 and therefore in I3C-ME uses the ∇T_+ in the subgrade layer. Then the ∇T_+ measured at the frost front for all sections were significantly higher at the beginning of the season than what is proposed in the CHAUSSEE2 model, which will affects the frost penetration rate, and should be integrated into the q+ calculation.

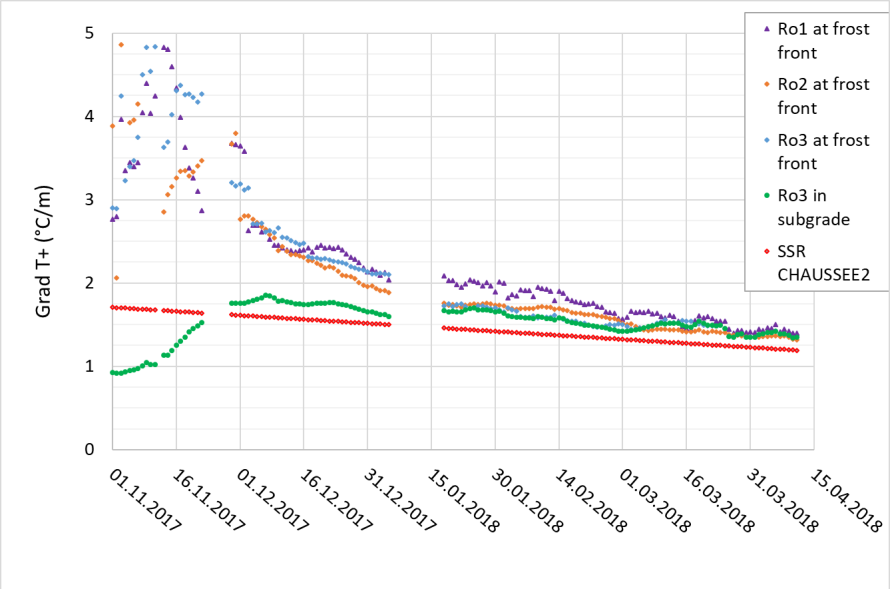

Figure 56: Thermal gradient according to time at Røros test site for winter 2017-18

Côté and Konrad (2009) developed the Canadian (Quebec) model by directly calculating heat flow at the freezing front (q+), which is physically more close to field observations. They demonstrated that soil type and stratigraphy had a negligible effect on the geothermal heat flux at the freezing front, therefore reducing the necessary input to time of year and mean annual temperature. However, most research in Finland and Canada has been on structures with relatively thin layers. The direct uses of the q+ therefore had to be tested and assessed for use in the SSR model for future research on Norwegian conditions.

6.3.5 Design optimization

The SSR model was found to be a good model for assessing frost penetration and heave on the different FPL grading sections at the Røros test site. The thick layers of Norway's road structure have proven efficient at preventing high frost heave in high freezing index conditions. However, due to economic and environmental considerations, thick pavement structures may not be acceptable in the future, in which case the SSR model is likely to prove a powerful tool for optimizing layer thickness based on the material's properties. The concept of allowable frost heave been developed by Quebec, Finnish and Swedish roads Administration. They are presented in Table 18.

Table 18: Allowable frost heave (mm) according to road class (Quebec, Finland), and speed limit in km/h (Sweden). (Doré and Zubeck, 2009; Swedish Road Administration (2004)

Road class	Freeways	National	Regional	Local
Finland	<30	<50	---	<100
Canada	<50	<55	<60	<70

Speed limit	110	100	90	70	<50
Sweden	<20	<50	<80	<120	<160

Finland and Quebec proposed allowable frost heave according to experience and observations. Analytical methods that relates the allowable frost heave to International Roughness Index (IRI) and pavement service are relatively new but with promising outcomes, as presented by Bilodeau and Doré (2013) and Sylvestre (2017).

An analysis of heaving in function of the surface freezing index (FIs) was modelled for Ro-3 section, as presented in Figure 57.

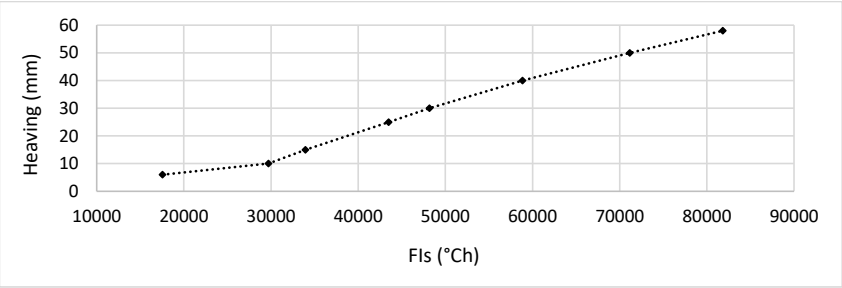

Figure 57: Modelled heaving in function of surface freezing index for Ro-3

This means that a road built like the Ro-3 test section would withstand a winter with 71000 °C·h, which represents more than the 100-year return period design of 62000 °C·h, when allowing 50 mm of frost heave. Ro-3 would withstand a freezing index of 48000 °C·h when allowing 30 mm of frost heave. It is

therefore possible to optimize the structure, significantly reducing both the cost and the environmental impact of road building. Therefore a second analysis of heaving in function the frost protection layer thickness was modelled for the using the 2017-18 surface freezing index (35000 °C·h), as presented in Figure 58.

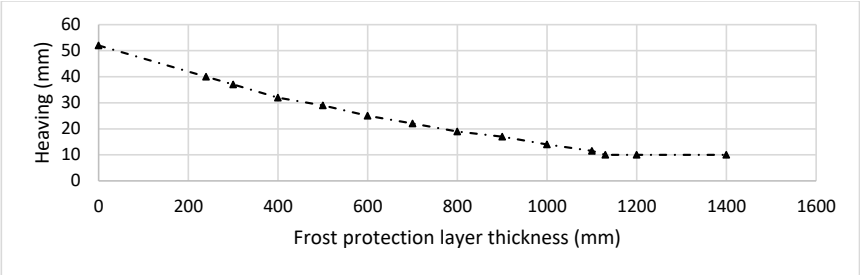

Figure 58: Modelled heaving in function of the frost protection layer thickness for Ro-3

Here it was observed that for a surface freezing index ≈ 35000 °C·h and an allowable frost heave of 50 mm, the thickness of frost protection layer could be reduced from 1 to 0.1 meters, therefore almost removing it completely. For 30 mm of allowable frost heave, the frost protection layer could be reduced from 1 to 0.4 m. This would considerably reduce the cost of such a project and provide confidence in a tolerable amount of heave that would not significantly affect the integrity of the pavement. For sensitive projects with no tolerance for frost heave such as high speed train lines, the NPRA procedure for preventing the frost front penetrating the subgrade and tight control of the frost susceptibility of the materials used is suggested. For other projects, standardizing the allowed frost heave is suggested and then using the SSR model to assess maximum frost depth and heave using sensitivity analysis, mainly of water content, dry densities and ground heat flow variation.

In summary, the SSR model was run using the I3C-ME software with data from three road sections at the Røros test site. The model was run with data parameters measured in the laboratory from crushed rock aggregates and silt, i.e. reliable and precise data. The SSR model was found to be applicable for the evaluation of frost depth and frost heave in thick-layered road structures. It was possible to back calculate key parameters such as water content, dry density (porosity), thermal conductivity and segregation potential from a site. The segregation potential estimated in laboratory tests using a multi-ring apparatus was found to be accurate for the determination of frost susceptibility and estimation of frost heave at steady state, i.e. when the frost front stabilizes in depth. Use of a laboratory segregation potential function was found necessary in transient regimes to evaluate a realistic segregation potential value for the model, as it proved to be higher than the segregation potential at steady state in this case. This study has found that the thermal gradient ∇T_+ in CHAUSSEE2 (and I3C-ME) is evaluated for the underlying subgrade. This is helpful for pavement structures with thin layers but could lead to bias in the evaluation of frost heave in the upper layers of thick-layered pavement structures. Direct evaluation of the ground heat flux q+ is therefore recommended, as applied in Quebec. Finally, the SSR model showed its capacity for optimizing design. The potential economic and environmental gains from such optimization will help to meet future challenges in road design.

7. CONCLUSION

Several conclusions can be drawn from this study. The conclusions for frost heave susceptibility of crushed rock aggregates, for the estimation of the segregation potential of crushed rock aggregates using index parameters, the investigation

The frost susceptibility of crushed rock aggregates using the segregation potential theory was expanded for different, mostly good quality rock type typically encountered in Norway. Their segregation potential proven to be medium to high, from 60 to 197 mm2/°C·h for 0-4 mm crushed rocks containing between 12.5 to 30.7 % of fine <63 µm. The % of fines < 63 µm and <20 µm found to not accurately relates to the segregation potential magnitudes. The % of fine <2 µm measured from the fraction < 75 µm gave the better correlation between % fine and the frost heave susceptibility of a material. I was than proven that the grain-sized base criterion have to be used with care. No conclusions were achieved from the mineral content of the first frost heave tests, but the ones run for the assessment of the use of the normalized SP concept showed that mineral enrichment in the fine fraction affected the segregation potential of crushed rocks. The segregation potential showed to be 17.6% higher for crushed gabbro between the blasted material and the one processed in three crushing phases. Also, the segregation potential showed to be between 59.3 to 135% higher for crushed gneiss from when comparing first stage crushing to fourth stage crushing phase.

The estimation of the segregation potential of 0-4 mm crushed rock aggregates using the normalized SP was investigated on 23 different samples of 7 different minerals. The method uses the following index parameters: the average particle size of the fine <75 µm (d_{50ff}), the specific surface area of the fine <75 µm (Ss), the liquid limit (w_L) and the water content of the samples. All index were measured in laboratory conditions. In parallel, frost heave tests were performed on the same materials and their segregation potential determined from a graphical solution. The investigation shown that the normalized SP concept gave a good estimation of the segregation potential when compared to those determined from the frost heave tests, in ca ± 15 % margin. The analysis of the specific surface area shown that there is a possibility to directly estimate the segregation from the specific surface area only, and an equation was presented. It was shown that the crushed rock aggregates with specific surface >8 m^2/g in this study were from early stage crushing, therefore potentially having weak mineral enrichment of the fine <75 µm at early crushing stage and/ or asperities and micro-cracking of crushed particles again, at an early crushing stage, leading to overestimation by the methylene blue test. The estimation of the segregation potential of crushed rock aggregates using parameters index would save time and money in road and railway construction projects.

The estimation of frost heave for transport infrastructure is tightly link to a good estimation of the frost depth in function of time, as the different layers will have different frost heave susceptibility. The thermal performance of three different grading of frost protection layers were investigated at the test site for both winters 2016-17 and 2017-18. All the road structures prevented the frost to penetrate the subgrade for winter 2016-17, where a surface freezing index of 22630 °C·h was observed. For 2017-18 winter, only the Ro-2 section (fine, well graded 0-32 mm) prevented the frost to penetrate in the sub-grade soil for a surface freezing index of 36683 °C·h, but Ro-3 was judged to perform satisfactorily. The design of the three sections would therefore resist a 100 years period of return freezing index for most populated area as Trondheim, Oslo, Narvik and Tromsø. Therefore, best cost-benefit frost protection layers would seem to be on the coarser, open graded crushed rock material, but convective effects might happen and have to

be taken into the design. The frost depth estimation using the contributive freezing index tended to over estimate the maximal depth, even with a fully characterized site. It was shown that the over estimation in depth can result in a significant bias when analyzing the overestimation by the contributive freezing index, leading to 25% overestimation for Ro-3 in winter 2017-18. A part of the overestimation in calculation comes from the initial thermal state of the soil that is considered. It was shown that most realistic frost depth results were achieved when using the mean road temperature before the freezing season, which was set to November 1 at Røros.

Finally, the SSR model was run with the I3C-ME software for the same three road sections were frost depth was investigated at the test site, Ro-1,2 and 3. The model was run with parameters measured in laboratory from crushed rock aggregates and silt. It was found that the SSR model proven to be applicable for the evaluation of frost depth and frost heave fro thick-layered road structures. It was found that key parameters as water content, dry density (porosity), thermal conductivity and segregation potential can be back calculated from a site, therefore being also useful to apply on the existent road network for rehabilitation purposes. Water content had to be adjusted to fit the model in Ro-1 and Ro-3 sections. No water content adjustment was necessary in Ro-2. It was found that the segregation potential estimated in laboratory tests using a multi-ring apparatus was accurate for the determination of frost susceptibility and estimation of frost heave at steady state, i.e. when the frost front stabilize in depth. Use of a segregation potential function from the laboratory was found necessary in transient regimes to evaluate a realistic segregation potential value for the model, since it proven to be higher than the segregation potential at steady state in this case. This study has found that the thermal gradient ∇T_+ is evaluated in the subgrade. This is helpful for pavement structures with thin layers but could lead to a bias in the evaluation of frost heave in the upper layers of thick-layered pavement structures. Finally, the SSR model showed its capacity for optimization design purposes. Economic and environmental gain from such optimization answers to future challenges in road design.

8. REFERENCES

Aldrich, H.P and Paynter, H.M. (1953). First interim report, analytical studies of freezing and thawing in soils. Arctic construction and frost effect laboratory, New England division, Corps of Engineers, ACFEL. Technical report 42.

Bilodeau, J.P. (2009). *Optimisation de la granulométrie des matériaux granulaires de fondation des chaussées.* Ph.D. Thesis, Department of Civil Engineering, Université Laval, Quebec City, Canada (*In French*).

Bilodeau, J.P. and Doré, G. (2013). *A new pavement design procedure for frost protection in seasonal frost areas*. Bearing capacity of roads, railways and airfields: proceedings of the ninth International Conference on the Bearing Capacity of Roads, Railways and Airfields: Trondheim, Norway 25-27 June 2013. pp 299-308.

Brandl, h. (2008). *Freezing-thawing behaviour of soils and unbound road layers*. Slovak Journal of Civil Engineering. Slovak University of Technology. 12 p.

Casagrande, A. (1932). *A new theory of frost heaving: discussion*. Proceedings of US Highway Research Board, Vol. 11, Pt I, pp. 168-172.

Chamberlain, E. J. (1981). *Frost susceptibility of soils – Review of index tests*. CRREL Monograph 81-2. United States Army Corps of Engineers, Cold Regions Research and Engineering Laboratory, Hanover New Hampshire.

Côté, J. and Konrad, J.M. (2009). *A regional model of heat flow under the frost front for the thermal design of pavements in Nordic conditions*. Report S-10 for Quebec road administration. Chaire industrielle de recherche en exploitation des infrastructures soumises au gel CREIG, phase 2. Laval University, Quebec City, Canada. (*In French*).

Côté, J., Konrad, J.-M. (2005). *Thermal conductivity of base-course materials*. Canadian Geotechnical Journal, Vol. 42, 61 -78.

Côté, J., Konrad, J.-M. (2005). *A generalized thermal conductivity model for soils and construction materials*. Canadian Geotechnical Journal, Vol. 42, 443 - 458.

Côté, J., Konrad, J.-M. (2003). *Assessment of the hydraulic characteristics of unsaturated base-course materials: a practical method for pavement engineers*. Canadian Geotechnical Journal, Vol. 40, 121 - 136.

Doré, G. (1997). *Détérioration des chaussées en condition de gel: une nouvelle approche prévisionnelle.* Ph.D. Thesis, Department of Civil Engineering, Université Laval, Quebec City, Canada (*In French*).

Doré, G., Grellet, D., Richard, C., Bilodeau, J.P., Pérez-Gonzales, E.L. and Barón, M.F. (2019). *Mechanistic-empirical flexible pavement design software: I3C-ME, user manual.* I3C Chair team. Laval University, Quebec City, Canada.

Doré, G. and Zubeck, H.K. (2009). *Cold regions pavement engineering*. American Society of Civil Engineering. Reston, VA.

Dysli, M. (1991). *Le gel et son action sur les sols et les fondations (Frost action on soils and foundations)*. Complément au traité de Génie Civil. École polytechnique fédérale de Lausanne. Presse polytechniques et universitaires Romandes. 250 p. (*In French*)

Federal Highway Administration (2017). Geotechnical Aspects of Pavement Reference Manual. Chap.7. U.S. Department of Transportation. Revision of 2017/06/27. https://www.fhwa.dot.gov/engineering/geotech/pubs/05037/07c.cfm.

FROST I JORD (1976). *Sikring mot teleskader*. The Royal Norwegian Council for scientific and industrial research and the Public Road Administration's Committee on frost action in soils. Nr.17, Nov. 1976. Oslo (*In Norwegian*).

GEO365 (2015). *Gneiss til pukk*. Halfdan Carstens (author). (*In Norwegian*). https://geo365.no/bergindustri/gneis-til-pukk/

Håndbok N200 (2018 & 2014). *Vegbygging.* Statens Vegvesen Handbook series, National Public Road Administration, Norway (*In Norwegian*).

Håndbok R210 (2016). *Laboratorieundersøkelser.* Statens Vegvesen Handbook series, National Public Road Administration, Norway (*In Norwegian*).

Hoff, I., Watn, A., Øiseth, E., Emdal, A. and Amundsgård (2002). *Light weight aggregate (LWA) used in road pavement*. Sixth International conference on the Bearing Capacity of Roads, Railways and Airfields, Lisbon, Portugal, 24-26 June 2002. pp. 1013-1022.

Knuttson, S., Domaschuk, L. and Chandler, N. (1985). *Analysis of large scale laboratory and in situ frost heave tests*. IV International symposium on ground freezing. Sapporo, Japan. 65-70.

Konrad, J.M. (1980). *Frost heave mechanics*. Ph.D. Thesis. Department of Civil Engineering, University of Alberta.

Konrad, J.M. (1987). *Proceeding for determining the segregation potential of freezing soils*. Geotechnical Testing Journal, Vol.10, No.2, June 1987. 51-58.

Konrad, J.M. (1994). *Frost heave in soils: concepts and engineering.* Sixteenth Canadian Geotechnical colloquium. Canadian Geotechnical Journal, Vol. 31, 223-245.

Konrad, J.M. (1999). *Frost susceptibility related to soil index properties.* Canadian Geotechnical Journal, Vol. 36, 403-417.

Konrad, J.M. (2005). *Estimation of the segregation potential of fine-grained soils using the frost heave response of two reference soils.* Canadian Geotechnical Journal, Vol. 42, 38-50.

Konrad, J.M. (2008). *Freezing-induced water migration in compacted base-course materials.* Canadian Geotechnical Journal, Vol. 45, 895-909.

Konrad, J.M. (2014). Course material of GCI-7076: Géotechnique des regions froides. Department of Civil and Water engineering, Université Laval, Quebec City, Canada (*In French*).

Konrad, J.M. and Lemieux, N. (2005). *Influence of fines on frost heave characteristics of a well-graded base-course material.* Canadian Geotechnical Journal, Vol. 42, 515-527.

Konrad, J.M. and Morgenstern, N.R. (1980). *A mechanistic theory of ice lens formation in fine-grained soils.* Canadian Geotechnical Journal, Vol. 17, 473-486.

Konrad, J.M. and Morgenstern, N.R. (1981). *The segregation potential of a freezing soil.* Canadian Geotechnical Journal, Vol. 18, 482-491.

Konrad, J.M. and Morgenstern, N.R. (1982a). *Prediction of frost heave in the laboratory during transient freezing*. Canadian Geotechnical Journal, Vol. 19, 250-259.

Konrad, J.M. and Morgenstern, N.R. (1982b). *Effects of applied pressure on freezing soils.* Canadian Geotechnical Journal, Vol. 19, 494-505.

Konrad, J.M. and Valencia Gabezas, F.A. (2008). *Caractérisation des particules fines d'un matériau granulaire de foundation par l'essai au bleu de methylene.* Report GCT-2008-01. Presented to: Ministère des Transports du Québec. CREIG phase II Industrial chair, Université Laval, Quebec, Canada. 99 p (*In French*).

LC22-331 (2010). *Détermination du potentiel de ségrégation des sols*. Laboratoire des Chaussées, secteur sols et fondation, Ministère des transports du Québec (MTQ).

Loch, J.P.G. (1978). *Thermodynamic equilibrium between ice and water in porous media*. Soil Science journal, Vol. 126 (2), 77-80.

Mahoney, J.P., Rutherford, M.S. and Hicks, R.G. (1986*). A research summary report: Guidelines for spring highway use restrictions*. Washington State Transportation Center, University of Washington. Research project Y-2811, Task 28.

Nordal, R.S. (1989). Frysedjup i vegkonstruktar (frost depth in roads). Institute of rad and railway construction, Norwegian University of Science and Technology. Notat 522. Revised in 1998 (*In Norwegian*).

Nixon, J.F. (1991). *Discrete ice lens theory for frost heave in soils*. Canadian Geotechnical Journal, Vol. 28, 843-859.

Nurmikolu, A. (2005). *Degradation and frost susceptibility of crushed rock aggregates used in structural layers of railway track.* Ph.D. Thesis. Tampere University of Technology, Publication 567.

Rieke, R.D. (1983). *The role of specific surface area and related index properties in the frost susceptibility of soils*. Master Thesis. Oregon State University.

Rieksts, K. (2018). *Heat transfer characteristics of crushed rock and lightweight aggregate material*. Ph.D. Thesis, Norwegian University of Science and Technology, 2018:228.

Saarelainen, S. (1992). *Modelling frost heaving and frost penetration in soils at some observation sites in Finland: The SSR Model.* Technical Research Center of Finland, VTT publication 95.

Saarelainen, S., Gustavsson, H., Korkiala-Tanttu, L. and Tieaho, I. (2015). *Applying site and laboratory studies to determine frost-heave coefficient*. XVI European conference on soil mechanics and geotechnical engineering, Edinburgh, U.K. Vol.3, 919-924.

Santamarina, J.C., Klein, K.A., Wang, Y.H. and Prencke, E. (2002). *Specific surface: determination and relevance.* Canadian Geotechnical Journal, 39: 233-241.

St-Laurent, D. (2006). *Chaussée 2, Logiciel de dimensionnement des chaussées souples : Guide de l'utilisateur.* Direction générale du laboratoire des chaussées. Ministère des transports du Québec. July 2006, revised in August 2019 (*In French*).

St-Laurent, D. (2012). Routine mechanistic pavement design against frost heave. 15th International conference on cold regions engineering, Quebec City, Canada.

Stenberg, Lars (1994). Design of frost protection in roads. Road and Transport Research Institute, Swedish National Road and Transport Administration. Project 4204004-8.

Skaven-Haug, S. (1971). Frostfundamenters dimensionering, frysevarme og jordvarme. Fost I jord 3. 9 – 27 (*In Norwegian*).

Sylvestre, O. (2017). *Influence du soulèvement au gel sur la durée de vie utile des chaussées*. Master Thesis. Department of Civil and Water Engineering, Université Laval, Quebec City, Canada (*In French*).

Teknisk Ukeblad - Bygg (2010a). *Ny motorvei ødelagt for alltid (New highway destroyed for good)*. Truls Tunmo (author). Teknisk Ukeblad Media AS, Bygg division. (*In Norwegian*). https://www.tu.no/artikler/ny-motorvei-odelagt-for-alltid/238209

Teknisk Ukeblad - Bygg (2010b). - *Vil bedre kjørekomforten (… will improve driving comfort)*. Truls Tunmo (author). Teknisk Ukeblad Media AS, Bygg division. (*In Norwegian*). https://www.tu.no/artikler/vil-bedre-kjorekomforten/241986

Teknisk Ukeblad - Bygg (2014). *Så mye koster det egentlig å bygge vei i Norge (It really costs that much to build a road in Norway)*. Mari Gisvold Solberg (author). Teknisk Ukeblad Media AS, Bygg division. (*In Norwegian*). https://www.tu.no/artikler/sa-mye-koster-det-egentlig-a-bygge-vei-i-norge/231083

Uthus, L., Hermansson, A., Horvli, I. and Hoff, I. (2006). *A study on the influence of water and fines on the deformation properties and frost heave of unbound aggregates*. Cold Regions Engineering – Current Practices in cold Regions Engineering, American Society of Civil Engineers.

Uthus, L. (2007). *Material properties of unbound granular aggregates and the effect on the deformation behaviour*. Paper IV, Ph.D. T*hesis: Deformation properties of unbound granular aggregates. Ph*.D. Thesis. Norwegian University of Science and Technology, department of civil and transport engineering.

Zhang, Y., Korkiala-Tanttu, L.K., Gustavsson, H. and Miksic, A. (2019). Assessment of sustainable use of quarry fines as pavement construction materials: Part I – Description of basic quarry fine properties. Materials journal, Vol.12, Issue 8.

Øiseth, E., Aabøe, R. and Hoff, I. (2006). *Field test comparing frost insulation materials in road construction. 2001*. Cold Regions Engineering 2006: Current practices in cold regions engineering, the 13th International Conference on Cold Regions Engineering, 23–26 July 2006, Orono, Maine, USA.

APPENDIX A – PAPER I

Loranger, B., Hoff, I., Scibilia, E. and Doré, G. (2019a).

Frost heave laboratory investigation on crushed rock aggregates.

Québec 2019: 18th International Conference on Cold Regions Engineering and the 8th Canadian Permafrost Conference. Quebec City, Canada. (August 18th to 22nd 2019).

Frost Heave laboratory investigation on crushed rock aggregates

B. Loranger, Ph.D. Candidate
Norwegian University of Science and Technology, Trondheim, Norway

I. Hoff, Ph.D.
Norwegian University of Science and Technology, Trondheim, Norway

E. Scibilia, Ph.D.
Norwegian University of Science and Technology, Trondheim, Norway

G. Doré, Ph.D.
Université Laval, Quebec City, Quebec, Canada

ABSTRACT: Crushed rock aggregates are widely used for transport infrastructure construction in Norway. During winters 2009/10 and 2010/11, differential frost heave severely affected the Norwegian transport network. Currently there is no system in the Norwegian road design to calculate expected frost heave from sub-grade and crushed rock aggregates. The segregation potential (SP) can be used to estimate heaving according to climatic data with the SSR Model (Saarelainen, 1992). Consequently, The Frost Protection of Roads and Railways project was created in part to improve knowledge about the frost susceptibility sensibility of crushed rock aggregates. The goals of this paper are to a) introduce the Norwegian University of Science and Technology (NTNU) freezing cell apparatus and laboratory methodology b) present soil characterization and SP results of 7 different rock types and c) discuss SP relationship with fine fraction content and mineralogy. A 150 mm diameter by 200 mm high multi-ring frost heave apparatus was used to perform the tests. Samples were frozen from top and hydraulic pressure other than cryosuction was avoided. Temperatures, heaving rate and magnitude, and water mass were recorded for the 96 hours duration of each test. A wide variety of rocks, including granitic gneiss, gneiss, anortosite, granodiorite, slate, gabbro, gneiss and porphyr, was chosen. Fine fraction <63, <20 and <2 μm varies from 12.5% to 25.6%, 7.1% to 14.8% and 0.53% to 2.45% respectively. The SPs varied from 60 to 197 $mm^2/°C \cdot d$. SP results are in accordance with value range showed by Konrad (2005), Konrad and Lemieux (2005), and Nurmikolu (2005) for granitic aggregates. SPs for the other rock type are proposed to be used as reference values. The SP as a function of fine content <2 μm calculated from the <80 μm fraction showed a trend of $R^2 = 0.84$ for this study.

KEY WORDS: Crushed rock, frost heave, multi-ring frost cell, segregation potential, frost susceptibility.

1 INTRODUCTION

One objective of The Frost Protection of Roads and Railways project (FROST) is to improve knowledge about frost susceptibility of crushed rock aggregates. Frost susceptibility refers to the propensity of natural or manufactured aggregates to induce significant ice segregation when

required moisture and freezing conditions are present (Chamberlain, 1981). Three conditions are necessary to experience frost heave: soil frost susceptibility, freezing temperature, and presence of water (Rieke, 1983). High frost susceptibility of fine-grained natural soils, as silt and clays, is established. However, few studies focused on the frost susceptibility of crushed rock aggregates. Those aggregates are widely used in Norway for construction of linear transport infrastructure because of the abundance of resource (tunneling, cuts, and earthwork).
The present study focused on three objectives. The first was to describe laboratory apparatus and methodology, the second was to present index values of tested samples, and finally, the third one was to present the results with a brief discussion using the segregation potential (SP) as a comparative tool. Particular attention was paid to granite/ gneiss of granitic origin as they were the most studied/documented rock type in references consulted. The SP was chosen as frost susceptibility criteria for its simplicity, comparison purposes, and the possibility to evaluate frost heave magnitude using methodology described by Konrad (1999) or Saarelainen (1992).

2 BACKGROUND

Few studies focused on crushed rock material mainly because their frost sensibility was considered low when used as a base layer material. In Norway, crushed rock aggregates are the main construction materials for all layers in transportation infrastructure. A frost protection layer below the sub-base layer is commonly used to prevent frost front to reach the sub-grade. A wide range of particle size distribution can be used into this layer, with no restriction about the mineralogy. There is a knowledge gap concerning frost susceptibility of such materials. The actual criteria described in the Norwegian Road Construction Handbook (Håndbok N200, 2018) use a particles size-distribution classification in four frost susceptibility group, T1 to T4.

Konrad (2005) proposed SPs for six different crushed rock mineralogy: basalt, dolostone, granite, limestone, quartzite, and greywacke. The same year, Konrad and Lemieux (2005) presented SPs of well-graded, crushed rock granite base layer (0-20 mm) as a function of fine content fraction <80 µm and clay fraction (kaolinite) variations. Nurmikolu (2005) presented a thesis on degradation and frost susceptibility of crushed rock aggregates for 0-32 mm railway ballast layers. His study included a considerable amount of frost heave tests that include crushed granite aggregates. Table 1 presents detailed information on materials, particle size distribution (PSD), SP, and percentage of fine.

2.1 Crushed Rock Aggregates

Crushed rock aggregates come from various Norwegian quarries: Aplitt, Hadeland, Hellvik, Legruvbakken, Vassfjell, Lørenskog and Velde. Different laboratory characterizations were completed as particle density (ASTM D854), X-Ray Diffraction (XRD), full particle size distribution (ASTM C136 and ASTM D7928) and grain density (ASTM D854). Samples for frost heave tests were prepared using a steel split mold, where the different crushed rock were intensively compacted in 7 layers using an electrical hammer (Kango 900X) at a water content close to 7%, for reaching an estimated 95-98% of the maximum modified proctor value.

Table 1. Segregation potential of different crushed rock aggregates.

Ref.	Material	PSD (mm)	SP $mm^2/°C \cdot d$	% fine
Konrad 2005	Basalt	< 0.08	329	55% <20 µm; 16% <2 µm
	Dolostone	< 0.08	84	53% <20 µm; 9.5% <2 µm
	Granite	< 0.08	98	38% <20 µm; 6.5% <2 µm
	Limestone 1	< 0.08	98	55% <20 µm; 17% <2 µm
	Limestone 2	< 0.08	104	55% <20 µm; 17% <2 µm
	Limestome 3	< 0.08	91	55% <20 µm; 17% <2 µm
	Quatzite	< 0.08	202	50% <20 µm; 16% <2 µm
	Greywacke	< 0.08	139	47% <20 µm; 14% <2 µm
Konrad & Lemieux 2005	Granite	< 0.08	84	100% <80 µm
	F5K50	0-20	145	5% <80 µm, including 2.5% kaolinite
	F10K10	0-20	144	10% <80 µm, including 1% kaolinite
	F15K10	0-20	217	15% <80 µm, including 1.5% kaolinite
Nurmikolu 2005	Granite (test 4)	0-31.5	84	9.6% <63 µm; 5% <20 µm
	Granite (test 51)	0-31.5	66	10.5% <63 µm; 5.5% <20 µm
	Granite (test 5)	0-31.5	81	12.3% <63 µm; 6.5% <20 µm
	Granite (test 64)	0-31.5	104	15.2% <63 µm; 5% <20 µm

The sample had to be cohesive enough to hold together when unmolded directly on the experimental setup and strong enough to avoid any deformation due to creep. All samples were built from the 0-4 mm sieved material but two: one was prepared using Lørenskog (>125 µm - 4 mm) and Velde (0 - <125 µm) fractions (referred as C.S., for constructed sample, in different tables and figures), and the other one was already in a 0 - 0.500 mm grading (Velde). The samples were 150 mm in diameter and close to 200 mm in height.

2.2 The Multi-Ring Frost Cell

The frost cell consists of 18 rings that can accommodate sample heights up to 200 mm (225 mm with rubber spacers between rings), and 150 mm diameter (Figure 1). The rings were made of high-density polyethylene. Eighteen thermistors with a 0.1°C accuracy were inserted in each ring, with the tip of the thermistor secured with epoxy glue flush at the inner diameter side of the sample, taking temperature measurement at each 11.1 mm before heaving. The cell was insulated during test to minimize radial heat transfer. The cell is rigid enough to not deform under radial pressure during ice formation with 50 mm wall thickness.

The NTNU frost cell was built at Laval University, Quebec, Canada, based on a design modified from the one developed by the U.S. Army Cold Region Research and Engineering Laboratory (CRREL), illustrated in ASTM D5918. The sample was placed between two plates (with filter paper and porous stone) where temperature was imposed using two cryostat units.

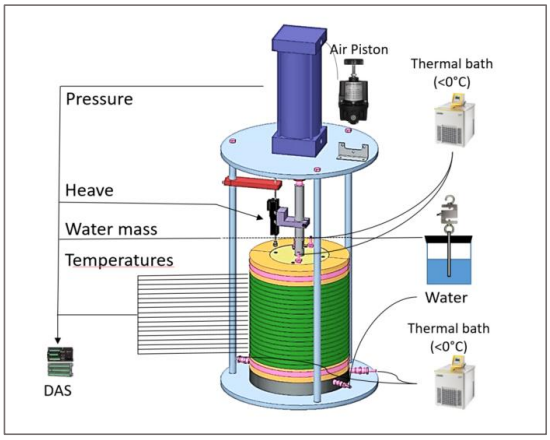

Figure 1. NTNU Multi-ring frost heave cell.

A 0.635 mm thick rubber membrane was placed on the sample after being unmolded on the base plate. A split ring at the base was tightened with a steel collar to seal the membrane. Rings were placed one by one and another split ring sealed the sample at the top. The multi-ring cell included an air piston, allowing pressure control during test. No vertical pressure was imposed in this present study. A potentiometer was used to measure heaving with a 0.01 mm precision. The water was free to flow inside the sample for the 24 hours conditioning phase, with level placed 3-4 cm higher than the sample top. The water level was lowered at the base of the sample prior to the freezing phase. A glass recipient with a cork, in which a glass tube inserted, was used to have a constant pressure head at a chosen height (Mariotte's bottle), therefore allowing water to flow only by the cryosuction process.

The cell was placed into a fridge at 2°C to further limit temperature variation during test. The sample was conditioned at 2°C before starting the freezing. The freezing was applied from top with an aimed temperature of -4°C. Samples were submitted to freezing for a 96 hours period. All the data were recorded at each 5 minutes using a data acquisition system (18 temperature, sample height and water mass). Rings' position variation during tests were measured using graduations on the frame, allowing thermistors heights correction versus time for the SP calculation.

2.3 Segregation Potential (SP) Calculation

The SP is defined as a relationship between water velocity intake and thermal gradient when at steady state (Konrad and Morgenstern, 1981), (Equation 1).

$$SP = {}^{v}/_{\nabla T} \qquad [1]$$

Where ∇T is the temperature gradient (°C/mm), v is the water intake velocity (mm/d) at thermal steady state. The SP is therefore expressed in mm^2/degree-day. Some works also express SP in mm^2/degree-hour. The notation mm^2/°C-d will be used in this paper.

The methodology to find the SPs is a graphical interpretation, as described in the Quebec Transport Administration (MTQ) LC-22.331 standard. It was adapted from its original version since it was previously developed for fine grained-soils (silt and clay), without compaction phase (sample are put in place in cell at relatively high water content followed by a consolidation phase) and by using a split-mold freezing cell type (no thermistors height variation).

The principle of the method is to use both frost depth vs. time and temperature profile graphs in order to find at which moment the temperature regime changes from transient to steady state. This moment defines the time at which the rate of heaving and the temperature gradient in the frozen fringe will be considered for calculation. This time indicates when the last ice lens in the sample begin to grow. Figure 2 shows an example from a laboratory test done on the Hadeland quarry aggregates for SP calculation methodology.

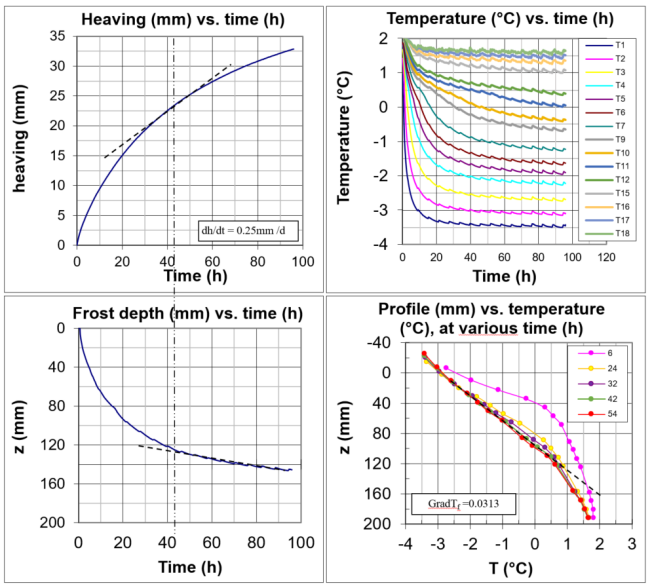

Figure 2. Detailed graphical solution of the segregation potential.

The top right corner portion of Figure 2 presents the temperature evolution of each thermistors for the 96 hours duration of the test. Note that three thermistors were faulty (T8, T13 and T14) and therefore have not been plotted. The cyclic variations of ± 0.05 °C are due to the fridge temperature variation during the test (due to evaporator coil defrost cycle). Left section of Figure 2 presents heaving, and frost penetration vs. time respectively. The bottom right portion shows different temperature profiles at different times in the sample.

The steady state was reached around 42 hours based on a) frost penetration that became linear and b) the temperature gradient in the fringe became constant in the frozen fringe, i.e. [-0.1, 0]°C. At this time, the rate of heaving (dh/dt) was 0.25 mm/h and the thermal gradient in the frozen fringe

($GradT_f$) was 0.0313 °C/mm. The SP is calculated by dividing the rate of heaving by the temperature gradient, and by 1.09 to accommodate volume difference between ice and water. Consequently, the SP for this 0-4 mm crushed rock aggregates was 192 mm^2/°C-d.

3 RESULTS

The particles size distribution, including fine fraction particle size distribution in mortise, of the different quarries are presented in Figure 3.

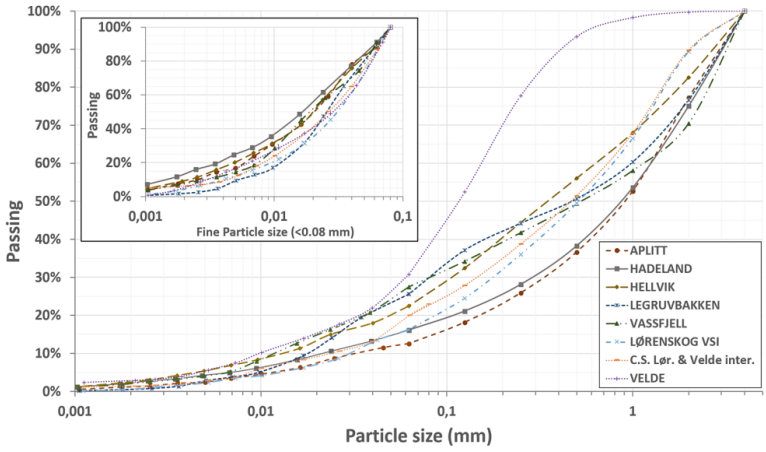

Figure 3. 0-4 mm, and <80 µm, crushed rock aggregates particle size distribution.

The XRD results are presented in Table 2 and were performed sporadically from 2011 to 2018. The different rocks had all igneous or metamorphic origin. The table 3 presents rock type, density of grain ρ_s , dry density ρ_d, porosity n (after compaction), initial water w_i content before testing (after compaction), and % fine fraction for <63, <20 and <2 µm. The dry densities ranged from 1.983 to 2.170 g/ cm^3 for 0-4 mm material. Percentages of fine material < 63 µm varied from 12.5 to 30.7. Table 4 presents temperature boundaries at top and bottom of the sample during test, rate of heaving and temperature gradient at steady state, and SPs. Despite a relatively low amount of <2 µm, the observed SPs were relatively high, from 60 to 197 mm^2/°C·d.

Table 2. Mineralogical content (%) using XRD analysis.

	Aplitt	Hadeland	Hellvik	Legruvbakken	Vassfjell	Lørenskog	Velde*
Quartz	29.0	7.0	0.0	35.8	0.0	28.0	25.0
Plagioclase	37.0	53.7	78.2	32.8	21.3	47.5	30.0
K-Feldspar	13.4	32.0	3.7	4.3	1.7	6.4	35.0
Hornblend	0.6	2.2	0.0	3.9	35.1	0.0	0.0
Epidote	6.0	0.0	6.2	5.7	30.0	0.0	0.0
Pyroxene	0.0	4.3	2.4	0.0	1.0	0.0	0.0
Amphibole	0.0	0.0	0.0	0.0	0.0	14.1	0.0
Chlorite	2.3	0.0	2.3	12.9	9.9	0.0	1.0
Mica	11.8	0.3	6.4	4.6	0.0	4.0	9.0
Others	0.0	0.5	1.0	0.0	1.1	0.0	0.0

* : % estimated from NGU and Velde Industri AS data.

Table 3. Characterization of crushed rock aggregates.

Quarry	rock type	PSD (mm)	ρ_s (g/cm^3)	ρ_d (g/cm^3)	n %	w_i %	<63 µm %	<20 µm %	< 2um %
Aplitt	Granodiorite	0-4	2.712	2.132	20	7.0	12.5	7.4	1.23
Hadeland	Porphyr	0-4	2.653	2.088	20	7.4	16.1	9.7	2.30
Hellvik	Anortosite	0-4	2.720	2.163	20	7.5	22.4	13.2	2.45
Legruvbakken	Slate	0-4	2.663	1.983	29	7.4	25.6	11.5	0.56
Vassfjell	Gabbro	0-4	3.064	2.137	29	7.3	24.9	14.8	2.05
Lørenskog	Gneiss	0-4	2.690	2.170	18	7.0	16.2	7.1	0.53
C.S. Lør.+ Velde	Gneiss/Granite	0-4	2.670	2.165	20	6.8	20.0	9.1	1.41
Velde	Gneiss/Granite	0-0.5	2.610	1.825	31	9.6	30.7	15.2	2.83

Table 4. Segregation potential of crushed rock material.

Quarry	rock type	T_c (°C)	T_w (°C)	dh/dt (mm/d)	*Grad* T_f (°C/mm)	SP (mm^2/°C-d)
Aplitt	Granodiorite	-3.5	2.0	5.40	0.0333	149
Hadeland	Porphyr	-3.4	1.6	6.00	0.0313	176
Hellvik	Anortosite	-3.3	2.2	6.97	0.0324	197
Legruvbakken	Slate	-3.5	1.9	2.18	0.0333	60
Vassfjell	Gabbro	-3.2	2.1	7.27	0.0379	111
Lørenskog	Gneiss	-3.7	1.9	4.00	0.0350	105
C.S. Lør.+ Velde	Gneiss/Granite	-3.7	1.8	5.33	0.0376	130
Velde	Gneiss	-4.2	1.1	5.42	0.0253	197

4 DISCUSSION

All tests were performed with NTNU multi-ring cell test. The multi-rings cell has proven to be a reliable and precise tool to perform frost heave tests. Frost heave tests are time-consuming, require specialized, costly equipment, and are therefore suggested i) for building a database of reference values for different materials, or for ii) particularly sensitive projects (e.g. high-speed railway) requiring high degree of data accuracy. No particular difficulties were encountered for during the tests, but it was necessary to find a way to automatize the rings position during heaving phase in order to get more precise positioning of the thermistors as they heaved along with the rings. The graphical solution to find SP is suspected to be user variable, but to an unknown degree.

All crushed rock aggregates in this study are classified as highly frost-susceptible but for the slate rock type. No reliable trend has been observed regarding SPs according to fine content percentages

of <63, <20 µm from the 0-4 mm fraction regarding this study tests. An acceptable trend was observed for <2 µm from the 0-4 mm fraction, presenting a $R^2 = 0.68$.

The different percentages of <20 and <2 µm fraction were evaluated from the <80 µm fraction in order to compare the different results. Figure 4 presents the SP values as function of percentages of the <20 and <2 µm from the <80 µm fraction for this study.

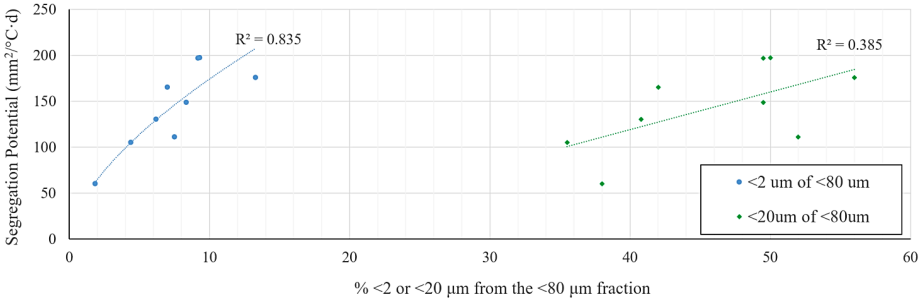

Figure 4. Segregation potential of the <2 and <20 µm fraction from the <80 µm.

According to <80 µm fraction, a significant relationship was observed between SP and the %<2 µm, but a poor one for the <20 µm fraction. SP results from Konrad (2005), and Konrad and Lemieux (2005) did not present correlation for both grading fractions. SP results from Nurmikolu (2005) did not present a good relationship for the %<20 µm but a better one for the %<2 µm.

According to Nurmikolu (2005), a strong correlation exists between percentages of the <20 µm fraction from the total fraction of a same crushed rock type vs. SP. The granite and granitic gneiss of this study (0-4 mm), Konrad and Lemieux 2005 (0-20 mm) and Nurmikolu 2005 (0-31.5 mm) were compared together and are presented in Figure 5.

Nurmikolu and this study SPs for granite and granitic gneiss followed a similar trend with a $R^2 = 0.8023$. Same mineralogy seems to follow a similar trend, independently of the fraction. By using mixes of granitic materials and kaolinite, Konrad and Lemieux showed the effect of mineral content on SP. For similar grain sizes, clay minerals have higher SPs than non clay minerals as shown in Figure 5, and observed by Rieke (1983).

5 CONCLUSION

The multi-ring frost cell apparatus at NTNU has been used to investigate the segregation potential (SP) of commonly found crushed rock aggregates. The frost cell has been proven to be a reliable and precise tool for frost heave testing. Different index values and SPs are proposed following the investigation.

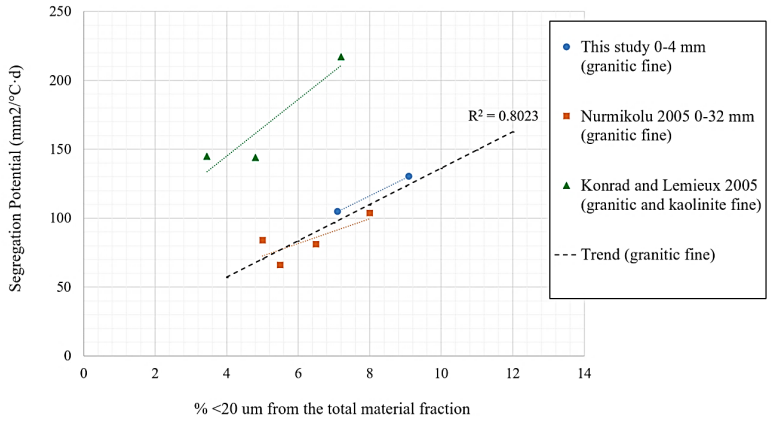

Figure 5. Segregation potential of granitic crushed rock aggregates.

The graphical methodology is established to be an adequate method for SP determination, but the processing time is long and there is always possibility of having interpretation variability. Moreover, the displacement of the rings (and thermistors) leads to few available data when assessing the thermal gradient at different time as the heave has to be manually measured. There is ongoing work in order to produce a mathematical tool that will shorten the processing time and eliminate any interpreter variability.

The same SP magnitude values were measured as in other studies for granite/granitic gneiss rock. SP values for granodiorite, porphyr, anortosite, slate and gabbro were not found in the literature; the values therefore can be used as a reference.

The amount of the different <63, <20 and <2 μm fraction for all types of rock did not reveal satisfactory correlation with SP. When normalizing the <2 μm fraction to the <80 μm one, the correlation for this study was of $R^2 \approx 0.84$, but no satisfactory correlation was obtained in other consulted studies.

According to Nurmikolu (2005), a strong relationship exists between percentages of the <20 μm fraction from the total fraction of a same crushed rock type vs. SP. Correlation of $R^2 \approx 0.80$ was observed when putting in relation the <20 μm fraction from the total fraction for granite/ granitic gneiss in both this study and Nurmikolu (2005). The effect of clay (kaolinite) content when used along with granite fines was observed from Konrad and Lemieux (2005) for <20 μm fraction from the total fraction.

It is known that mineralogy will play a substantial role when rocks are crushed, which affects the fine grain-shape, and indirectly, the unfrozen water content and hydraulic conductivity in the frozen fringe (Konrad 1999). Further investigation is necessary in order to determine the effect of mineralogy on SP for crushed rock aggregates.

ACKNOWLEDGMENTS

The Frost Protection for Roads and Railways project is an national Norwegian research project supported by the Norwegian Research Council (NRC, under grant 246826/O70), the Norwegian Public Roads Administration (NPRA), the Norwegian National Rail Administration (NNRA) and The Foundation for Scientific and Industrial Research at the Norwegian Institute of Technology (SINTEF).

REFERENCES

ASTM C136 (2014). *Standard test methods for sieve analysis of fine and coarse aggregates.* ASTM International, West Conshohocken, PA.

ASTM D5918 (2013). *Standard test methods for frost heave and thaw weakening susceptibility of soils.* ASTM International, West Conshohocken, PA

ASTM D7928 (2017). *Standard test methods for particle-size distribution (gradation) of fine-grained soils using the sedimentation (hydrometer) analysis.* ASTM International, West Conshohocken, PA.

ASTM D854 (2014). *Standard test methods for specific gravity of soil solids by water pycnometer.* ASTM International, West Conshohocken, PA.

Chamberlain, E.J. (1981). *Frost susceptibility. Review of index tests.* US Cold Regions Research and Engineering Laboratory, Monograph 81-2, CRREL, Hanover, N.H.

Håndbok N200 (2018 & 2014). *Vegbygging.* Statens Vegvesen Handbook series, National Public Road Administration, Norway.

Konrad, J.M. (1999). *Frost susceptibility related to soil index properties.* Canadian Geotechnical Journal, 36: 403-417.

Konrad, J.M. (2005). *Estimation of the segregation potential of fine-grained soils using the frost heave response of two reference soils.* Canadian Geotechnical Journal, 42: 38-50.

Konrad, J.M. and Lemieux, N. (2005). *Influence of fines on frost heave characteristics of a well-graded base-course material.* Canadian Geotechnical Journal, 42: 515-527.

Konrad, J.M. and Morgenstern, N.R. (1981). *The segregation potential of a freezing soil.* Canadian Geotechnical Journal, 18: 482-491.

LC-331 (2010). *Détermination du potentiel de ségrégation des sols*. Laboratoire des Chaussées, secteur sols et fondation, Ministère des transports du Québec (MTQ).

Nurmikolu, A. (2005). *Degradation and frost susceptibility of crushed rock aggregates used in structural layers of railway track.* Ph.D. Thesis. Tampere University of Technology, Publication 567.

Rieke, R.D. (1983). *The role of specific surface area and related index properties in the frost susceptibility of soils*. Master Thesis. Oregon State University.

Saarelainen, S. (1992). *Modelling frost heaving and frost penetration in soils at some observation sites in Finland: The SSR Model.* Technical Research Center of Finland, VTT publication 95.

APPENDIX B – PAPER II

Loranger, B., Rieksts, K., Hoff, I. and Scibilia, E. (2019b).

Frost depth and frost protection capacity of crushed rock aggregates based on particle size distribution.

Québec 2019: 18th International Conference on Cold Regions Engineering and the 8th Canadian Permafrost Conference. Quebec City, Canada. (August 18th to 22nd 2019).

Frost Depth and Frost Protection Capacity of Crushed Rock Aggregates Based on Particle Size Distribution

B. Loranger, Ph.D. Candidate
Norwegian University of Science and Technology, Trondheim, Norway

K. Rieksts, Ph.D.
Norwegian University of Science and Technology, Trondheim, Norway

I. Hoff, Ph.D.
Norwegian University of Science and Technology, Trondheim, Norway

E. Scibilia, Ph.D.
Norwegian University of Science and Technology, Trondheim, Norway

ABSTRACT: A common road insulation practice in Norway is to use a layer of crushed rock material, which is called a frost protection layer (FPL). The current regulations allow a large variation of particle size distribution into this layer. This paper presents field investigations on frost insulation performance of crushed rock material with three distinct grading. A full-scale test site was built in Røros, Norway, with each FPLs composed of 1 meter of crushed rock aggregates and built as: Ro-3 section was a coarse dense-graded material (0/120 mm), Ro-1 section, a coarse open-graded material (40/120 mm) and section Ro-2, a fine dense-graded material (0/32 mm). The sections were monitored for two winters (2016-17 and 2017-18). The results showed a significant difference in frost penetration and capacities between the sections. For winter 2016-17, the frost depth reached 194, 136 and 175 cm in Ro-1, Ro-2 and Ro-3 sections respectively, for a surface freezing index of 22630 ºC·h. For winter 2017-18, the frost depth reached 232, 171 and 209 cm in Ro-1, Ro-2 and Ro-3 sections respectively, for a surface freezing index of 36683 ºC·h. The 0/32 mm material provided the best insulation capacity with a frost protection capacity of 443 °C·h/cm. The frost protection capacity for the 0/120 and 40/120 mm material were of 253 and 85 °C·h/cm respectively. The study showed that fine dense-graded material provided superior frost protection mostly due to the larger amount of water retained that increased latent heat. For similar road design and layer thicknesses, the coarse, well-graded material seemed to be the most cost-effective material adapted to Norwegian regions with F_{100} < 28000 °C·h. Coarse, open-graded material should be used in low FI areas, and convection effect should be taken into account.

KEY WORDS: Crushed rock aggregates, frost depth, frost protection capacity, frost protection layer.

1 INTRODUCTION

It is typical to estimate the maximum frost depth in order to choose adequate frost protection measures for transport infrastructure design (Andersland and Ladanyi, 2004; Doré and Zubeck,

2009). In Norway, the National Public Road Administration (NPRA) follows the principle of not allowing frost to penetrate the underlying frost susceptible sub-grade for main roads, i.e. with an average annual daily traffic above 8000. A frost protection layer (FPL), situated between the sub-base and sub-grade, is used for frost protection design. This layer is composed of crushed rock aggregates and has no bearing capacity purposes requirements. A large variation of particle size distribution is accepted as frost protection material. As stated in The Road Construction Handbook N200, i) the material has to be crushed (not blasted), ii) the maximum rock size shall not exceed half of the layer thickness, with a maximum of 500 mm, iii) the proportion of material less than 90 mm must be at least 30% and iv) the proportion of fines <63 μm shall be between 1 and 7 percent, calculated from the less than 90 mm fraction. Note that a new revision of The Handbook was released in 2018, and the proportion of fines that was accepted in the 2014 version (i.e. when the test site was built) was 2 to 15 percent, calculated from the less than 22.4 mm fraction.

This case study first presents the in-situ maximum frost depth with the ones calculated using modified Stefan's equation that accounts for the cooling of the soil below the freezing front. Secondly, the frost protection capacity, in necessary freezing index per centimeter (°C·h/cm) are compared together. The objectives of this paper are to i) present grading and material properties of 3 different FPL composed of crushed rock aggregates, ii) present maximum calculated and observed frost depth and iii) compare frost protection capacities between the sections.

2 FIELD TEST SITE

A field test site was constructed at the end of fall 2016 in Røros, Norway. The test site was composed of six road and four railway sections. However, this study focuses on the first three road sections (Ro-1 to Ro-3) due to the different particle gradations used in their FPLs. A more detailed description of the test site and instrumentation was presented by Loranger et al. (2017).

Each test section had a width and length of 6 and 8 meters respectively and was constructed off-road (no traffic load except for snow removal). Figure 1 shows the cross-section of the first three road sections investigated in this study. Each section is equipped with nine thermocouples located either at the interface or in the middle of each layer. Some moisture sensors were installed in the silt layer, FPL and base layer. An artificial silt layer at 2 meters depth below the road surface was put in place to act as a highly frost susceptible material for frost heave demonstration purpose.

The FPL gradations used between sections are within the accepted range described in the 2014 national standard N200 for road construction. All gradations are shown in Figure 2. An open-graded material (20/120 mm) was used for the frost protection layer for the first section (Ro-1). This material is characterized with minimal amount of fines and an open pore structure. A fine-graded material (0/32 mm) was used for the Ro-2 section. This material was selected for water retention purposes. In addition, the increased fines fraction (11.2% < 63μm) could make this material frost-susceptible . The third road section (Ro-3) had a typical frost protection grading (0/120 mm) and was acting as a reference section. This material is characterized with a coarse, well-graded particle distribution. The fines fraction for this material was approximately 5 percent.

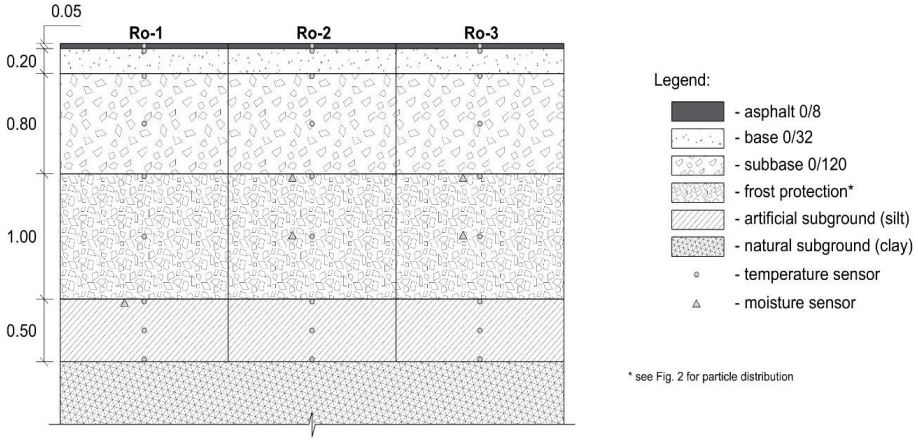

Figure 1. Cross-section of road sections with thicknesses expressed in meter.

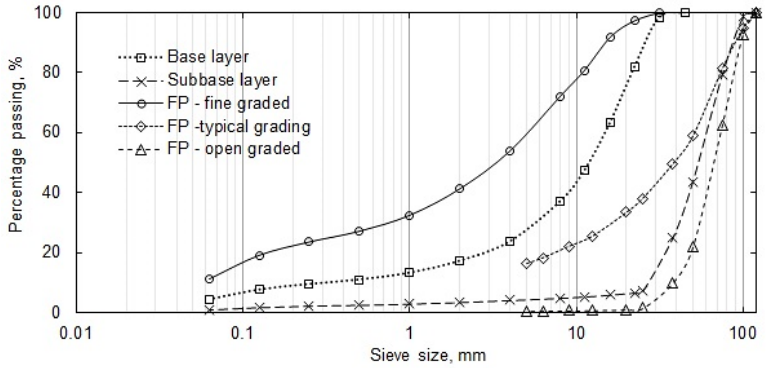

Figure 2. Material gradation of base, subbase and frost protection layers (FP).

3 MATERIAL PROPERTIES

Table 1 lists the material properties for each soil layers. Material properties, such as porosity and mineralogy, were measured under laboratory conditions. Moisture contents were obtained from field measurements. Thermal conductivities were calculated based on the model proposed by Côté and Konrad (2005). The properties for asphalt, silt and clay standard values were taken from Heiersted (1976).

Table 1. Material properties.

	Porosity (n)	ρ_d, (kg/m^3)	C (kJ/(m^3·°C))	w (%)	λ_u (W/(m·°C))	λ_f (W/(m·°C))
Asphalt	0.07	2400	1840	0.5	1.45	1.25

Base	0.29	1980	1817	4	1.46	1.46
Subbase	0.42	1623	1218	1	0.51	0.46
FPL – open graded (Ro-1)	0.45	1535	1152	1	0.44	0.41
FPL – fine graded (Ro-2)	0.24	2116	1986	5.5	1.80	1.87
FPL – typical grading (Ro-3)	0.36	1780	1542	2	0.85	0.77
Silt	0.41	1600	2959	26.3	1.50	2.14
Clay	0.50	1400	2725	28.6	1.19	1.70

4 METHODOLOGY

The compilation of freezing indexes was done using the ISO 13793 standard. The surface freezing indexes were compiled directly from the upper thermocouple in the asphalt layer. The measured *n* factor relating FI_{air} to FI_s were of 0.96 and 1.0 for winter 2016-17 and 2017-18 respectively. The winter 2016-17 showed a FI_s of 22630 °C·h, and winter 2017-18, a FI_s of 36683 °C·h. The Road Construction Handbook N200 is giving a FI_{air} of 21000 °C·h for a 2-years period of return winter and a FI_{air} of 32000 °C·h for a 5-years period of return winter.

Frost depth (FD) monitored at the site were given by thermocouples at variables depth. In parallel for comparison purposes, frost depths were calculated using the modified Stefan's equation, a derived method with addition of heat capacity. Equation 1 shows the modified Stefan's solution that adds the sensible heat to the latent heat factor (ISO-13793). The total amount of sensible heat of the frozen layer is obtained by the multiplication of the volumetric heat capacity and the mean annual air temperature (T_m). The depth at which sensible heat was considered reached 2 m below the freezing front, as estimated from the 2016-2018 temperature curves of road sections 1 to 3. The cooling effect linearly decreases from the freezing front downward to the depth of 2 m.

$$FD = \sqrt{\frac{7200 \cdot FI_s \cdot \lambda_f}{L + C \cdot T_m}} \quad [1]$$

where FI_s is the surface freezing index (°C·h), λ_f is the thermal conductivity of the frozen ground (W/(m·°C)), L is the latent heat of water in the soil ($L_w \cdot w_{vol}$ = J/m^3), C is the specific heat capacity of unfrozen ground (J/(m^3·°C)) and T_m is mean air annual temperature (°C).
It is possible to calculate the necessary FI for the frost front to penetrate a depth h in layer *i* (FI_i) in a multi-layered system from the integration of the modified Stefan's solution for a multi-layered system (Nordal, 1989).

$$FI_i = f \cdot L_i \cdot h_i \cdot \left(\frac{h_1}{\lambda_1} + \frac{h_2}{\lambda_2} + \cdots + \frac{h_{i-1}}{\lambda_{i-1}} + \frac{h_i}{2\lambda_i}\right) \quad [2]$$

where FI_i is the freezing index that is necessary for the frost front to reach h_i in the layer i, i is the number of layers considered, f is a convertion factor from MJ to W·h (1 MJ = 277.78 W·h), L_i is

the soil latent heat of layer i (MJ/m^3), h_i is the frozen thickness of layer i (m), and h/λ is the thermal resistance of layers (°C/W). The estimation of the total frost penetration in that case is the sum of each contributive FI_s for each layer.
The frost protection capacity was used to express the relative insulation performance of each frost protection layers regarding its grading. The different frost protection capacities (β) were calculated using equation 3.

$$\beta = (FI_{z_2} - FI_{z_1})/(z_2 - z_1) \quad [3]$$

where FI_{z_2} and FI_{z_1} are the surface freezing indexes (°C·h) that are necessary for the frost front to reach depth z_2 and z_1 respectively. The depth z_2 and z_1 are expressed in cm and the frost protection capacity is therefore expressed in FI_s/cm.

5 RESULTS AND DISCUSSION

Figure 3 shows the evolution of the frost depth measured in 2016-17 and 2017-18 winters. A total cumulative FI_s of 22630 and 36683 °C·h were compiled for winter 2016-17 and winter 2017-18 respectively.

As expected, finer material grading had procured a better frost protection. The latent heat released during the freezing process, governed by the layer's water content, was acting against the frost penetration.

The maximal FD comparison between measured and calculated frost depths is presented in Table 2 and 3. The site measurement FD were estimated using an intercept function between temperature and thermocouples depths. Calculated ones were done using parameters of Table 1 and designated FI_s. The measured mean air annual temperature for both years was 1.3°C, warmer than the mean air annual temperature stated in N200 of 0.2 °C. The variation is presented between calculated and observed values, in percentage.

The modified Stefan's solution is over-evaluating the frost depth of all sections for 2016-17 winter, with bigger variation as the aggregates get finer. For winter 2017-18, the FD in section Ro-1 was underestimated, and overestimated in sections Ro-2 and Ro-3.

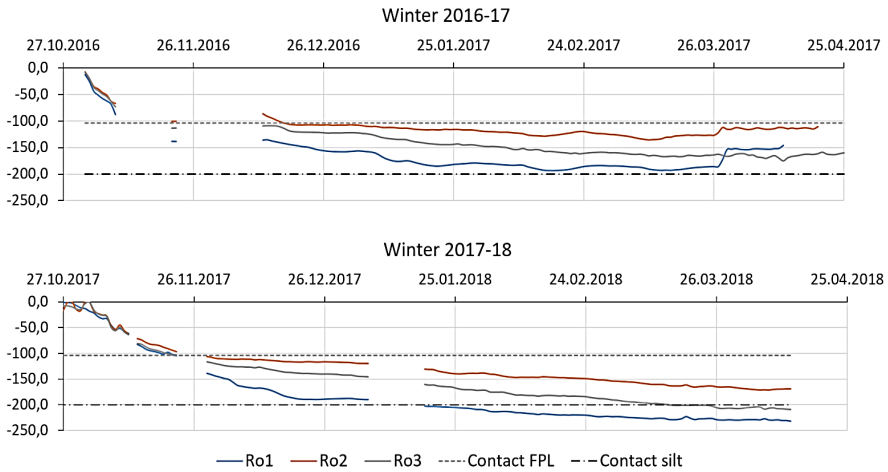

Figure 3. Frost depth according to time for winter 2016-17 and 2017-18.

Table 2. Observed and calculated maximum frost depth (FD, cm) for winters 2016-17, with FI_s = 22630 $^oC \cdot h$.

Road section	Observed field FD (cm)	Calculated FD (cm)	% variation
Ro-1	193.9	207.7	+6.6
Ro-2	136.0	170.0	+20.0
Ro-3	175.2	207.5	+15.6

Table 3. Observed and calculated partial frost depths (FD, cm) for winter 2017-18 with FI_s = 36683 $^oC \cdot h$.

Road section	Observed field FD (cm)	Calculated FD (cm)	% variation
Ro-1	232.9	215.7	-8.0
Ro-2	171.4	208.9	+18.0
Ro-3	209.3	218.2	+4.1

If some centimetres of difference can be considered as correct for designing purpose, one should be careful when using this solution. In fact, the necessary FI_s to penetrate the high water content silt below the FPL implies large values. Field observations showed that FI_s of roughly 1000 to 1500 $^oC \cdot h$ were necessary to penetrate each cm of silt below the FPLs. The use of the mean annual

temperature in Equation 1 is suspected to be responsible for the over-evaluation of the FD. The temperature data from the test site showed that the ground was approximately at 6.5°C at the end of October, just before the freezing period. This temperature is probably the one that should be used as in Watzinger's solution (Nordal, 1989), when considering sensible heat for FD calculation. Further research is necessary to assess the considered depth and temperature if the Watzinger's solution is preferred.

The necessary FI_s for the frost front to advance 1 cm is proposed as a performance index, and was named frost protection capacity (β). The necessary FI_s from the top of the different FPL to a depth of 50 cm which was used to calculate βs as the frost penetration was mainly linear and therefore judged as not significantly affected by the cooling of the sub-grade silt. The β allows to compare the frost protection efficiency according to FPL grading. The β of the different FPLs are presented in Table 4.

Table 4: Frost protection capacity, β (FI_s/ cm) for winters 2016-17 and 2017-18.

Road section	β (FI_s/cm) 2016-17	β (FI_s/cm) 2017-18	Mean
Ro-1	95	75	85
Ro-2	395	485	443
Ro-3	265	240	253

Field results show that it took 4 to 5 times more FI_s amount to penetrate 1 cm of FPL between the coarser and the finer grading (Ro-1 vs. Ro-3). For each winter day with -10°C of mean temperature (≈ average daily temperature for January and February in Røros (N200)), the frost front progressed of 3.2, 0.5 and 1.0 cm/day in road section Ro-1, Ro-2 and Ro-3 respectively.

The β were calculated using the modified Stefan's solution, and gave 89, 255 and 111 FI_s/ cm for road section Ro-1, Ro-2 and Ro-3 respectively. The β comparison for Ro-1 between the field and calculated value was the same magnitude. Calculated βs for Ro-2 and Ro-3 underestimated the capacity by a factor of 1.74 and 2.28 respectively. Again, the use of the mean annual temperature instead of the ground temperature prior to the freezing is believed to be responsible for the under-calculated frost protection capacity.

The frost protection capacity has the same limitation for analysis purposes as the FI. It therefore didn't include wind factor or winter severity (FI build up). Climatic factor such as wind can be calculated using methodology proposed by Dysli (1991). Currently there is no tool other than modelling to assess FI build up effect.

According to frost design N200, finer, well-graded crushed rock aggregates (0-32 mm) as in section Ro-2, is the only section that prevents the frost to penetrate the sub-grade for both winters. The results also confirmed that this grading had the highest frost protection capacity. On the other hand,

Ro-2 is the only material which could have a substantial frost susceptibility. New revision of the Norwegian Road Construction Handbook N200 is lowering the accepted amount of fine <63 μm from 15 to 7%, calculated from the less than 90 mm fraction. Therefore, a 0-32 mm grading would need to have <7% fine to be in agreement with the legislation. This amount is considered to produce limited frost susceptibility risk when referring to particle size distribution criteria (N200). The use of a fine-graded frost protection layer could therefore be considered for extreme cold regions, or for particularly sensible projects.

The use of coarse-graded crushed rock aggregates (20-120 mm) as in Ro-1 should be limited in warmer zones, with limited FI. This conclusion corroborates the Norwegian regulation N200 (2018) regarding FD of open, coarse aggregates for FPL. Rieksts (2018) showed that open graded material in the frost protection could be subject to convection, lowering the anticipated frost protection capacity of such aggregates. An extremely rapid frost front progression in such materials can be expected.

The coarse, well-graded crushed rock aggregate (0-120 mm), as in Ro-3, presents the most cost-efficient grading according to Norwegian climatic realities. Most of the coastal and populated areas generally have F_{100} (100 years period of return freezing index) from ≈3000 - 4000 °C·h (i.e. Bergen, Ålesund, Stavanger) to ≈19000 - 24000 °C·h (i.e Trondheim, Oslo, Narvik, Tromsø). The field data showed that a FI_s of ≈ 28000 °C·h was necessary to reach the sub-grade soil.

CONCLUSION

Different grading of frost protection layers, which are situated below the sub-base layers in the pavement structure, have been tested at the Røros experimental site, in Norway. Norwegian frost design methods use this layer to prevent frost front to penetrate the sub-grade. The results from both winters 2016/17 and 2017/18 showed a clear difference of the thermal response between each FPL toward frost penetration.

For winter 2016-17, the frost depth reached 194, 136 and 175 cm in Ro-1, Ro-2 and Ro-3 section respectively, for a surface freezing index of 22630 °C·h. For winter 2016-18, the frost depth reached 232, 171 and 209 cm in Ro-1, Ro-2 and Ro-3 section respectively, for a surface freezing index of 36683 °C·h.

The average observed frost protection capacities (β, necessary FIs per cm into the different frost protection layers) were 85, 443 and 253 °C·h/cm for Ro-1, Ro-2 and Ro-3 respectively.

When using the Stefan's modified solution, frost depth and frost protection capacities should be calculated using the field temperatures prior to the freezing season at the considered depth. The low mean annual air temperature of the Røros region causes the magnitude of the cooling of the underlying soil to be underestimated, thus FD to be overestimated and frost protection capacity to be underestimated for all sections.

The best performance can be observed with the fine-graded frost protection layer. The performance is related to high water retention compared to the two other materials (5.5% vs. 1.5% and 1%). According to N200 design guideline, Ro-2 is the only section which prevents the frost to penetrate the sub-grade in both winters. However, it is the section with the highest frost susceptibility risk if fine content is relatively high. The typical, well-graded material of Ro-3 (0-120 mm) was judged as the more cost-efficient grading for most Norwegian regions presenting a F_{100} of less than 28000 $^{o}C \cdot h$ for a similarly built road structure. Coarse, open-graded material should be used in low FI areas, and convection effect should be taken into account.

ACKNOWLEDGMENTS

The Frost Protection for Roads and Railways project is a national Norwegian research project supported by the Norwegian Research Council (NRC, under grant 246826/O70), the Norwegian Public Roads Administration (NPRA), the Norwegian National Rail Administration (NNRA) and The Foundation for Scientific and Industrial Research at the Norwegian Institute of Technology (SINTEF).

REFERENCES

Aldrich, H. and Paynter, H. (1953). *Analytical studies of freezing and thawing of soils.* U.S. Army Snow, Ice and Permafrost Research Establishment, First Interim Report 42.

Andersland, O. and Ladanyi, B. (2004). *Frozen ground engineering.* US Cold Regions John Wiley & Sons Press.

Berggren, W. (1943). *Prediction of temperature-distribution in frozen soils.* Eos, Transactions American Geophysical Union, 24(3): 71-77.

Côté, J. and Konrad, J.M. (2005). *A generalized thermal conductivity model for soils and construction materials.* Canadian Geotechnical Journal, 42(2): 443-458.

Doré, G., and Zubeck, H. K. (2009). *Cold Regions Pavement Engineering*. American Society of Civil Engineers Press, Reston, VA.

Dysli, M. (1991). *Le gel et son action sur les sols et les fondations.* Complément au traité de génie civil de l'école polytechnique fédérale de Lausanne. Presses polytechniques et universitaires romandes.

Heiersted, R.S. (1976). *Sikring mot teleskader: Norges teknisk-naturvitenskapelige forskningsråd og Statens Vegvesens.* Frost i jord.

Konrad, J.M. and Morgenstern, N.R. (1981). *The segregation potential of a freezing soil.* Canadian Geotechnical Journal, 18: 482-491.

N200 (2014). *Hånbok N200 Vegbygging.* Statens Vegvesen, Vegdirektoratet.

N200 (2018). *Hånbok N200 Vegbygging.* Statens Vegvesen, Vegdirektoratet.

Nordal, R.S. (1989). *Frysedjup i vegkonstruksjonar.* Institutt for Veg –og Jernbanebygging. Norwegian University of Science and Technology, Notat 522.

Rieke, R.D. (1983). *The role of specific surface area and related index properties in the frost susceptibility of soils*. Master Thesis. Oregon State University.

Rieksts, K. (2018). *Heat transfer characteristics of crushed rock and lightweight aggregate material*. Ph.D. Thesis, Norwegian University of Science and Technology, 2018:228.

Saarelainen, S. (1992). *Modelling frost heaving and frost penetration in soils at some observation sites in Finland: The SSR Model.* Technical Research Center of Finland, VTT publication 95.

APPENDIX C – PAPER III

Loranger, B., Doré, G., Hoff, I. and Scibilia, E. (2020a).

Assessing soil index parameters to determine the frost susceptibility of crushed rock aggregates.

Submitted to Cold Regions of Science and Technology Journal (May 12th 2020).

This paper is awaiting publication and is not included in NTNU Open

APPENDIX D – PAPER IV

Loranger, B., Doré, G., Hoff, I. and Scibilia, E. (2020b).

Evaluation of the SSR model on thick-layered road structures using the I3C-ME frost module and analyses of key parameters.

Submitted to the Journal of Cold Regions of Science and Technology (July 7th 2020).

This paper is awaiting publication and is not included in NTNU Open

APPENDIX E – PAPER A

Loranger, B., Kuznetsova, E., Hoff, I., Aksnes, L. and Skoglund, K.A. (2017).

Evaluation of Norwegian gradation based regulation for frost susceptibility of crushed rock aggregates in roads and railways.

10th International Conference of the bearing capacity of roads, railways and airfield. Athens, Greece. (June 28th to 30th 2017).

This paper was the first evaluation of the Norwegian road design from a foreigner point of view.

Judged as too general to be integrated as scientific contribution to the thesis, it is however interesting to consult in order to get the work environment in which I was to work for the next years.

Erratum: Railway ballast gradation is 0-62.5 mm, and not 20-120 mm as showed on figure 12.

This paper is not included due to copyright

APPENDIX E - PAPER B

Rieksts, K., Loranger, B., Hoff, I. and Scibilia, E. (2019).

In-situ thermal performance of lightweight aggregates (expanded clay and foam glass) in road structures.

Québec 2019: 18th International Conference on Cold Regions Engineering and the 8th Canadian Permafrost Conference. Quebec City, Canada. (August 18th to 22nd 2019).

This paper presents thermal performance of lightweight aggregates at the Røros test site. It was decided to be placed in this section because it was judged that no deep analysis were performed, and it is mostly showing results. However, it brought interesting observations on the role, or necessity, of an underlying frost protection layer below lightweight aggregates.

In-situ thermal performance of lightweight aggregates (expanded clay and foam glass) in road structures

K. Rieksts, Ph.D.
Norwegian University of Science and Technology, Trondheim, Norway

B. Loranger, Ph.D. Candidate
Norwegian University of Science and Technology, Trondheim, Norway

I. Hoff, Ph.D.
Norwegian University of Science and Technology, Trondheim, Norway

E. Scibilia, Ph.D.
Norwegian University of Science and Technology, Trondheim, Norway

ABSTRACT: Transport infrastructures built on frost-susceptible soils may require insulation layer to minimize frost penetration. In Norway, one of the approaches is the use of lightweight aggregates (LWA) as an insulation layer, especially when there are specific restrictions for pavement thickness. Performance and design thicknesses of LWA are included into the Norwegian Road Design Handbook. The current regulations allow the use of LWA layers with or without an underlying lower frost protection layer (LFPL). The goals of this paper are to a) observe the frost insulation capacity of lightweight aggregates and b) investigate the necessity of lower frost protection layer below the lightweight aggregate layer. A full-scale road test site was built in Røros, Norway, with three sections using LWA for insulation purposes. For these sections, a 0.6 m thick insulation layer of expanded clay (Leca) with particle size of 10/20 and 0/32 mm and foam glass (Glasopor) with particle size of 10/60 mm was constructed. An underlying LFPL with a thickness of 0.7 m was made of crushed rock material with particle size of 0/120 mm. Temperature was monitored for two winters (2016/2017 and 2017/2018). The cumulative surface freezing index (FI_s) for the two winters resulted in 22630 and 36683 °C·h respectively. Field observations show that the performance of all three insulations layers was generally the same. The results showed that for both winters the frost front remained in the LWA layer. The study shows that lightweight aggregates could be placed directly on frost-susceptible soils and the frost front will remain in the 60 cm insulation layer even at FI_s of 36683 °C·h.

KEY WORDS: Expanded clay, foam glass, lightweight aggregates, road insulation.

1 INTRODUCTION

Transport infrastructures built in seasonally freezing environments may require insulation layer to minimize the frost penetration if built on frost-susceptible soils (Andersland & Ladanyi, 2004; Doré

& Zubeck, 2009). In Norway, the National Public Road Administration (NPRA) defines in their guidelines that roads with an annual average daily traffic above 8000 should be built so that the frost does not penetrate the frost-susceptible soils (N200, 2018). One of the approaches to limit the frost depth is the use of lightweight aggregates (LWA) as an insulation layer, especially when there are specific restrictions for pavement thickness (Kestler, 2003; Øiseth et al., 2006). Two LWA are commonly used in Norway: expanded clay and foam glass.

Performance and design thicknesses of LWA are included into the Norwegian Road Design Handbook (N200, 2018). The current guidelines, which were revised in 2018, allow the use of LWA with or without a lower frost protection layer (LFPL) which is typically made of crushed rock material. The main purpose of the lower frost protection layer is to provide a thermal barrier by retaining moisture and therefore increasing sensible and latent heat. Hence, this layering is based on the approach that the insulation layer provides a large resistance for the heat that must be extracted from the layer below. The thickness of the LFPL depends on the design thickness of the LWA layer. The current design of layer thicknesses is chart-based in which the charts are produced using a modified Stefan's equation. The modification considers the heat capacity of the soil by adding it to the latent heat term. The test site was built when the previous guidelines (N200, 2014) were still active which required the LFPL layer as a mandatory layer. However, if the insulation layer can retain the frost front within the layer, the LFPL layer might not be necessary.

The paper first describes the full-scale test site that was built to test three different LWA. The results of frost penetration of two consecutive winters are then presented. Finally, the results are compared with the current guidelines and the recommendations of the thicknesses of insulation layers. The main objectives of this study are twofold: i) to observe the frost insulation capacity of lightweight aggregates, and ii) to investigate the necessity of lower frost protection layer below the lightweight aggregate layer. This study is a part of a larger research project on frost protection of roads and railways at Norwegian University of Science and Technology (Kuznetsova et al., 2017).

2 TEST SITE

The location of the test site is in the central part of Norway in Trøndelag region in the municipality of Røros. The location of the test site was chosen for the very low mean annual temperature of 0.2 °C, which is based on 30-year observation data from 1981 to 2010. The corresponding air freezing index (FI_a) for a 10-year and 100-year return period is 38681 and 60599 °C·hours respectively. The test site was constructed during the fall of 2016 and incorporated six road and four railway sections. Each section had a width and length of 6 and 8 m respectively. Figure 1 shows the test site after the construction. The test site was placed in an off-road location and was not subjected to any traffic loading. Winter maintenance was performed to limit the snow and ice buildup.

Figure 1. Test site: a) road section; b) railway sections.

This study focused only on three road sections that were constructed with a layer of lightweight aggregates. Figure 2 shows the cross section of the three road sections.

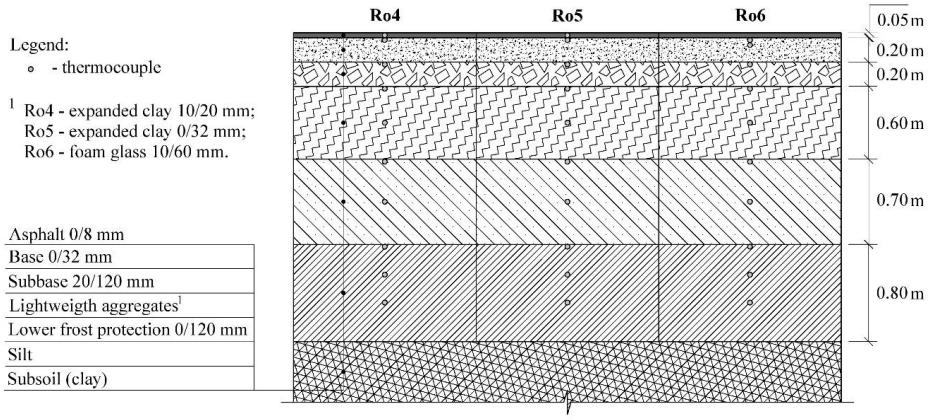

Figure 2. Cross section of road sections with lightweight aggregates.

All three sections were constructed with an overlaying asphalt layer, 0/32 mm crushed rock base layer and 20/120 crushed rock subbase layer. The insulation layer was constructed with three different lightweight aggregates. Examples of lightweight aggregate particles are shown in Figure 3.

Figure 3. Example of particles of foam glass and expanded clay.

Expanded clay material with a particle size distribution of 10/20 mm was used for the Ro4, 0/32 mm expanded clay material for the Ro5, and 10/60 mm foam glass material for the Ro6. Particle size distribution for the three insulation materials are shown in Figure 4. The thickness of the LFPL was 0.7 m and was made of 0/120 mm crushed rock material. All three sections were underlain with an artificial layer of silt with a thickness of 0.8 m. The natural subgrade soil was clay. For a more detailed description see Loranger et al. (2017).

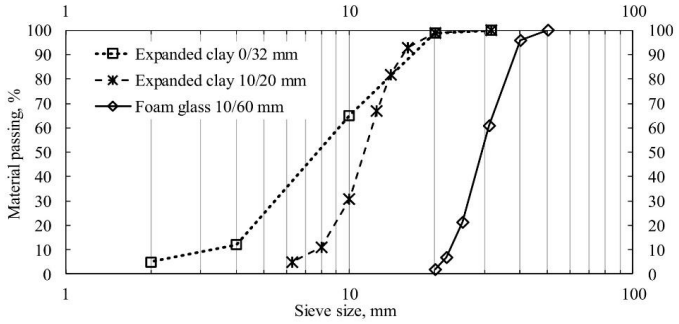

Figure 4. Grain size distribution of lightweight aggregates.

Table 1 lists the final layer thicknesses which were accurately measured during the construction process.

Table 1. Thickness of structural layers.

	Section 1, cm	Section 2, cm	Section 3, cm
Asphalt layer	5	5	5
Base layer	17	18	14
Subbase layer	28	31	41
Insulation layer	64	64	62
Lower frost protection layer	62	59	53
Silt layer	80	80	80

Expanded clay is produced by heating clay up to around 1200 °C in a rotary kiln. The 0/32 mm expanded clay material is the particle gradation straight from the production line whereas the 10/20 mm is a sieved material with removed fine and coarse fractions. The foam glass material is produced by sintering crushed glass powder. The material naturally breaks down to an approximate particle gradation of 10/60 mm during the cooling process. Both materials have very similar thermal properties with thermal conductivity of 0.1 W/m·°C at dry state and about 0.18 W/m·°C with a field moisture content (Øiseth et al., 2006; Øiseth & Refsdal, 2006). The method for determining the thermal conductivity of lightweight aggregates under laboratory conditions is based on ASTM-C518-17 (2017)

To monitor the temperature distribution, each section was instrumented with 10 thermocouples per section. Thermocouples were placed on the interfaces between two layers or in the midsection of each layer. The maximum depth of temperature sensor was 2.25 m. The approximate locations of temperature sensors are shown in Figure 2.

3 RESULTS AND DISCUSSION

Temperature distribution in the three sections was observed for two consecutive winters. Figure 5 shows the air and surface temperature for the period from October 2016 to May 2018. The winter of 2016/2017 resulted in a FI_a and FI_s of 23527 °C·h and 22630 °C·h respectively. The consecutive winter was colder and resulted in FI_a and FI_s of 36536 °C·h and 36683 °C·h.

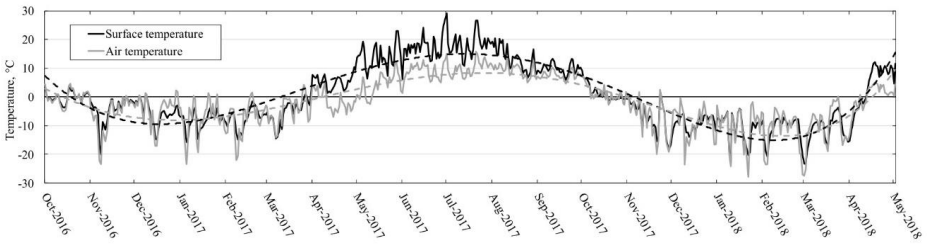

Figure 5. Air and surface temperature measurements from October 2016 until May 2018.

Figure 6 shows the frost penetration in each of the three sections during the winter of 2016/2017. The frost front penetrated down into the insulation layer in a very short period. However, it remained within the insulation layer relatively close to the bottom of the layer for the rest of the winter. The general performance of all three materials was very similar.

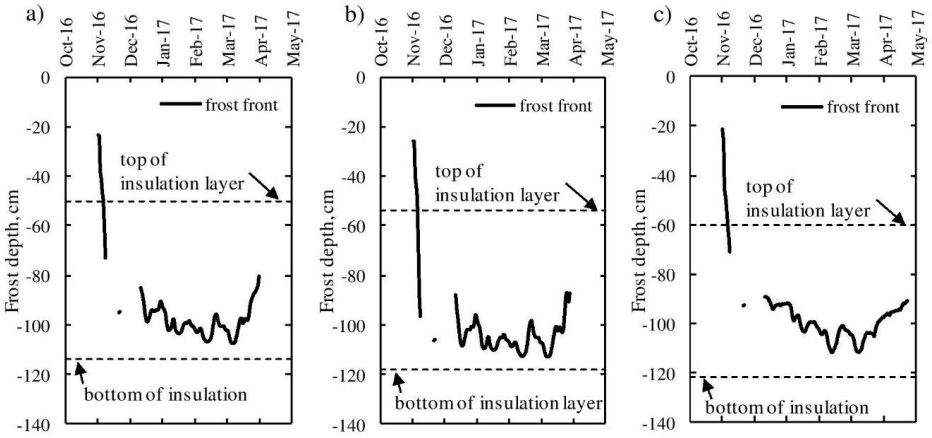

Figure 6. Frost penetration during the winter 2016/2017: a) Ro4; b) Ro5; c) Ro6.

Figure 7 shows the frost penetration for the second winter from October 2017 until May 2018. Given that the second winter was considerably colder than the first one, the frost front penetrated deeper and reached the interface between the insulation layer and LFPL. However, it remained within the insulation layer throughout the winter season and did not penetrate the LFPL.

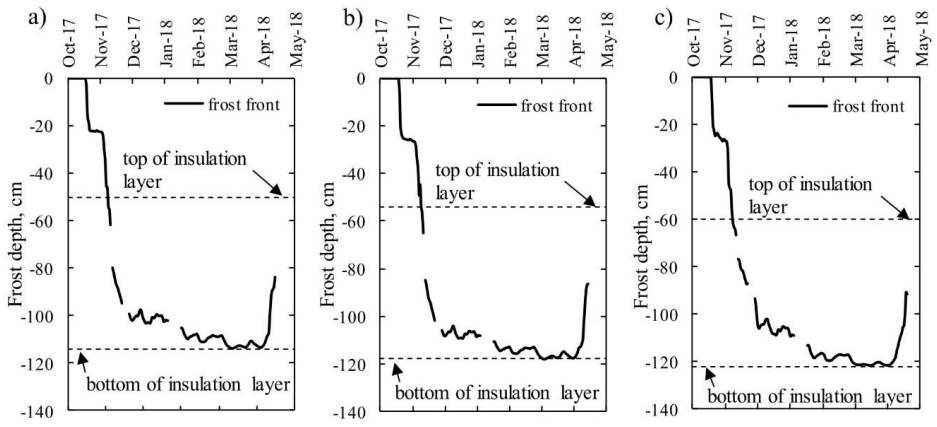

Figure 7. Frost penetration during the winter 2017/2018: a) Ro4; b) Ro5; c) Ro6.

The second winter had a frost index with an approximate return period of 8 years. The design of the sections was made with an FI_{10} which corresponds to 38681 °C·h based on the N200 (2014). This means that based on the design guidelines, the frost front should stay above the frost-susceptible soils during winters with freezing index below FI_{10}. The results show that the insulation layer alone could withstand a freezing index very close to the $FI_{10,}$ meaning that the lower frost protection layer might not be necessary. Possibly, if the structure would be subjected to a winter with FI_{10}, the frost front might penetrate through the insulation layer. When comparing the two winters it can be seen that when the FI_s increased from 22630 to 36683 °C·h, the frost front advanced only by about 0.1 m. This in turn means that slightly increasing the thickness of the insulation layer would keep the frost front within it even at FI_{10}.

The designed manual N200 (2018) calculates the necessary layer thicknesses (LWA layer and LFPL) with a modified Stefan's equation. This approach considers the heat capacity of the unfrozen soil by assuming yearly mean temperature for it. Given that the long-term observations show a yearly mean temperature of 0.2 °C, this factor gives a negligible contribution to the heat extraction during the winter time. Considering only a 0.6 m of insulation layer without any LFPL and the soil temperature of 0.2 °C, the calculations indicate that the frost front would penetrate through the insulation layer at FI_s of approximately 8000 °C·h. This result significantly underestimates the insulating capacity of the lightweight aggregate layers.

During the two-year observation period from 2016 to 2018 a yearly mean temperature of 1.3 °C was measured which is considerably warmer than the long-term observations of 0.2 °C. Considering a soil temperature of 1.3 °C and no LFPL would result in maximum FI_s of 12000 °C·h when frost front would penetrate through the insulation layer based on the N200 (2018) calculations. This result is still far from the insulating capacity that was observed for all three sections. During both winters it was observed that the actual soil temperature at the -beginning of the cooling season

varied between 5 and 6 °C, which is significantly higher than the mean annual temperature. Considering 5 and 6 °C temperature of soil and no LFPL would result in threshold FI_s of approximately 28000 and 32000 °C·h based on the N200 (2018) calculations. This result is much closer to the FI_s what was observed in the field conditions and indicates that using a yearly mean temperature of the soil results in underestimation of insulating capacity of the LWA materials.

4 CONCLUSION

A full-scale test sections were constructed to test the frost insulation performance of three lightweight aggregates: expanded clay with particle size distribution of 10/20 and 0/32 mm, and foam glass material with particle size distribution of 10/60 mm.

The temperature distribution in all three sections were monitored throughout two consecutive winters from 2016 to 2018. The first winter had a FI_s of 22630 and the second winter had a FI_s of 36683 °C·h. The results show that the relative performance of all three materials is very similar. During both winters the frost front remained within the insulation layer. However, during the second winter the frost front stopped at the bottom of the insulation layer.

The results show that the lower frost protection layer is not required if the insulation layer is thick enough. For the given structure, the limit of frost insulation was reached during the second winter which corresponds to a FI_s with approximately of 8-year return period. For a colder winter a thicker insulation might be required to withstand the design winter with FI_{10}. This result confirms that the insulation layer could be placed directly on frost-susceptible soils without the lower frost protection layer.

The design manual N200 (2018) considers a yearly mean temperature for the unfrozen soil. Considering a 0.2 °C temperature of the soil and no LFPL results in the threshold FI_s of only 8000 °C·h which significantly underestimates the insulating capacity of LWA. The field observations showed that yearly mean temperature was 1.3 °C and that the actual soil temperature at the beginning of the cooling season varied between 5 and 6 °C. Considering a temperature of 5 to 6 °C in the calculation based on the design manual results in a more realistic insulating capacity of LWA in terms of the necessary FI_s to penetrate through the insulation layer. This indicates that the calculation gives better results when the actual soil temperature is used rather than the yearly mean temperature.

ACKNOWLEDGMENTS

This study was funded by the Research Council of Norway under grant 246826/O70 and partly by the Norwegian Public Road Administration and the Norwegian National Rail Administration for funding this study.

REFERENCES

Andersland, O., & Ladanyi, B. (2004). *Frozen ground engineering, 2nd edition*: John Wiley & Sons.

ASTM-C518-17. (2017). Standard Test Method for Steady-State Thermal Transmission Properties by Means of the Heat Flow Meter Apparatus.

Doré, G., & Zubeck, H. K. (2009). *Cold regions pavement engineering*: American Society of Civil Engineers Press, Reston, VA.

Kestler, M. A. J. T. r. r. (2003). Techniques for extending the life of low-volume roads in seasonal frost areas. *1819*(1), 275-284.

Kuznetsova, E., Hoff, I., & Danielsen, S. W. (2017). FROST – Frost Protection of Roads and Railways. *Mineralproduksjon, 7*(B1-B8).

Loranger, B., Kuznetsova, E., Hoff, I., Aksnes, J., & Skoglund, K. A. (2017). Evaluation of Norwegian gradation based regulation for frost susceptibility of crushed rock aggregates in roads and railways. *Tenth International Conference on the Bearing Capacity of Roads, Railways and Airfields*.

N200. (2014). Vegbygging (Road construction). Statens vegvesens håndbokserie. Norway.

N200. (2018). Vegbygging (Road construction). Statens vegvesens håndbokserie. Norway.

Øiseth, E., Aabøe, R., & Hoff, I. (2006). Field test comparing frost insulation materials in road construction. In *Current Practices in Cold Regions Engineering* (pp. 1-11).

Øiseth, E., & Refsdal, G. (2006). Lightweight Aggregates as Frost Insulation in Roads—Design Chart. In *Current Practices in Cold Regions Engineering* (pp. 1-11).

APPENDIX E - PAPER C

Kjelstrup, S., Ghoreishian Amiri, S.A., Loranger, B. and Grimstad, G. (2020).

Transport coefficients and pressure conditions for growth of ice lens in frozen soil.

Submitted to Acta Geotechnica journal (July 2nd 2020).

This paper presents the coupled transport of heat and mass across the frozen fringe using the non-equilibrium thermodynamics. It is presented here as extended work involving PoreLab at NTNU.

This paper is awaiting publication and is not included in NTNU Open